# Investigation into Fluidization and De-Aeration Characteristics of Powders and Yield Stress Determination

*A Dissertation submitted*
in partial fulfilment of the requirements
for the award of degree of

**Master of Engineering**

in

**Thermal Engineering**

by

**Kathi Tejaswi**

**Registration No.: 801483012**

**Under the Supervision of**

**DR. S.S. MALLICK**
(Associate Professor)

**Mr. GAUTAM SETIA**
(Lecturer**)**


**DEPARTMENT OF MECHANICAL ENGINEERING**

**THAPAR UNIVERSITY, PATIALA**

July, 2016

# CERTIFICATE

I hereby declare that the thesis entitled **"Investigation into fluidization and de-aeration characteristics of powders and yield stress determination"** is an authentic record of my work carried out as requirements for the award of the degree of Master of Engineering in Thermal Engineering at Thapar University, Patiala, Punjab under the supervision of **Dr. S.S. Mallick**, Associate Professor and **Mr. Gautam Setia**, Lecturer, Mechanical Department, Thapar University, Patiala during July, 2014 to July, 2016. No part of the matter embodied in this report has been submitted to any other university or institute for the award of any degree.

Date: 27/06/2016

27/06/16

**Kathi Tejaswi**

It is certified that the above statement made by the student is correct to the best of my/our knowledge and belief.

27/6/16

**Dr. S.S. Mallick**
Associate Professor
Mechanical Engineering Department
Thapar University, Patiala – 147004

**Mr. Gautam Setia**
Lecturer
Mechanical Engineering Department
Thapar University, Patiala – 147004

Countersigned by

**Dr. S.K. Mohapatra**
Head, Mechanical Engineering Department
Thapar University, Patiala – 147004

**Dr. S.S. Bhatia**
Dean of Academic Affairs
Thapar University, Patiala - 147004



i

*Dedication*

*I dedicate this thesis to my beloved father Kathi Mallesham and my mother Kathi Sharadha, who are an ever supporting and encouraging with their great patience. I also dedicate this to my sister Kathi Jyothsna, who is as an impression for me and to all my dearest friends.*

# Acknowledgements

First of all, I would like to thanks to my most esteemed supervisors Dr. S.S. Mallick, associate professor and Mr. Gautam Setia, Lecturer, Thapar University, Patiala for their

worthy guidance, continuous encouragement and having high patience to listen to all my queries and suggest accordingly. The faith of Dr. S.S. Mallick in me always compelled me to work hard, apart from research his attitude towards life and work and his valuable words taught me many things. The hard work and practical knowledge of Mr. Gautam Setia stood as an inspiration for me. A special thanks to Mr. Atul Sharma, Lecturer and Mrs. Anu Mittal, Lecturer, mechanical department, Thapar University for their assistance to make my avail with the material required for my project work.

I would like to acknowledge all the members of mechanical workshop, Thapar University for helping me out in improving the fabricated test set up and carry out experimental work.

I appreciate the facilities provided by Thapar University to carry out my studies and gain practical knowledge. I gratefully acknowledge SAI labs, Thapar University for providing the results in time.

A special debt of gratitude is owed to the authors whose work I have consulted and quoted in this work.

Last but not least I am always grateful to my family and friends for their unconditional support, encouragement and best wishes, without which I have not come this far.

# Abstract

The study has two major purposes; one is to investigate into the fluidization and de-aeration behaviour of fine powders (belonging to Geldart group A and C) to determine the minimum fluidization velocity and propose a model by considering basic properties to predict the minimum fluidization velocity and the other is to determine the yield stress of fine powders at different depths of spindle immersions and to compare the shear stress behaviour of fine powders with bingham plastic fluids at varying strain rates.

Initially, a model to predict the minimum fluidization velocity has been proposed by considering the experimental data adapted from the literature and by inputting the basic particle parameters. Necessary improvements in the experimental set up have been made to obtain more certain results. Experimental investigations were conducted on different fly ash materials collected from different fields of ESP hoppers from different powder plants and the proposed model was checked for validation. From the obtained experimental data the air retention capability of the fine powders has been analyzed. Shear stress behavior with varying strain rates have been investigated initially for mustard powder and mustard paste at two different depths of spindle immersion. Further investigation is conducted on fly ash from different fields of ESP hoppers of different power plants under fluidized and un-fluidized conditions.

The model developed for predicting minimum fluidization velocity was found to be well suitable for fine powders, especially for powders that fall under A/C boundary. It has been found that the model shows large deviation from the experimental results for very cohesive powders with mean particle size $d_{50} \leq 8$ μm.

The fluidized powders behave same as non-Newtonian bingham plastic fluids (mustard paste) with varying strain rates. The yield stress value of fine powders increases with increasing depths of spindle immersion. Shear stress value is lowered at high speeds of spindle rotation. Furthermore, investigation into shear stress behavior of fine powders is required to involve this as a parameter for accurate modelling of fluidized dense phase flow.

*Key words:* Pneumatic conveying, fluidized dense phase, minimum fluidization velocity, yield stress.

## TABLE OF CONTENTS

## LIST OF FIGURES

## LIST OF TABLES

**LIST OF SYMBOLS AND ABBREVIATIONS**

## Nomenclature

| | | |
|---|---|---|
| A | : | Cross section area of bed ($m^2$) |
| Ar | : | Archimedes number |
| d | : | Volume surface mean diameter (m) |
| $d_{50}$ | : | Mean particle size (μm) |
| D | : | Pipe diameter (m) |
| $F_b$ | : | Buoyancy force (N) |
| $F_d$ | : | Fluid drag force (N) |
| $F_g$ | : | Gravitational force (N) |
| g | : | Acceleration due to gravity ($ms^{-2}$) |
| H | : | Bed height (m) |
| K | : | Power function constant |
| n | : | Exponent |
| P | : | Gas pressure (Pa) |
| $\nabla P$ | : | Pressure drop per unit length (kPam) |
| Re | : | Reynolds number |
| $Re_{mf}$ | : | Reynolds number at minimum fluidization velocity |
| $U_{mf}$ | : | Minimum fluidization velocity ($ms^{-1}$) |
| $U/V_f$ | : | Superficial air velocity ($ms^{-1}$) |
| $W_{fo}$ | : | Settling velocity in calm air of round particles ($ms^{-1}$) |

**Greek symbols**

| | | |
|---|---|---|
| $\alpha$ | : | Constant used in Coltters and Rivas equation |
| $\xi$ | : | Bed voidage |
| $\xi_{mf}$ | : | Bed voidage at minimum fluidization velocity |
| $\rho/\rho_g$ | : | Density of fluidizing air ($kgm^{-3}$) |
| $\rho_p$ | : | Particle density ($kgm^{-3}$) |
| $\rho_b$ | : | Bulk density ($kgm^{-3}$) |
| $\rho_{fl}$ | : | Fluidized bulk density ($kgm^{-3}$) |
| $\rho_{lb}$ | : | Loose poured bulk density ($kgm^{-3}$) |
| $\rho_{tb}$ | : | Tapped bulk density ($kgm^{-3}$) |
| $\sigma_z$ | : | Normal stress in z-direction (Pa) |
| $\tau_w$ | : | Wall shear stress (Pa) |
| $\Phi_s$ | : | Sphericity |
| $\Psi$ | | Permeability factor ($m^3skg^{-1}$) |

## Acronym

| | | |
|---|---|---|
| ESP | : | Electro Ptatic Precipitator |
| FCC | : | Fluidized Cracking Catalyst |
| MsFRB | : | Mechanically stirred Fluidized Bed Rheometer |
| PCC | : | Pneumatic Conveying Characteristics |
| PSD | : | Particle size distribution |
| RPM | : | Rotations per minute |
| SEM | : | Scanning Electron Microscopy |

# Chapter 1

# Introduction and Objectives

## 1.1 Introduction

Bulk material handling and transportation is an important field of engineering that is focused on the design of equipment dealing with the materials such as coal, fly ash, ores, cereals, wood chips, pharmaceutical powders, sand etc. There are certain kind of systems that tackle with the bulk material transportation, one of them is pneumatic conveying. Pneumatic conveying systems are widely used for the transportation of bulk solid materials in chemical (soap powders, detergents), food (sugar, flour), cosmetic (talc, face powder), pharmaceutics and energy (coal and ash) industries. This is normally done by moving the process materials through a totally enclosed pipeline, in a clean, contained stream of air generated either by a vacuum pump, positive displacement blower, or compressor, which is attached to the system. The purpose of preferring pneumatic conveying over other transportation systems is to ensure that the materials are conveyed in a contained environment for preventing contamination (primary requirement for food transportation), ensures dust free operation, flexibility and easy automation. In industries a major proportion of the cost of bulk materials is accredited to its handling and transportation [Wiiliams, 2008]. To ensure minimal cost of handling and transportation appropriate operating parameters are to be chosen.

Pneumatic conveying is generally classified into two modes of flow, dilute-phase and dense-phase. These are classified based on the solid air mass ratio of the material [Klinzing, 2010]. Dilute-phase flow is a suspension flow, whereas dense-phase is non-suspension flow type (shown in Fig. 1.1). The dense-phase is gaining popularity in industries such as power, cement, pharmaceutical, food etc due to its advantages over dilute-phase such as reduced gas flow rate requirement and hence reduced power consumption, which results in more efficient conveying system and therefore, less environmental emissions; lower transport velocities and hence reduced pipeline wear and product degradation; smaller sizes of pipe, filtration equipment, fitting and support sizes/structures for same conveying capacities [Setia, 2012]; improved product quality, reduced wear rate of pipelines, bends and increased workplace safety [Mallick, 2009].

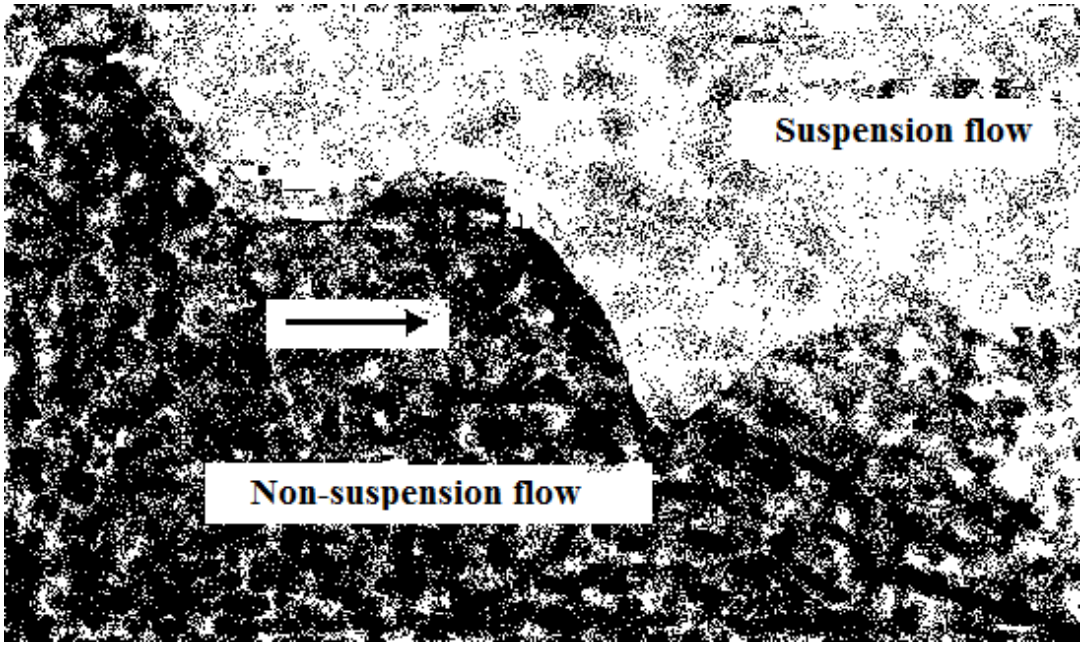


**Figure 1.1:** Two layered flow of fine powders in dense phase

Fluidized dense-phase flow is best suitable for fine powders belonging to Geldart type A [Mallick, 2010] such as fly ash, cement, pulverized coal etc, and that has good air retention properties [Klinzing, 2010] and Geldart type C which are difficult to fluidize, but those exhibits good air retention capability once fluidized [Geldart, 1973]. Therefore, to adopt appropriate operating parameters, it is necessary to understand the behavior of the powders.

For optimum design of fluidized dense-phase flow two main parameters that are to be accurately modelled are total pipeline pressure drop due to solid-gas flows and minimum air flow rate required for fluidization of the fine powders. Accurate prediction of these two parameters is necessary for reliable operation of the pneumatic conveying systems. Over-prediction of pressure drop and air flow rate leads to the higher air velocity and hence causes pipeline wear, product damage and increased operating expenses. Under-prediction of pressure drop lead to reduced material flow rate, whereas under-estimation of air mass flow rate results in gradual material built-up in the pipelines, unstable flow of material and eventually pipeline blockage [Chawla, 2015]. Due to the highly concentrated and turbulent nature of the flow, which makes it difficult to fundamentally model important design parameters such as solid friction factor and minimum transport boundary, modelling of dense-phase flow remained as a significant challenge to the researchers. The proposed models by the researchers are based on power function formats using non-dimensional parameters like solids loading ratio, gas froude number, the ratio of air to particle density and particle to pipe diameter etc. These models have shown inaccuracy when tested under proper

scale-up conditions [Wypych, 1989]. This is because the existing models do not fundamentally address the flow mechanism of the powders when conveyed in fluidized dense phase flow.

Therefore, to understand the flow mechanism and to model the fluidized dense phase flow the pipeline pressure drop and air mass flow rate have to be predicted appropriately by considering the powder flow behavior. Powder yield stress is an important parameter for understanding the flow mechanism and for modelling the fluidized dense phase flow [Mallick, 2009; Chen, 2013; Bruni, 2005]. Fine powders are capable to exhibit fluid-like flow properties due to their natural ability to retain air and form pseudo-fluids. Certain researchers paid attention on the role of rheology in the design of pneumatic conveying systems. Yet none of the researchers have attempted to correlate particle and bulk properties or rheological properties of bulk solids to model dense phase [Chaudhry, 2015]. Considerable work was not done in this field. Hence the present work includes experimental and theoretical estimation of minimum fluidization velocity and study on the rheological properties of the fine powders that fall under the group of Geldart group A/C, so as to understand the flow behavior.

The basic knowledge of the present thesis concept and literature review of previous research in this area is provided in chapter 2 followed by a detailed explanation of the materials and the methodologies used in this project and the properties of each bulk material are exhibited in chapter 3. The experimental data and analysis of yield stress testing and air-particle parameter (fluidisation and de-aeration) testing are present in chapter 4 and chapter 5 respectively. The objectives of the present thesis work are mentioned as follows.

## 1.2 Objectives

Specific objectives are as given below:

- To perform rheology test and determine the yield stress at different depths of spindle immersion and rotational speeds.
- To ameliorate the existing fluidisation setup and perform fluidisation and de-aeration experiments on fine powders.
- To develop a model to predict minimum fluidisation velocity for the fine powders.

# Chapter 2

# Literature Review

## 2.1 Pneumatic conveying

Pneumatic conveying systems are widely used for the transportation of bulk solid materials. The purpose of the pneumatic conveying System is to ensure that materials are conveyed in a contained environment, utilizing air and avoiding spillage. This is normally done by moving the process materials through a totally enclosed pipeline, in a clean, contained stream of air generated either by a vacuum pump, positive displacement blower, or compressor, which is attached to the system. Following are the advantages and disadvantages of pneumatic conveying systems as mentioned by Wypych [2006].

Advantages of pneumatic conveying

a) Environmental clean transportation for a large variety of products.
b) Simplicity of pneumatic conveying system.
c) Flexibility in routing made possible by providing bends.
d) Multiple receiving and delivery points.
e) Low maintenance and manpower cost.
f) Easiness in automation and control of pneumatic conveying systems.

Disadvantages of pneumatic conveying

a) Relatively high power consumption.
b) Wear and abrasion of equipment.
c) Limitation in conveying distance.

### 2.1.1 Types of pneumatic conveying system

1. **Dilute phase**

   This is otherwise known as suspended flow. The basic premise in this is that the particles are picked up by the velocity of the airstream and remain airborne throughout the conveying process. The dilute phase system typically operates at a relatively high velocity and relatively low pressure. The air speed required depends on

the size and density of the particles to be transported. The advantage of dilute phase conveying is it has lower initial investment cost, however, it leads to high power consumption and involves a high maintenance cost. The dilute phase flow through a sight glass is shown in Fig. 2.1.

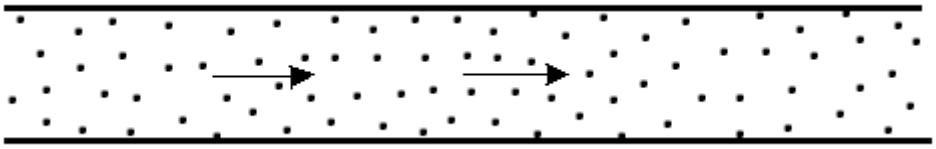

**Figure 2.1:** Dilute phase (suspension) flow

2. **Dense phase**

This is otherwise known as non-suspended flow shown in Fig. 2.2. This kind of flow uses relatively high pressure with relatively low air velocity. The solid loading ratio is high in this case, which provides a large amount of material transfer for same air flow rate when compared to dilute phase flow and thus decreases the total power consumption for pneumatic conveying. Hence dense phase flow is more preferable in industrial applications such as thermal power plants, cement, pharmaceuticals, advanced material and chemical etc. The problem faced in case of dense phase flow is blockage of material which is a critical issue of transportation. To avoid this blockage and to have control over the flow, the flow characteristics of the process material have to be determined.

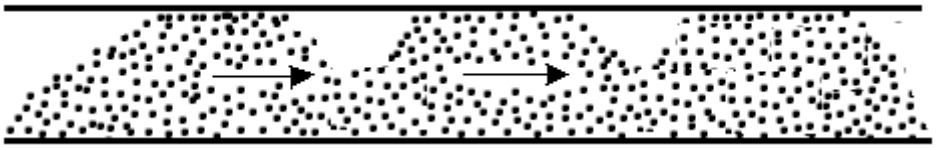

**Figure 2.2:** Fluidized dense phase (non-suspension) flow

## 2.1.2 Components in Pneumatic conveying system

A pneumatic conveying system consists of four distinct zones as mentioned by Klinzing et al., [2009]. These four zones are described as follows:

**a) Prime mover**

Compressed air/gas supply is the main requirement for pneumatic conveying. This is the zone where this air/gas supply is given. The prime mover is the device which includes a wide range of compressors, blowers and fans for supplying the compressed air. The air mass flow rate is controlled by these devices.

b) **Feeding device**

This is the part of pneumatic conveying system where the material is fed into the pipeline and mixed with the conveying gas. The majority of conveying system problems occurs due to a mismatch of feeder characteristics to the prime mover and/or pipeline conveying characteristics. The feeding devices are: 1) rotary valves, 2) Venturi, 3) Screw feeder, 4) Vacuum nozzle shown in Fig. 2.3. These are selected depending upon the pressure required and the material conveyed.

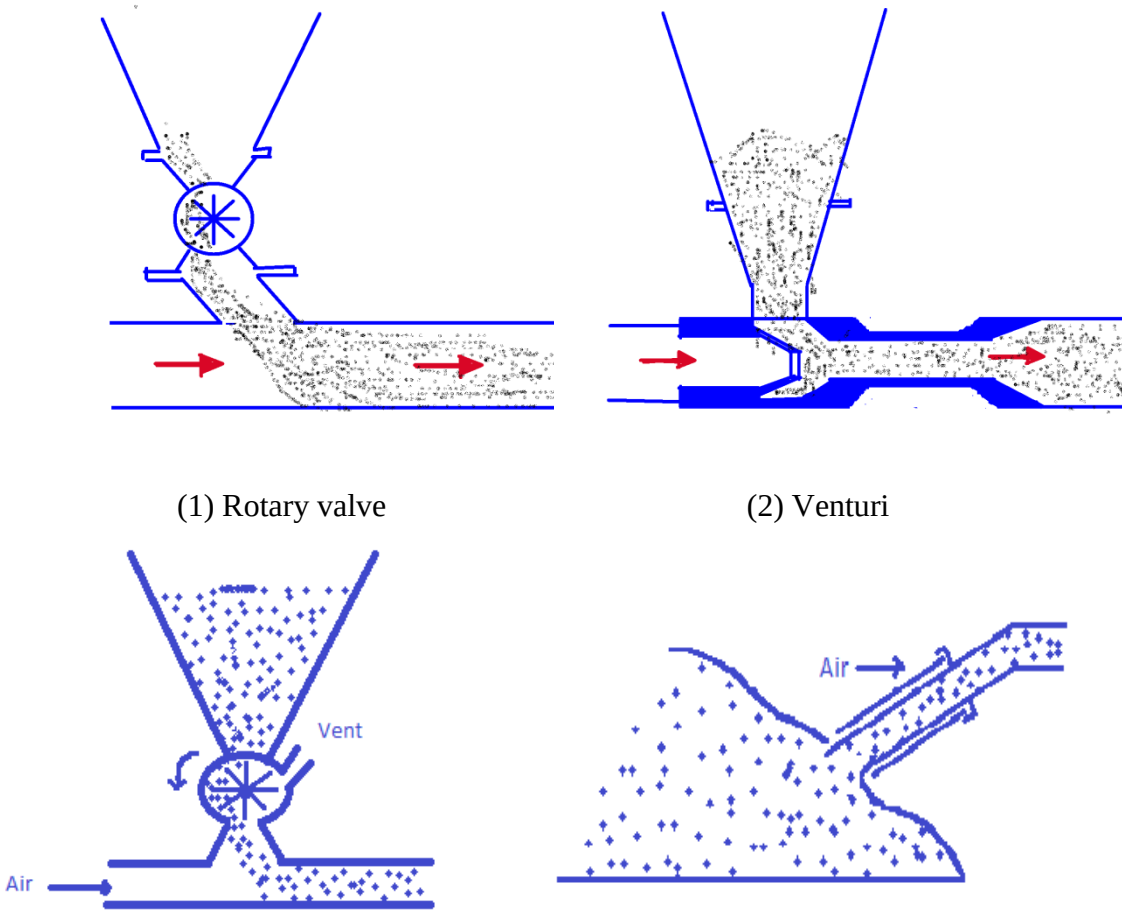


(1) Rotary valve (2) Venturi

(3) Screw feeder (4) Vacuum nozzle

**Figure 2.3:** Feeding devices

**c) Conveying line**

As the solids are fed into the pipeline, a region of the pipeline is needed which allows the solids to achieve final or terminal solids conveying velocity. The solids once accelerated till this velocity enters into the conveying zone. The conveying zone includes piping, bends, expansions, diverters, etc. [Wypych, 2006]. The piping material for this conveying zone depends on the pressure requirement and type of material conveying.

**d) Separating device**

In this device the gas/air supplied from prime movers for conveying is separated from the solids. The separation devices are usually cyclones and bag filters (shown in Fig. 2.4). Cyclones are used for granular materials and bag filters are used for powdered materials. In case the product has wide particle size distribution bag filter is arranged next to the cyclone.

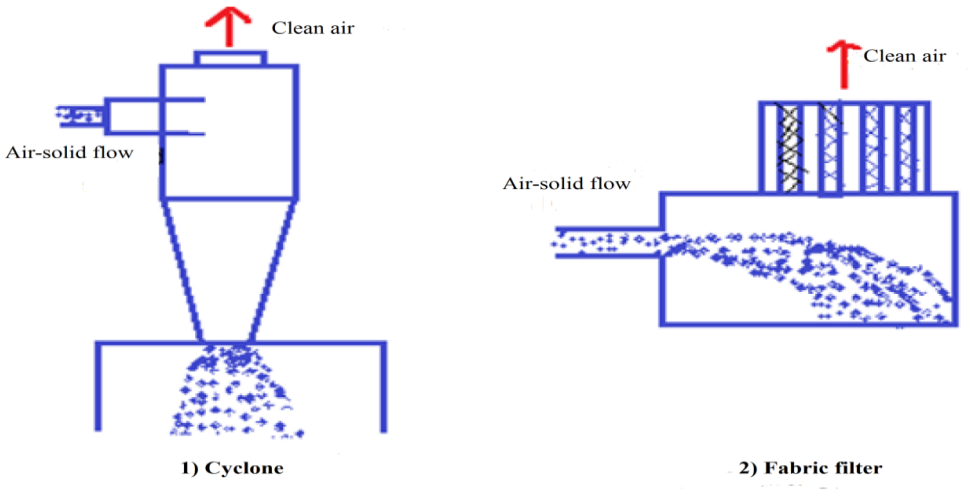


**Figure 2.4:** Separating device

## 2.2 Bulk solids and their properties

Bulk solids are defined as the mixture of at least two or all the three states of pure substances (solids, liquids, gases). The solid sin the mixture may contain diverged properties (size, density, shape, chemical composition etc.). To know the behavior of the bulk solids it is necessary to have abundant knowledge over their properties. These properties are interrelated to each other [Wypych, 2006]. They are divided into two categories; particle properties and bulk properties.

| Particle Properties | Bulk Properties |
|---|---|
| Size | Size distribution |
| Shape | Packing, compressibility |
| Particle density | Bulk density |
| Hardness, strength | Strength, cohesion, wall friction, time consolidation |
| Porosity | Moisture content |
| Toxity, corrosiveness, radioactive | Fluidization, de-aeration, permeability |
| Chemical composition | Explosibility |

### 2.2.1 Bulk properties

1. **Size distribution**

   The mechanical sieving method is most widely used for particle size distribution in industries. A sample of bulk material is placed over the sieve and the whole assembly is shaken for a certain period. The mass retained over the sieve is recorded and size distribution of the sample is determined. However, for small particle sizes, particularly for low density substances, normal, dry sieving becomes ineffective, so far below 75μm wet sieving is recommended [Wypych, 2006]. The most efficient method for size distribution is laser diffraction particle size analyses.

2. **Packing, bulk density, compressibility**

   Bulk solids are generally a random arrangement of a range of particle sizes and shapes. Bulk density depends on the packing of particles, the proportion of voids in the bulk solid. Compressibility determines the relationship between bulk density and the normal stress imposed on the sample.

3. **Moisture content**

   Moisture content has a major impact on the bulk solid behavior. In case of fine particles any amount of moisture leads to increase the internal and cohesive strength of the materials which creates handling difficulties. However the larger amount of moisture content will eventually reduce the internal strength because of slurry formation [Wypych, 2006]. It can also reduce the ignition temperature of dust particles which are prone to explosion.

**4. Internal strength, cohesion, wall friction, time consolidation**

These properties are applied in theoretical models to develop the guidelines in design of bins and silos. All these properties together determine the flow properties or flowability of a bulk solid.

**5. Fluidisation, Deaeration, Permeability**

Fluidisation is nothing but mixing of bulk solids with the gas to make it behave like a fluid. The minimum velocity required for fluidisation is called as minimum fluidisation velocity ($U_{mf}$). $U_{mf}$ is obtained from the fluidisation curve, which represents the variation of pressure drop with respect to superficial velocity ($V_f$) across a section of fluidised bed. The slope of the linear variation of this curve is known as permeability factor. De-aeration is the action of gas leaving the fluidised bed after the gas supply has been terminated.

The fluidization regimes change as a function of the fluid velocity. Certain regimes of fluidization that could be visualized while proceeding from the fixed bed stage to pneumatic conveying are as shown in the following Fig.2.5.

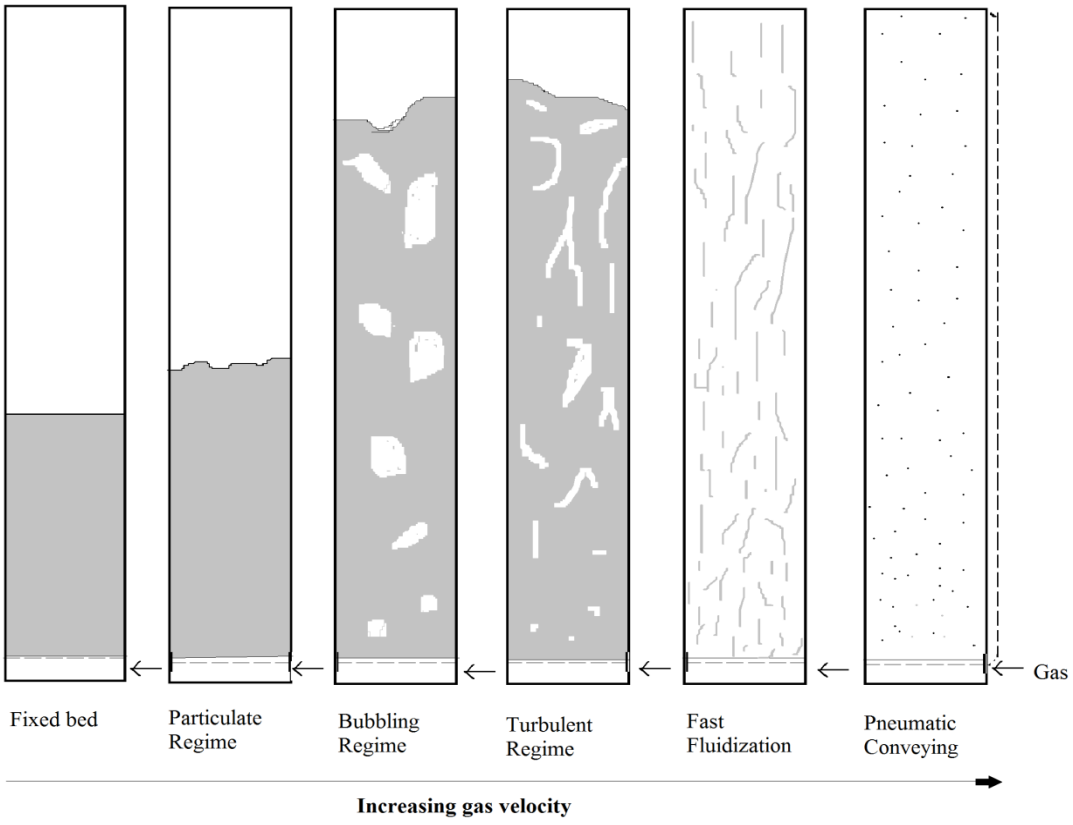


**Figure 2.5:** Flow regimes, adopted from the University of Flourida

6. **Explosibility**

   Any material which has a tendency to burn in bulk will explode when suspended in air at appropriate concentration. This kind of property is more prominent in fine powders. To avoid explosion vents have to be provided.

## 2.3 Flow patterns

Dilute phase and dense phase show different flow patterns. Depending on the gas velocity, product characteristics, conveying rate, pipe roughness and diameter the flow pattern in dense phase can vary from stable dune-flow to low velocity slug flow [Wypych, 2006]. Dilute phase flow apply a large volume of air at high velocities to maintain the solids in suspended flow [Klinzing et al., 2009]. Reducing this velocity the solid particulates start settling down and tend to act as dense flow. Some of the flow patterns in horizontal pipe are as shown in the following Fig. 2.6.

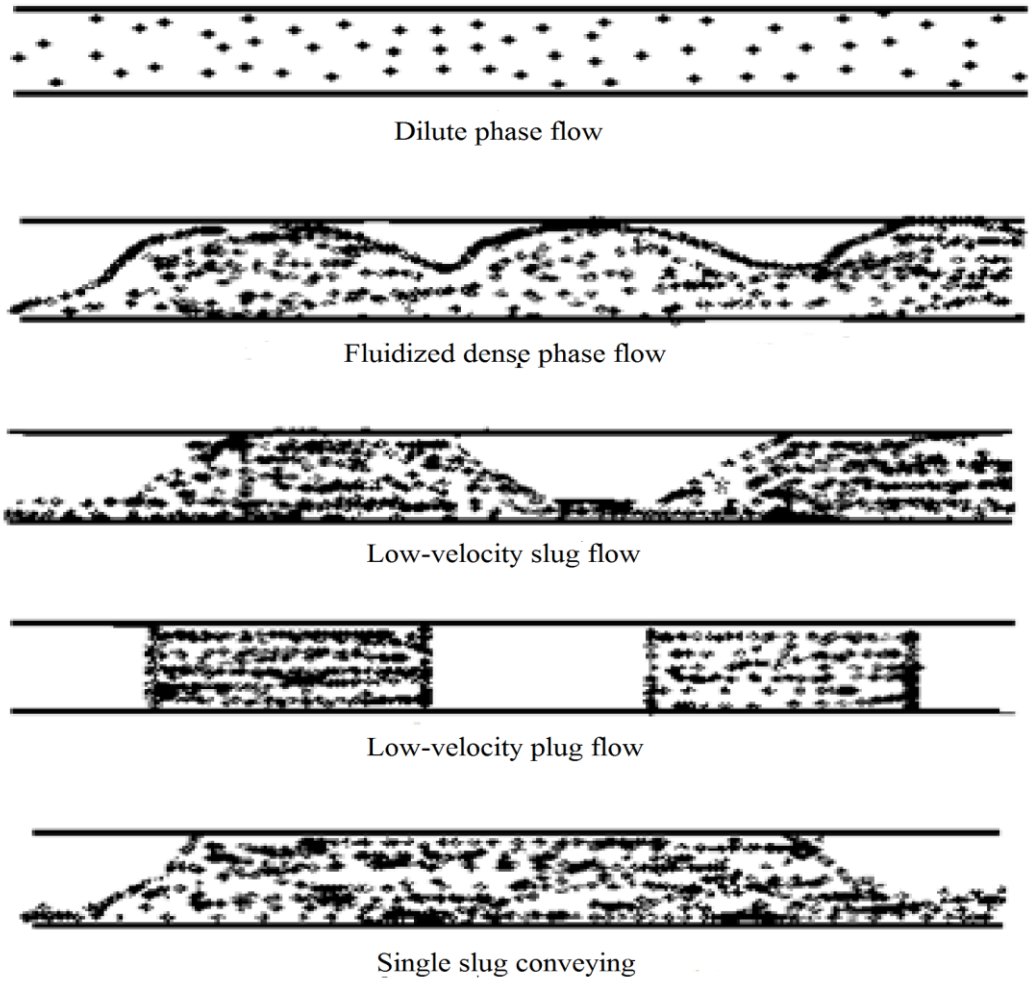


**Figure 2.6:** Flow patterns in horizontal pipe

The dense phase system is preferred as the best option for: 1) Materials that may get damaged by the high velocity in dilute phase system. 2) Abrasive materials. 3) Where a long conveying line is the requisite, as it typically uses a smaller pipe diameter and thus requires less air volume and is much lighter, making installation and replacement easier. Hence dense phase flow is more preferable in industrial applications, but the problem faced in case of dense phase flow is blockage of material which is a critical issue of transportation. To avoid this blockage and to have control over the flow, the flow characteristics of the process material have to be determined.

## 2.4 Geldart's Classification Diagram

Geldart [1973] developed a bulk material classification diagram (shown in Fig. 2.7) that predicts the capability of pneumatic conveying. The diagram indicates the classification of bulk material into any of the groups A, B, C or D on the basis of mean particle diameter and the difference in density between the particle and the gas density. According to the behaviour of the material undergoing the fluidization process, the material can be characterized in any of this group classification.

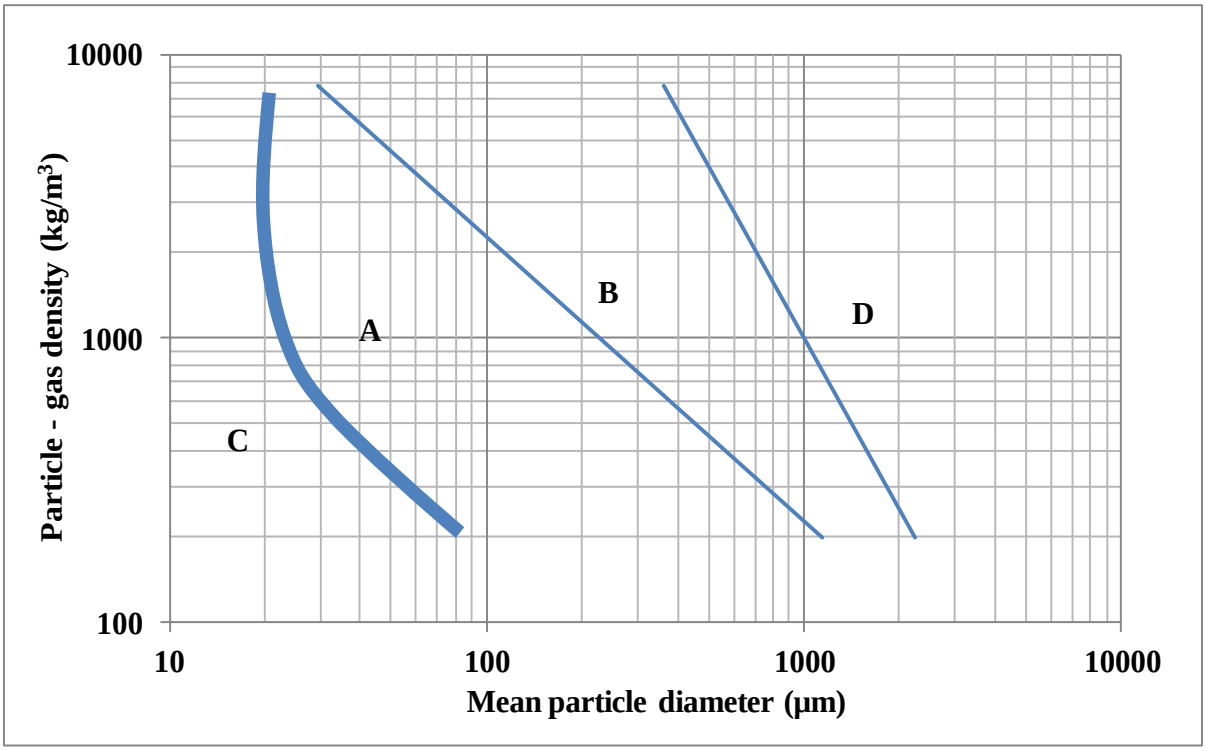


**Figure 2.7:** Fluidization Classification Diagram [Geldart, 1973]

- Group A: These materials have good air retention capacity and hence suited to fluidized dense phase flow. The fluidized bed collapses very slowly when the carrier gas supply is turned off. In these materials the bubbles may be observed later on after fluidization. Example: cement, fly ash.
- Group B: These materials are granular and therefore have less air retention comparing to group A materials because of poor permeability. The fluidized bed collapses very quickly after the gas supply is turned off. Bubbles are generally observed in the bed at or slightly above the minimum fluidization velocity Example: limestone dust, sugar granules.
- Group C: These materials are very fine and highly cohesive in nature. Fluidization of C group materials is difficult, but once aerated this has very good air retention and therefore well suited for fluidized dense phase flow. Difficulty in fluidization is in the form of lifting plug of bulk materials or vertical and the inclined cracks. Example: fly ash, talcum powder.
- Group D: These materials are the large granular materials and are difficult to fluidize because of its high permeability minimum fluidization velocity required for this material is high compared to group B materials. Example: wheat kernels, mustard seeds.

## 2.5 Powder rheology

Under applied stress material undergoes some deformation. The deformation may be elastic or plastic. The study of this flow behaviour of the material is known as rheology. Fluids are continuously deforming substances whereas powders deform under external forces. Fluids are categorized to newtonian and non-newtonian fluids based on its viscosity. High viscosity fluids are characterized as non-newtonian fluids. Fluidized powders exhibit non-newtonian fluid like behaviour. Rheology study of powders provides the similarity between powders and non-newtonian fluids.

### Yield stress:

In rheology study one of the important parameters is considered as the yield stress. Unlike fluids the molecules in powders have less freedom to move, hence have an inherent strength in them. A powder can be fluidized only when the applied stress exceeds the yield stress of the material. Below the point of yield stress the powder deforms elastically which shows the

transition from solids to liquid state. Above this point the powder starts behaving as a viscous fluid (non-newtonian). Hence, the yield stress is regarded as an important parameter in the rheology study of the powders [Chen, 2013] consequently in the design of pneumatic conveying systems. In case of aerated powders the packed molecules acquire the freedom to move freely, hence the yield stress value considerably decreases. So the minimum transport condition can be designed by studying the rheology of fluidized powders.

## 2.6 Fluidization and de-aeration test

The test is performed in a fluidized bed chamber. It consists of a vertical column of specific height made of acrylic tube materials along the periphery of the pressure tapings are installed to measure the pressure drop. The bulk material (powder) is loaded into the vertical column and under this there is a distribution plate and plenum chamber which allows air/gas from a prime mover to pass through bulk materials in the column to fluidize the packed bed particles. The flow of air/ gas is increased and then decreased and the pressure drop across the bed is recorded simultaneously and then the superficial velocity versus pressure gradient is plotted in order to get the fluidization behavior (minimum fluidization velocity) of bulk solids.

## 2.7 Previous research work

**Pan [1999]** developed a flow mode diagram for bulk solid materials depending upon the relation between the properties loose poured bulk density and mean particle diameter. The diagram is developed based on the experimental results and the theoretical analysis which indicates three classifications of pneumatic conveying PC1, PC2 and PC3. Wide range of bulk solid materials were considered in this work (fly ash, agricultural catalyst, alumina, barites, BPP, cement, coal, coarse sand copper ore, flour, granulated sugar, high silica flux, iron powder, magnesium sulphate, mustard seed, narasin, ply powder, plastic pellets, pulverised fuel ash, PVC powder, poly pellets, pulverised coal, pearlite, potassium chloride, potassium sulphate, sugar, silica sand, slate dust WPP, wheat and zircon sand) with mean particle diameter varying from 11 to 4000 μm , particle density from 800 to 4742 kg/$m^3$ and the loose-poured bulk density varying from 100 to 2778 kg/$m^3$. According to this classification if the material falls under the group PC1 it can be smoothly transported from dilute to fluidized dense-phase, material in group PC2 can be transported in dilute-phase,

unstable zone /slug flow and the materials under the group PC3 classification can be transported in dilute-phase only.

**Sanchez, L., et al. [2003]** tried to explore the combined effect of some basic parameters of particles to predict their feasibility to flow in dense phase. They have analyzed the properties of several particles which cover all the four groups (Group A, B, C, D) of Geldart's classification such as Alumina, glass beads, polyester, polyester polymer green, titanium dioxide, LDPE pellet and sand which are of different shapes. Various methods of classifying the particles in conveying mode that are found in the literature were reviewed by them to find out the factors that mainly influence the conveying mode. They found the best correlation using the dimensionless parameters that are functions of permeability factor, de-aeration factor and minimum fluidization velocity.

**Xu and Zhu [2006]** investigated the effect of mechanical vibration on fine particles in fluidization. They performed the experiments and studied the fluidizing behaviour of $Al^2O^3$ (4.8 μm), $TiO^2$ (5.2 μm), $CaCO^3$ (5.5 μm) and glass beads of various average particle size (6.1, 10, 39, 65 and 216 μm) particles which are pertaining to group C, group A and group B. The fluidizing quality of materials with vibrations depends on many factors such as Geldart type particles, particle size distribution, particle shape and also on a vibration parameter (amplitude, frequency, angle) applied. They have examined the particle properties such as particle shape and size on fluidization under vibrations and conclude that the effectiveness of vibrations is found to be more significant on group C particles than in group A and B particles and the irregular particles exhibit higher expansion ratios or larger bed wedges and are more difficult to be fluidized compared to spherical particles because of inter-particle forces. They also examined the role of vibration on fluidization of fine particles with respect to bed pressure drop, bed expansion ratio, agglomeration and tensile strength of bed materials. The vibration leads to decrease the minimum fluidization velocity with higher pressure drop. They observed dramatic reduction in average size and segregation of agglomerates and also lower the tensile strength of materials when the fluidization was assisted with vibration.

**Zhiping., et al. [2007]** investigated experimentally the effect of pressure on the minimum fluidization velocity of materials with larger, medium and smaller particle sizes. They inferred from their investigation that the $U_{mf}$ value decreases with increasing pressure

and, as the pressure increases the $U_{mf}$ of smaller particles is lesser influenced but that of larger particles is influenced strongly. In case of smaller particles the $U_{mf}$ decreases with increase in temperature, whereas in case of larger particles $U_{mf}$ increases along with the temperature and there is no change of $U_{mf}$ for medium particle size materials.

**Jones and Williams [2008]** developed a two dimensional diagram that could predict the three pneumatic conveying flow modes. The diagram was the result of the relation between loose-poured bulk density and permeability. The motive of the new developed flow mode diagram using the permeability factor was to discard the difficulty in determination of de-aeration value. The boundaries in this diagram are empirical in nature which may change according to data availability.

**Mallick and Wypych [2009]** conveyed different powders such as fly ash, ESP dust and cement in different pipe lengths and diameters. They developed Froude number based criteria for predicting minimum transport boundary. They developed a model which could be scaled up reliably from the laboratory test rig to the industrial systems to predict blockage points in dense phase conveying of powders. Initially Froude Number = 6 was predicted by Mallick and Wypych for reliable and safe conveying of powders, but recently, Setia and Mallick [2015] and Setia et al. [2015] have developed improved models for solid friction and better scale up of dense phase conveying of powders.

**Gupta et al. [2009]** investigated on several correlations predicted for minimum fluidization velocity by researchers for fine tailing materials such as zinc slime, iron ore tailings, pre and post hydro-cyclone uranium tailings and a coarse grain fly ash and compared the values with the experimental results. They found that most of the correlations under estimated the $U_{mf}$ value and the values calculated by the correlations predicted by Van Heerden et al. (1951), Noda et al. (1986), Coltters and Revas (2004) and Xu and Zhu (2009) shown good agreement with the experimental values of tailing materials whereas have a large deviation for coarse fly ash material belonging to Geldart group B. They suggested a modification in Coltters and Revas correlation by neglecting the air density in the numerator, the reduced equation is as shown in the Eqs. (2.1) to (2.4).

$$U_{mf} = K\left[\frac{d^2(\rho_p-\rho)g}{\mu}\left(\frac{\rho_p}{\rho}\right)^{1.23}\right]^{\alpha} \quad (2.1)$$

$$= K\left[\frac{d^2 {\rho_p}^2 g}{\mu \rho^{1.23}}\right]^{\alpha}$$

$$U_{mf} = KX^{\alpha} \tag{2.2}$$

$$X = \frac{d^2 {\rho_p}^{2.23} g}{\mu \rho^{1.23}} = R {d_p}^2 {\rho_p}^{2.23} \tag{2.3}$$

$$R = \frac{g}{\mu \rho^{1.23}} \tag{2.4}$$

From the analysis on the combined effect of particle size and density they have concluded that increase in particle size and density results in an increased minimum fluidization velocity.

**Zhu et al. [2009]** have investigated the multiple characterization techniques under different stress states ranging from relatively static to relative dynamic conditions to test powders. They investigated on two different formulations of coating powders, polyurethane and polyester-epoxy whose particle size is ranging from 22 μm to 31 μm. They analyzed the properties of each powder by characterizing them based on the particle size, bed expansion ratio, angle of repose, avalanche angle and cohesion. From their investigation they have concluded that the selection of appropriate technique which subjects the powders to similar conditions that are observed in hand has its own importance. To completely predict the performance of the powder in all processes, each process should be analyzed using a suitable characterization technique and the results obtained in individual characterization technique should not be generalized for all processes as the powders in each process is subjected to its own stress state condition. The results obtained from each technique should be investigated from application point of view.

**Rabinovich and Kalman [2011]** have developed a generalized flow regime diagram using Reynolds number and the Archimedes number for vertical pneumatic conveying and fluidized bed system. The most significant result was that the Geldart's classification diagram can be related to pneumatic conveying system also besides the fluidized bed. They modified the Geldart chart by replacing its boundaries by modified Re and Ar power law relationship. They performed various experiments and investigated the influence of various parameters such as solid concentration and pipe diameter on transition velocity in vertical pipe and found that the variation in pipe diameter has non considerable effect on transition velocity.

**Shabanian, J., et al. [2012]** discussed the fluidization behaviour of ultrafine powders. They described the forces that directly or indirectly affect the fluidization characteristics of the fine powders and the correlations that predict the magnitude of these forces. They mentioned the difficulties in fluidization of group C particles such as air bypassing due to the formation of channelling and behaviour of fine particles as larger particles due to agglomerates formed because of inter-particle forces. They have described some methods that assist to fluidize the fine and cohesive particles by overcoming the opposing forces for fluidization; described the experimental techniques to measure the size of agglomerates and models to predict the agglomerate size.

**Shaul, S., et al. [2012]** developed a generalized flow regime diagram for fluidized beds of Reynolds number as a function of Archimedes number to determine the fluidization state of the material. They performed fluidization tests on tabular alumina ($d_{50}$ = 36 μm), glass beads ($d_{50}$ = 41.6 μm, 69.5 μm) of group A, tabular alumina ($d_{50}$: 109 μm, 578 μm), glass beads ($d_{50}$: 250 μm) and sand ($d_{50}$: 350 μm) of group B, glass beads ($d_{50}$: 855 μm), steel beads ($d_{50}$: 1000 μm) and zirconium ($d_{50}$: 1100 μm, 1500 μm) of group D on fluidized beds of four different pipe diameters to find out the effect of bed height to diameter ratio on minimum fluidization velocity, bubbling velocity and slugging velocity. From the analysis they have concluded that if H/D > 4 the particles of group D start to fluidize by slugging, if H/D > 10 the group B particles tend to behave as group D particles and there is an effect on the minimum bubbling velocity and minimum slugging velocity of group A particles with different bed height to diameter ratios.

**Bruni [2013]** used a mechanically stirred fluidized bed rheometer (MsFBR) to study the rheology of ballotini ($d_{50}$: 350 μm) and alumina ($d_{50}$: 75 μm). Torque measurements were carried out near minimum fluidization velocities at different impeller depths of immersions and rotational speeds of the impeller. An elemental horizontal section of the material was taken and a force balance was provided at a depth z from the top surface. The forces of gravity, upward force due to aeration and forces due to the wall shear stress was taken into consideration. Assuming that stress is uniform at any horizontal section of the powder, the force balance equation was simplified to that provided by Eq. (2.5). This was further used to determine the torque at any given depth from the top surface.

$$\frac{d\,\sigma_z}{dz} + \frac{4\tau_w}{D} + \frac{dP}{dz} = \rho_{bl}\, g \qquad (2.5)$$

**Escudero and Heindel [2013]** investigated the effect of acoustic field on the minimum fluidization velocity of fluidized bed materials glass beads and ground walnut shell having a particle density of 2500 kg/m$^3$ and 1440 kg/m$^3$ respectively with three different particle size ranges (212-425 μm, 425-500 μm and 500-600 μm). They studied the effect of sound wave frequency and sound pressure level on the value of $U_{mf}$ in four fluidized beds of different bed height to diameter ratios (H/D: 0.5. 1.0, 1.5, 2.0). By using the sound frequency of loudspeaker ranging between 50-200 Hz acoustic source and the sound pressure level ranging from 90 to 120 dB they investigated the change in $U_{mf}$ value. As an outcome of their investigation, they conclude that the presence of acoustic field improved the case of material fluidization. The $U_{mf}$ value is affected by the changes in the sound frequency and as the sound pressure increases the $U_{mf}$ value decreases.

**Sharma, A.M., et al. [2013]** investigated into the fluidization behaviour of a mixture of gasifier solid residues (GSR), switchgrass and inert material in reactor bed having particle sizes of 80±2.6 μm, 10.3±1.7 μm and 348±1.6 μm respectively. Silica sand as inert material is held at 20 kg in the reactor with the composition of switchgrass ranging from 0.17 to 5% of the sand quantity and that of GSR ranging from 5 to 35% of switchgrass. They have stated that in all the conditions by increasing the superficial air velocity and the bed cross-sectional area the pressure across the bed increased to a maximum point which is considered as the point of minimum fluidization condition. From the obtained results they inferred that for a binary mixture of GSR and sand, with the increase in the percentage of composition of GSR from 5 to 35% the minimum fluidization velocity decreased significantly with bed pressure remained constant in all the compositions of GSR which indicates the improved fluidization with an increase in the percentage of GSR. Whereas in case of a tertiary mixture of GSR, switchgrass and sand there were significant effects of GSR and switchgrass and their interaction on the value of $U_{mf}$ and pressure drop across the bed, both the $U_{mf}$ and the pressure gradient increased with an increase in levels of GSR and switchgrass in the reactor bed composition. They compared the experimental $U_{mf}$ values of the tertiary mixture with theoretically calculated $U_{mf}$ values based on several correlations available in the literature and found that both the values does not match for throughout the range of the mixture

compositions. At higher levels of switchgrass (5% composition) they found ineffective fluidization resulting in segregation of bed material and channelling.

**Jiliang., et al. [2013]** proposed a correlation to predict $U_{mf}$ of wide sized particles given as Eq. (2.6). They investigated on the variation of $U_{mf}$ value quartz sand and bottom ash having wide spread particles with four size distributions; narrow cut, Gaussian type, binary type and uniform type over a range of temperature ranging from 30 – $600^0$C in a small bubbling type of fluidized bed reactors.

$$U_{mf} = 0.28 \sum_{i=1}^{n} X_i d_i^{0.599} \left(\frac{\rho_p}{\rho_g}\right)^{0.533} / v^{0.066} \quad (2.6)$$

From the experimental investigation, they concluded that in all the four distributions the $U_{mf}$ value decreases with increase in bed temperature and tend to be constant at higher temperature region. Coarser particles exhibit larger $U_{mf}$ value compared to others and this variation in $U_{mf}$ is reduced with an increase in temperature. Gaussian type samples exhibit more $U_{mf}$ than narrow-cut particles. Among the four distributions the $U_{mf}$ of uniformly distributed particles is higher than that of narrow-cut particles with same average diameter, unlike the behaviour of binary distributed particles. For the particles with wide PSD the semi-fluidized region extends with increase in bed temperature.

**Chen [2014]** measured the yield stress of three distinctive powders, alumina, bond and fly ash remains, at various air circulation levels utilizing the system of twofold finished cone penetration. It was presumed that the yield stress diminishes with an expansion in air stream rates and the diminishing pattern stops at minimum fluidization velocity. An empirical model was created to set up a connection between yield stress and bulk density. Be that as it may, the impact of particle size on yield stress was not contemplated. He upheld that the estimations of yield stress are to a great extent reliant on the sort of the estimation procedure received, i.e, the measurement of the shaft utilized and the amount of air circulation.

# Chapter 3

# Materials and methodology

This chapter includes the information about the materials used in bulk material testing methods such as basic parameters, air-particle parameter (fluidization and de-aeration), flow property (yield stress) tests and the basic material properties of each bulk material. A broad explanation of the experimental setup and the experimental procedure has been presented.

## 3.1 Bulk material testing methods

This comprises a basic parameter, air-particle parameter and flow property test methods which were conducted on each of the bulk materials to determine their values and behavior. The fly ash samples undergone the testing methods are very fine and cohesive; perhaps contain moisture content in them. Since the materials are delivered to the place of experimental laboratory in tight packed bags from the power plant, solidified powder and the agglomeration of the material was an observed behaviour. To ensure certain values of the experiments, all the materials are conditioned prior to testing by heating the samples at a temperature of $100^0$C in an electric oven for a period of two hours then after filtered the agglomerates by sieving.

### 3.1.1 Basic parameter test methods

The behavior of any powder material entirely depends upon its properties such as particle size, size distribution, shape and density. Hence the basic particle and the bulk properties of all the test materials are determined as follows:

1. **Mean particle diameter:** The bulk materials are very fine and cohesive; hence the particle size distribution was determined by preferring laser diffraction method over other methods. The size distributions of the materials presented in this chapter are $d_{10}$, $d_{50}$ and $d_{90}$.

2. **Particle density:** The particle density was determined by pycnometer method. Five readings were taken for each material and the average value is determined as the particle density of that material.

3. **Bulk density:**
    a) Loose poured bulk density: The value determined from the volume of material poured into a container. The bulk material is poured into the beaker of known volume. Care was taken not to compact the material while pouring into the beaker. The volume of material in the beaker is noted down from the graduated scale available inside of the beaker. This measured volume is divided by the known weight of the material into the beaker to determine the bulk density. The test was repeated for three times and the average value was defined as the loose poured bulk density.
    b) Tapped bulk density: After each loose poured bulk density the fine and cohesive materials were rammed in a sand rammer until there is no further reduction in the volume was observed. The tapped material volume is divided by the known weight to obtain bulk density. The test was repeated for three times and the average value is defined as the tapped bulk density.

4. **Voidage (ξ):** A single parameter value that represents the interstitial voids within the bulk material and for air at ambient conditions can be approximated as:

$$\xi = 1 - \frac{\rho_b}{\rho_s}$$

5. **Shape:** Irregular shape particles intend to interlock among themselves, hence have maximum packing fraction when compared to particles with smooth and spherical shape. To determine the shape of the particles scanning electron microscopy (SEM) analysis was conducted.

The determined values of all the above mentioned properties are provided at the end of this chapter.

## 3.1.2 Fluidization and de-aeration test methods

The basic methods used in conducting air particle parameter tests are fluidization and de-aeration. These tests are performed using a 0.102 m ID and 1 m height fluidization chamber which is made of acrylic tube material. Under this chamber there is a distributed plate with uniformly distributed holes of 3mm diameter drilled at every 1cm distance. There is a plenum chamber below the distribution plate which allows the air from the prime mover (a centrifugal type blower with 1 H.P and maximum air delivery of 145 $m^3$/hr) to pass through

the bulk material in the fluidizing chamber. The plenum chamber and the fluidization column are separated by a fine mesh which is placed over distributed plate for supporting the material and for uniform distribution of air supply. To control the air flow rate by changing the frequency (controlling the RPM of the blower) a variable frequency drive was attached to the blower. The superficial air velocity was measured via a series of Rotameters which are arranged in the air supply line. At each superficial air velocity setting the pressure drop across the fluidized bed is measured via U-tube manometers. The pressure tapings are provided at the bottom (10 cm above the bed) and top of the chamber. Two needle valves are used for precisely varying the air velocity. The fluidization chamber along with the individual parts is shown in Fig. 3.1. The bulk material bed height can be determined from the vertical scale attached on the side of the chamber. In Geldart 'C' type powders channelling would be the expected behaviour before fluidization. Tapping on the fluidization chamber or an external bypass air supply was required to break down the channelling. An anti-channelling air supply hose is provided at the bottom pressure tapping to break down the channelling.

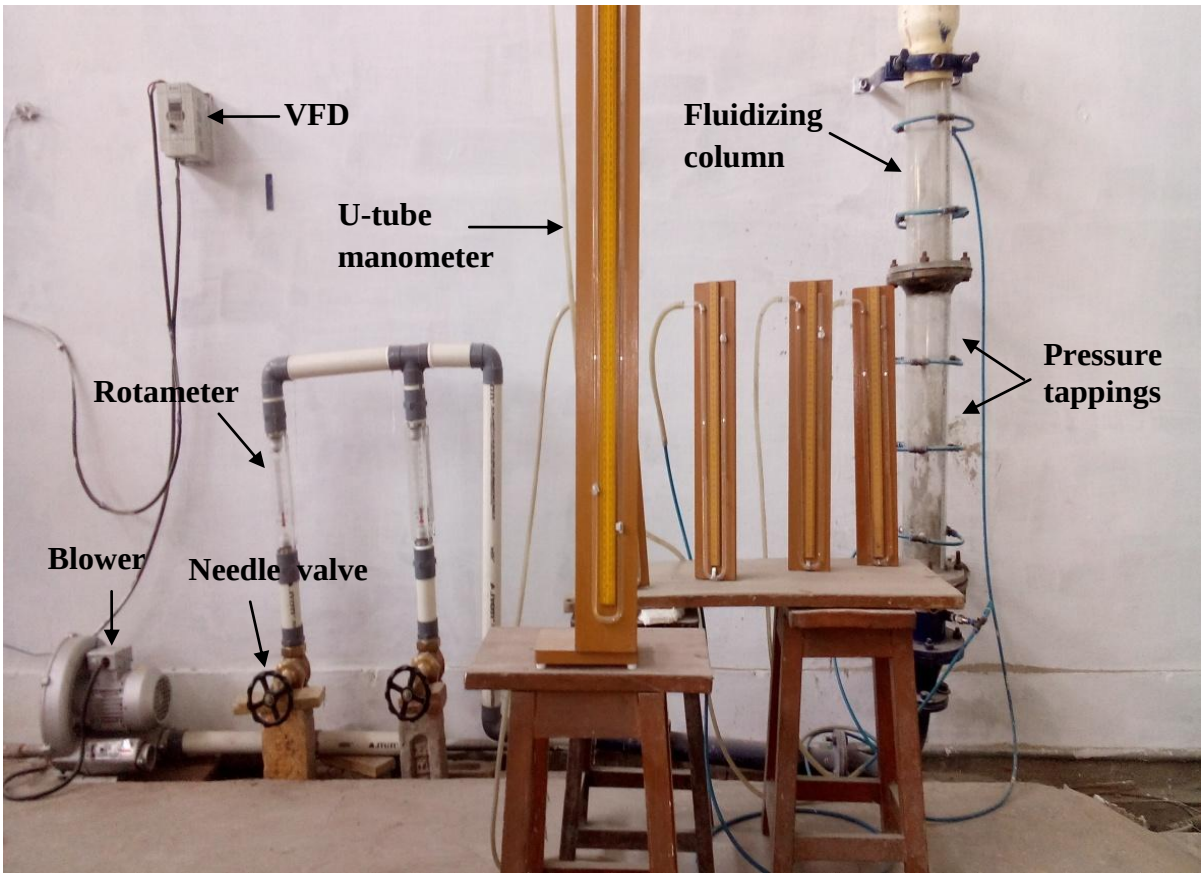


**Figure 3.1:** Experimental test setup of fluidization

1. Fluidization: The process of supplying the air for fluidizing the bulk material is known as fluidization. The flow of air is increased first and then decreased and the pressure drop is recorded simultaneously. The superficial air velocity is increased continuously with equal intervals until complete fluidization of the bed material and then the air velocity is reduced in the same air flow rate increments to zero. The bed height is recorded for each superficial air velocity setting to determine pressure drop per unit length and then the graph is plotted between pressure drop per unit length and superficial velocity in order to get the fluidization behavior of bulk solids.

2. De-aeration: The superficial air velocity is increased until complete fluidization occurs and a steady state pressure was achieved. The air supply is then shut down quickly and the pressure reading was recorded. This testing provided the information of air carrying capacity of the bulk material by bed height decay analysis. Data of reduction in bed height with tie is extracted from the videos recorded by a high speed camera. The reproduced figure of ideal fluidization and de-aeration diagram as given by Williams [2008] is shown below.

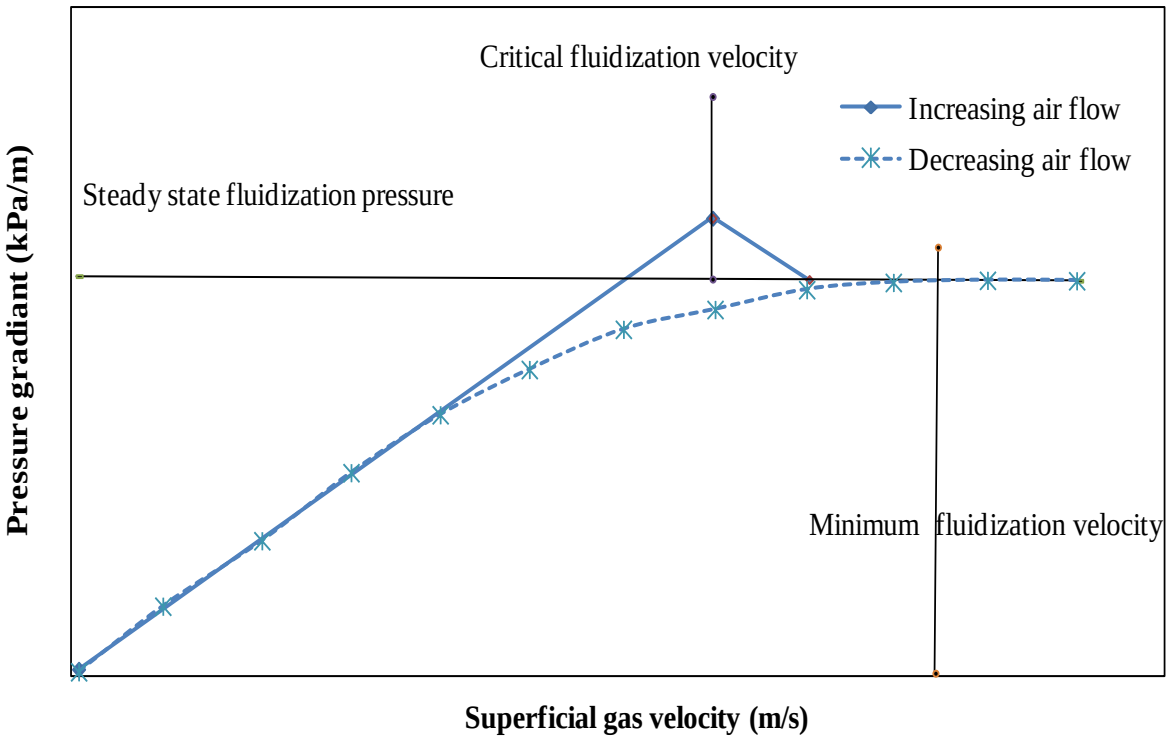


**Figure 3.2:** Ideal fluidization and de-aeration diagram

In order to obtain certainty in the experimental results all the experiments were performed on material after heating at a temperature of $100^0$C for a period of two hours to ensure the absence of moisture content in it. In case of cohesive powders before heating, sieving is performed to separate the lumps formed due to tight packing of material in the way of transportation from the power plant to the experimental laboratory. The detailed description of the operating procedure of the test set up for performing the experiments is provided below.

## Calibration

A standard procedure is employed for the calibration of test column. Before starting the calibration ensure the whole test column is properly fitted and with no leakage of air from any of the points. Then all the pressure tapping are attached to the manometers and air is blown into the test column with the help of a blower and then manometer readings are checked to ensure that all the manometer readings should come same.

**Operating procedure:**

Start up

1. Switch on the power supply and check the display of the VFD.
2. Connect the manometers to the experimental system using the connections provided. Fix all the flexible pipes at the designated points.
3. Start the blower with the help of a run button on VFD and check that it is functioning properly.

Shut down

1. Fully close the regulating valves.
2. Turn off the blower with the help of stop button on the VFD.
3. Turn Off the power supply.
4. Plug out all the pipes from the fluidizing column, then remove the testing particles by unbolt the nuts from bottom side of the column and clean the vessel with the help of compressed air.

**Fluidization testing:**

1. Pour the testing product of known mass into the acrylic tube and note down the initial bed height.
2. The frequency of the blower was set up with the help of VFD in order to get a specific flow rate at a certain pressure.
3. Increase the air flow rate in small increments with help of regulating valves.
4. Continuously note down air flow rate and corresponding pressure with the help of the manometer.
5. Continue the measurement up to the maximum flow and then decrease the air flow rate again to note down the air flow rate and pressure data.
6. Repeat steps 1 through 5.

**De-aeration testing:**

1. De-aeration testing can be done while doing the fluidization testing.
2. Increase the air flow rate up to fully fluidized state and run the system continuously for 3-4 minutes
3. Then air supply is cut off with the help of stop button of the VFD.
4. Record the pressure drop and the bed height with the help of high speed camera.
5. Plot the graph between pressure drop per unit length and time.
6. Plot the graph between bed heights against time.

The schematic diagram of test setup used for fluidization and de-aeration testing is shown in figure 3.3.

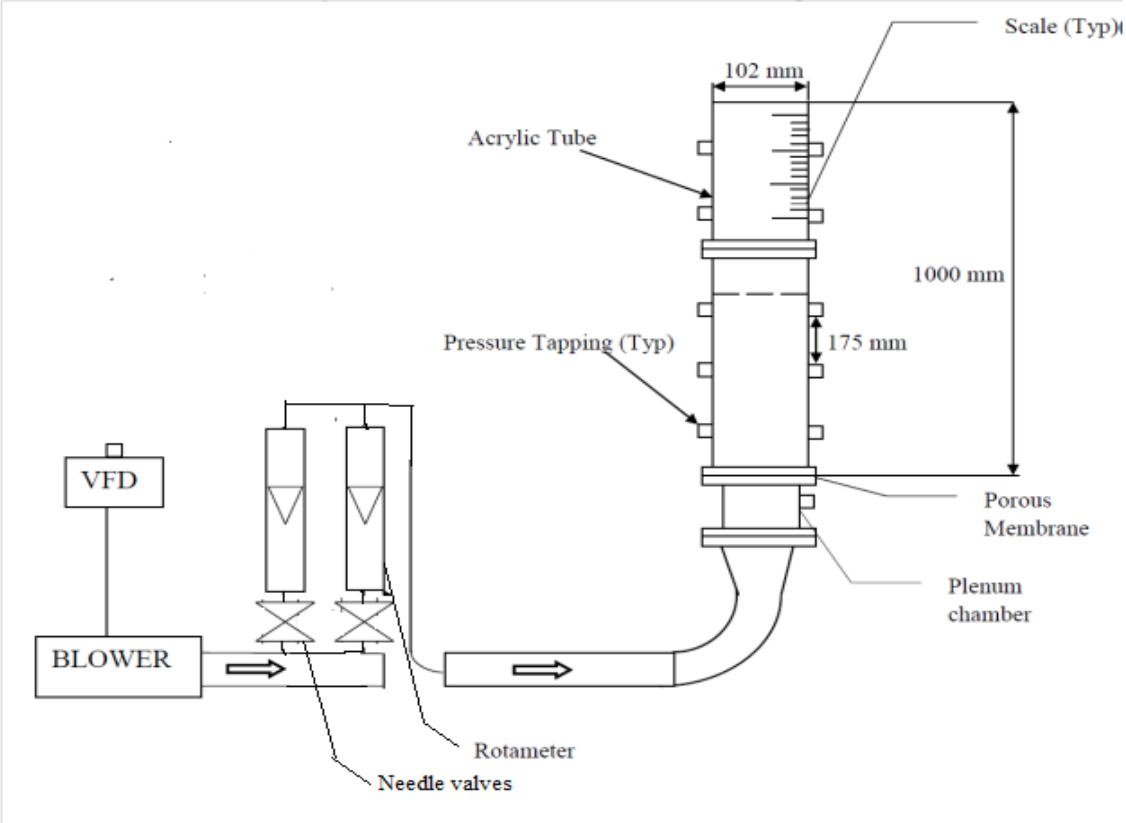


**Figure 3.3:** Schematic of fluidization and de-aeration test setup

### 3.1.3 Powder rheology test

**Description of Brookfield YR-1 rheometer**

Yield stress is defined as the point at which the material starts to deform plastically, the same point is assumed as the point of minimum transport on the PCC, as it also depicts the onset of material flow in a pipeline [Chaudhry, 2015]. The yield stress of fly ash materials and mustard is experimentally measured using a Brookfield YR-1 rheometer, shown in Fig. 3.4. The rheometer is capable of measuring the yield stress of materials of low to high viscous range such as mustard paste, ketchup, yogurt, gels, lotion, and toothpaste, besides it is also capable of measuring the yield stress of powders. EZ yield software is used for programming the required test parameters such as rotational speed of the spindle, spindle number and corresponding immersion mark of the spindle, zero speed and download the program into the rheometer.


**Figure 3.4:** Brookfield YR-1 Rheometer

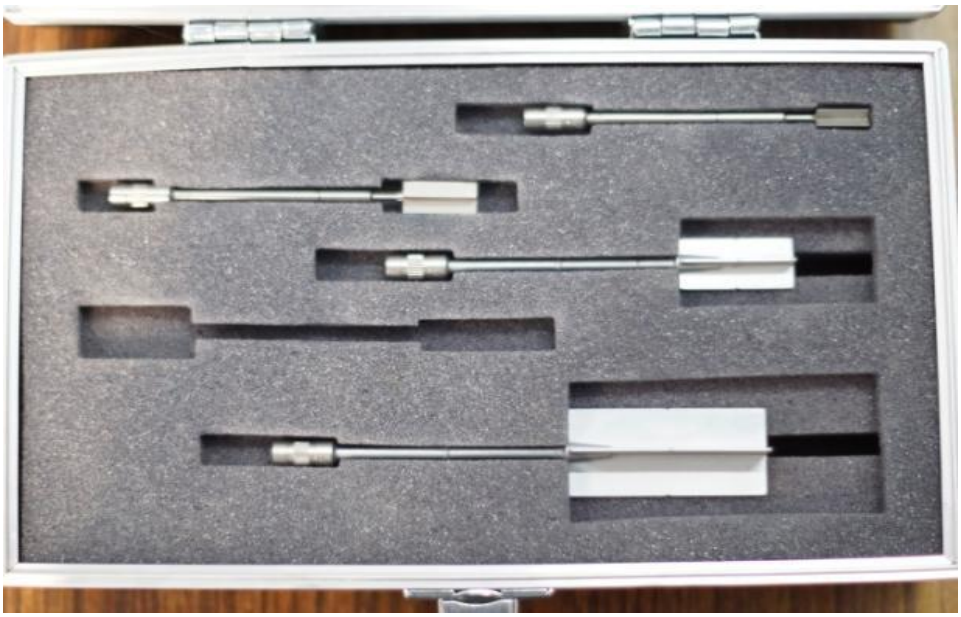

**Figure 3.5:** Brookfield vane spindles

Vane spindles available have different spindle length and diameter as shown in Fig. 3.5, all of which have their own corresponding range of stress measurement. Stress ranges of each spindle are specified in the following Table 3.1.

**Table 3.1:** Shear stress range of spindles

| Spindle | Shear stress Range (Pa) |
|---|---|
| V-72 | 2-20 |
| V-73 | 10-100 |
| V-74 | 100-1000 |
| V-75 | 40-400 |

The EZ yield software provides the graphical results between the torque versus time and stress versus apparent strain within the time of spindle rotation. The display of the results obtained from the EZ yield software is shown below in Fig. 3.6.

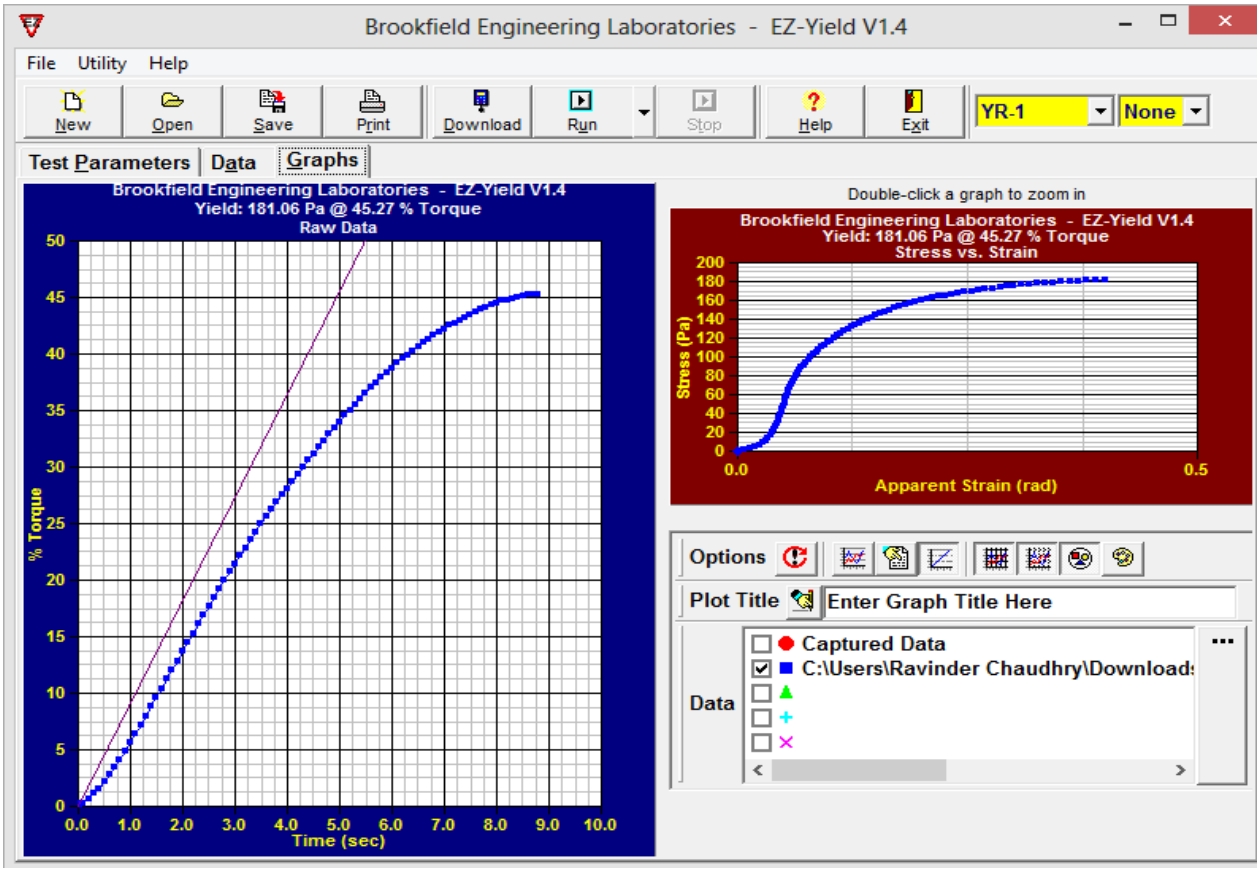


**Figure 3.6:** EZ yield software results display

The effect of aeration on yield stress is studied using the experimental setup available at the Laboratory for Particle and Bulk solids Technology in Thapar University, India. The experimental setup is able to fluidize the powder. The schematic diagram of the test setup is shown in Fig. 3.7.

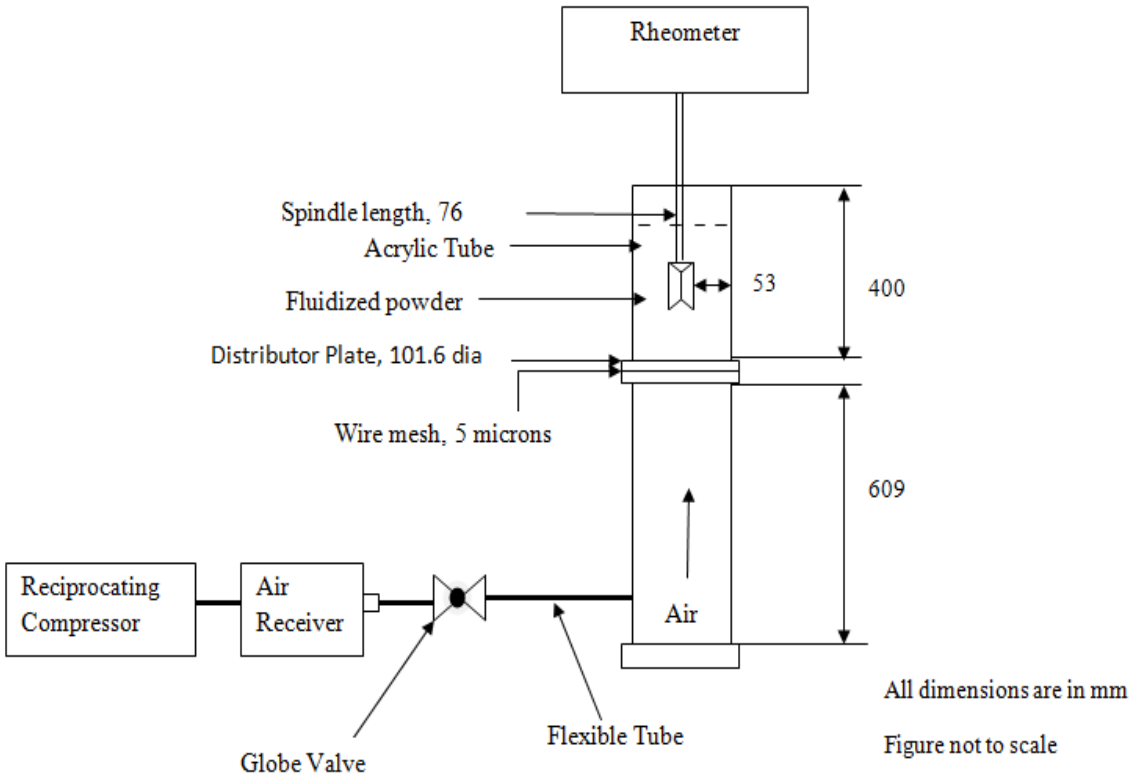


**Figure 3.7:** Schematic diagram of fluidizing rheology experimental test setup

Powders behave disparately when subjected to certain conditions. The flowability behaviour of the powder depends upon its nature and the conditions to which it has been suspended. In order to get a certain result, it was ensured that all the powder materials are conditioned. All the fly ash samples are heated at a temperature of $100^0$C for a period of two hours to remove the moisture content and then sieving test is performed to filter the agglomerates. Hence the final sample obtained was a uniformly distributed powder material with no agglomerates and moisture content in it, ensuring that the spindle is loaded uniformly throughout its circumference with no lumps of powder around it when immersed into the sample. Five repetition tests were performed on each sample and the value near to the average value was determined as the stress applied in powder to deform it at that particular spindle speed.

The background calculations that are being done in the EZ-Yield software to obtain stress and strain rate values are provided in Appendix A.

## 3.2 Bulk material data

Yield stress testing is conducted on eleven fine fly ash samples mustard powder and the mustard paste. The fly ash samples are collected from different fields of ESP hoppers from different power plants and the mustard paste is prepared from the same mustard powder by addition of water content. Fluidization and de-aeration testing is conducted on ten fine fly ash samples collected from different power plants. To validate the model predicted for the minimum fluidization velocity an additional experimental test results of yield stress, fluidization and de-aeration from the work conducted by Chaudhry [2015] and Chawla [2015] during their Masters dissertation were analyzed and are presented in this chapter.

The physical properties of the bulk materials that are tested for fluidization, de-aeration and yield stress testing are detailed in the following section. A total of seventeen fly ash samples are collected from different fields of ESP hoppers from power plants 1, 2, 3, 4 and 5. Four samples are collected from different fields of power plant 1 and seven fly ash samples are collected from all seven fields of ESP hoppers from power plant 2. All of the fly ash samples from power plant 2 are quite cohesive in nature. Remaining six fly ash samples are collected from the first two fields of ESP hoppers from power plant 3, 4 and 5. Mustard paste is prepared from the mustard powder which is considered as a standard bingham plastic fluid for testing the yield stress value.

The variation in mean particle size of all the powders was determined from the laser diffraction technique. The shape of the fly ash powders is determined from Scanning Electron Microscopy analysis.

### 3.2.1 Scanned Electron Microscopy (SEM)

The scanning electron microscopy (SEM) picture of the fly ash supports the general assumption that the fly ash samples are spherical in shape. Since all the powders are fly ash powders, fly ash samples from four different fields of ESP hoppers belonging to power plant 1 and 2 and two fields of ESP hopper from power plant 5 were analyzed for the shape of the fly ash. The SEM picture gives an idea of the shape of the bulk material and they are also capable of providing an idea of size of the particles and the change in particle size in each field of ESP hopper belonging to same power plant when viewed under same magnification. The images for all the fly ash samples of SEM analysis are shown in Fig. 3.8 to Fig 3.17.

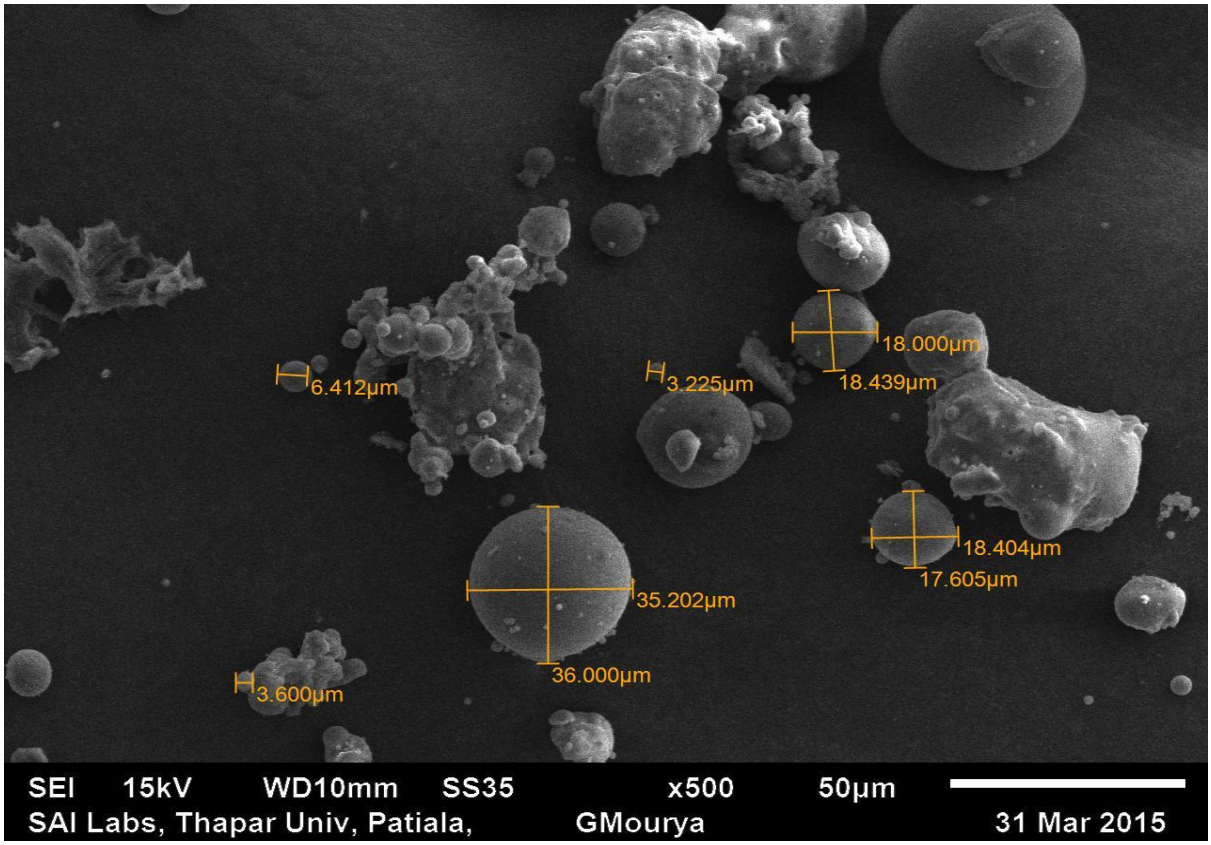


**Figure 3.8:** SEM picture of fly ash 1 from power plant 1

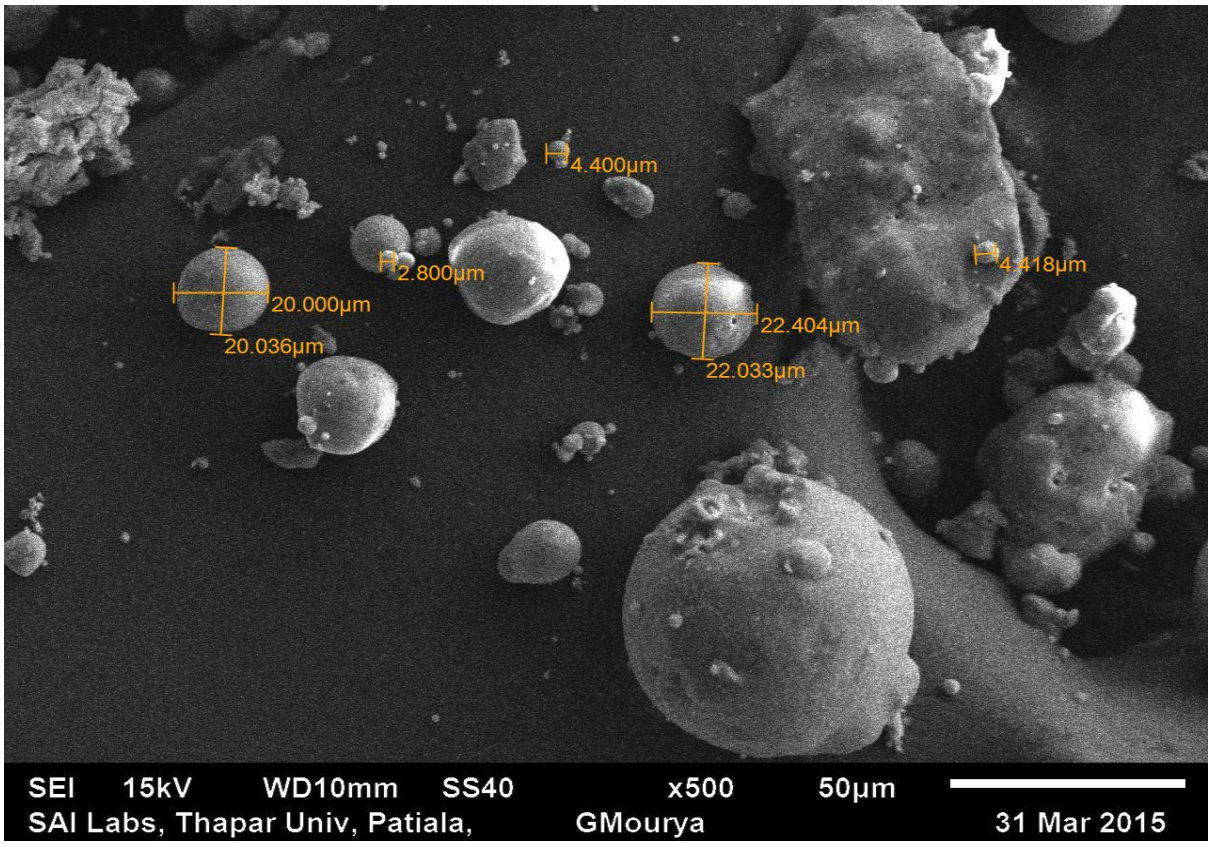


**Figure 3.9:** SEM picture of fly ash 2 from power plant 1

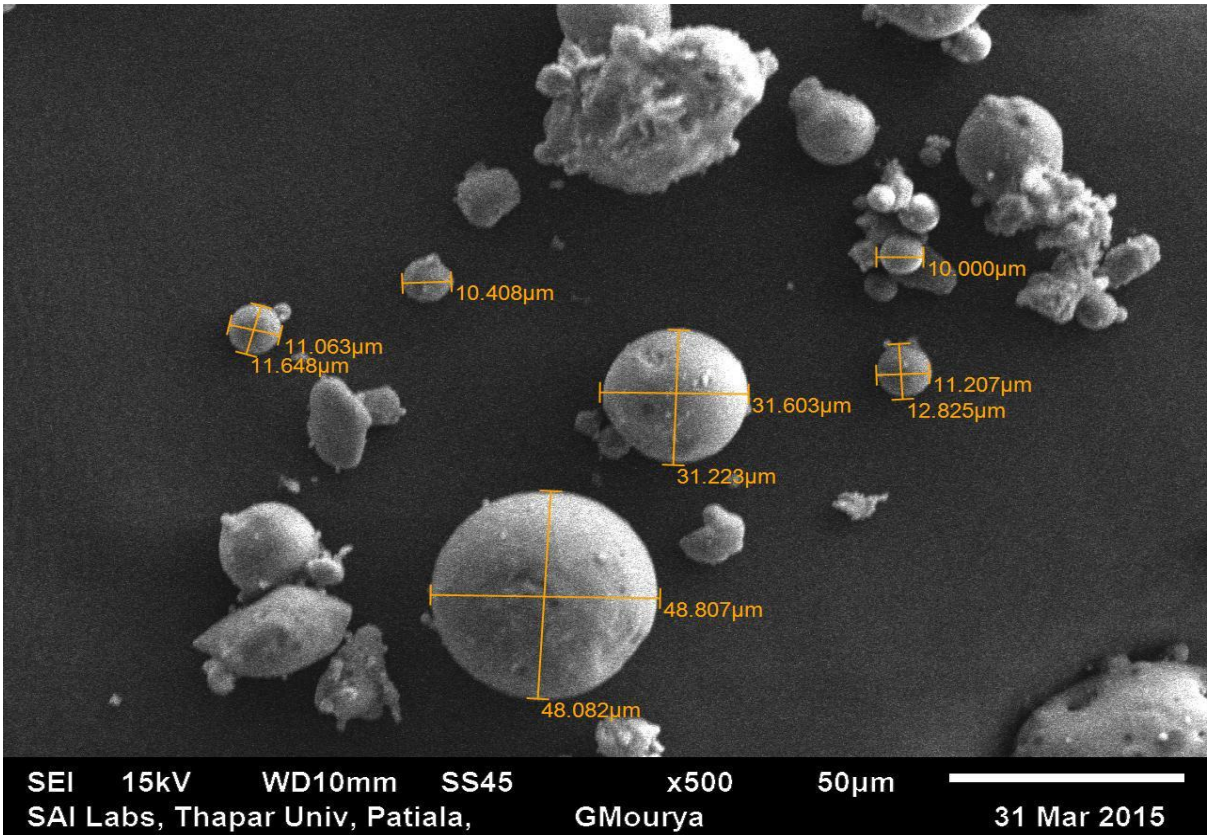


**Figure 3.10:** SEM picture of fly ash 4 from power plant 1

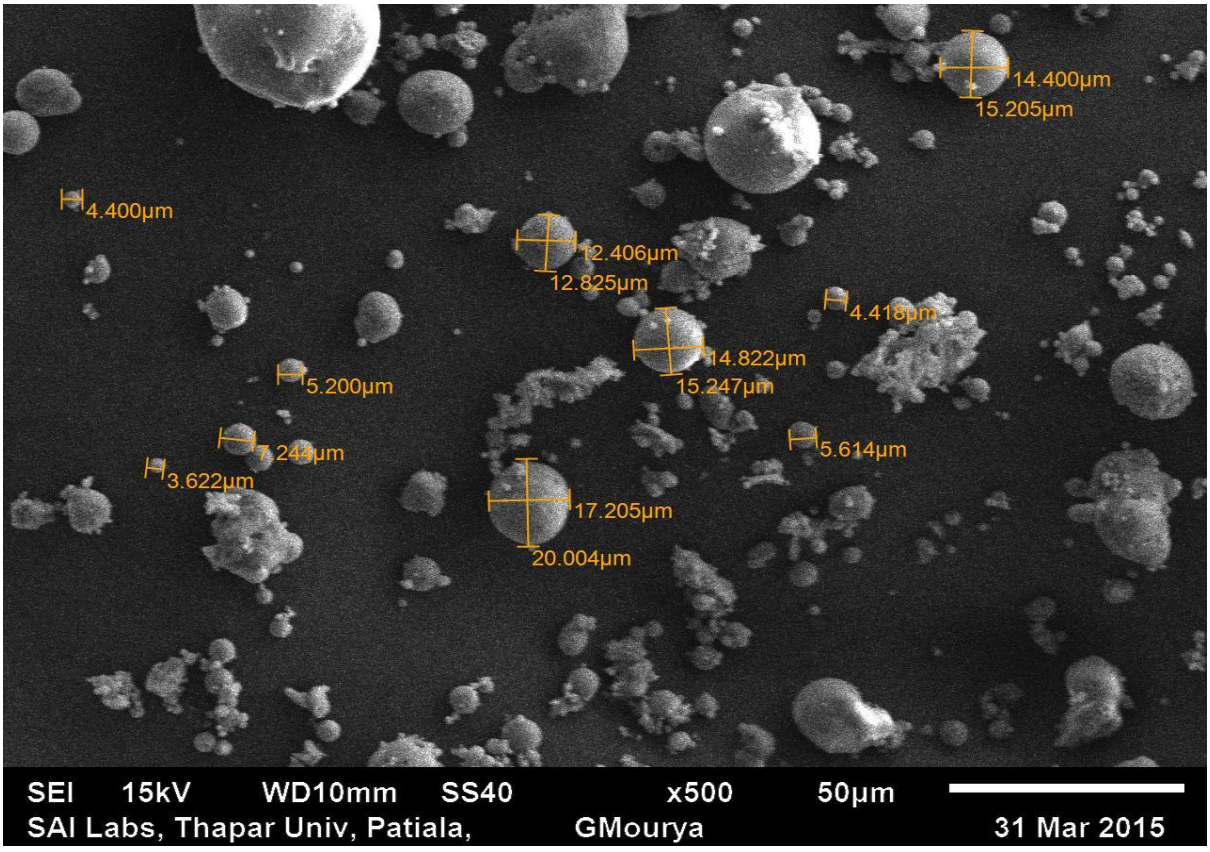


**Figure 3.11:** SEM picture of fly ash 7 from power plant 1

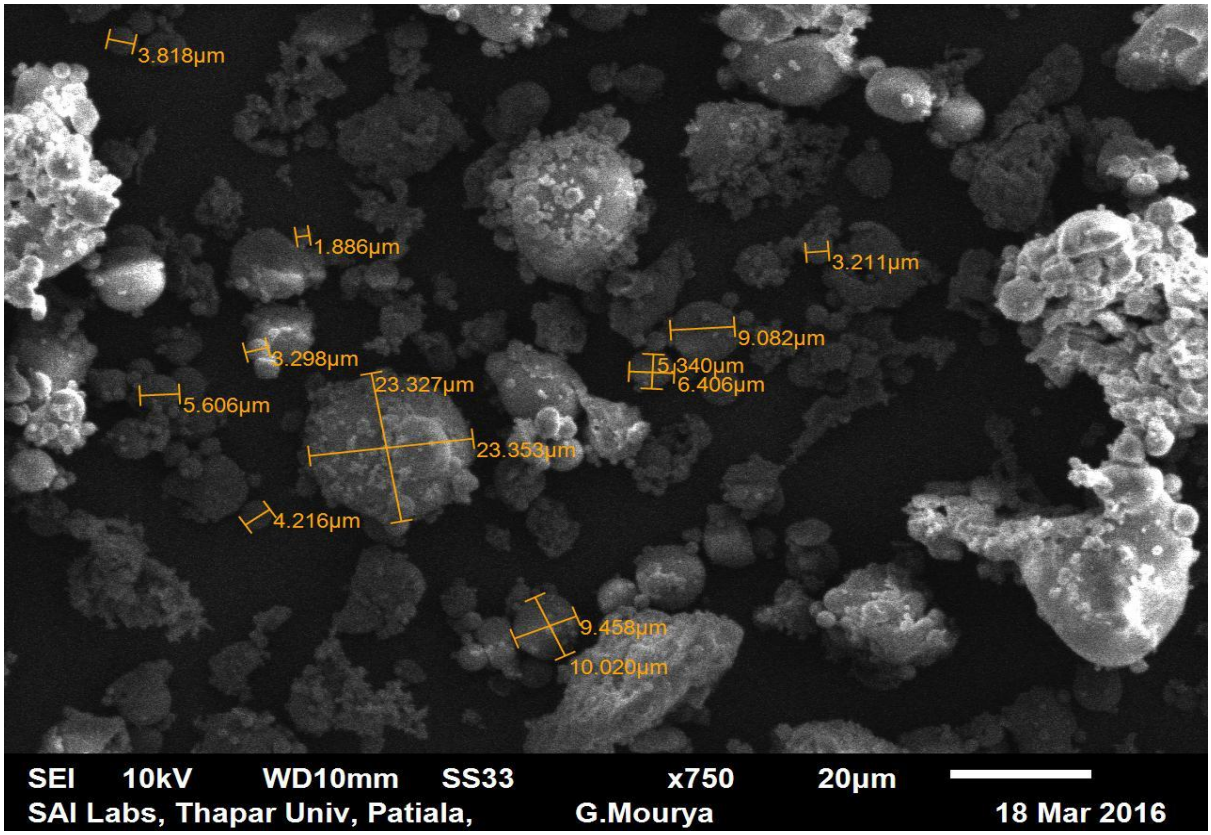


**Figure 3.12:** SEM picture of fly ash 1 from power plant 2

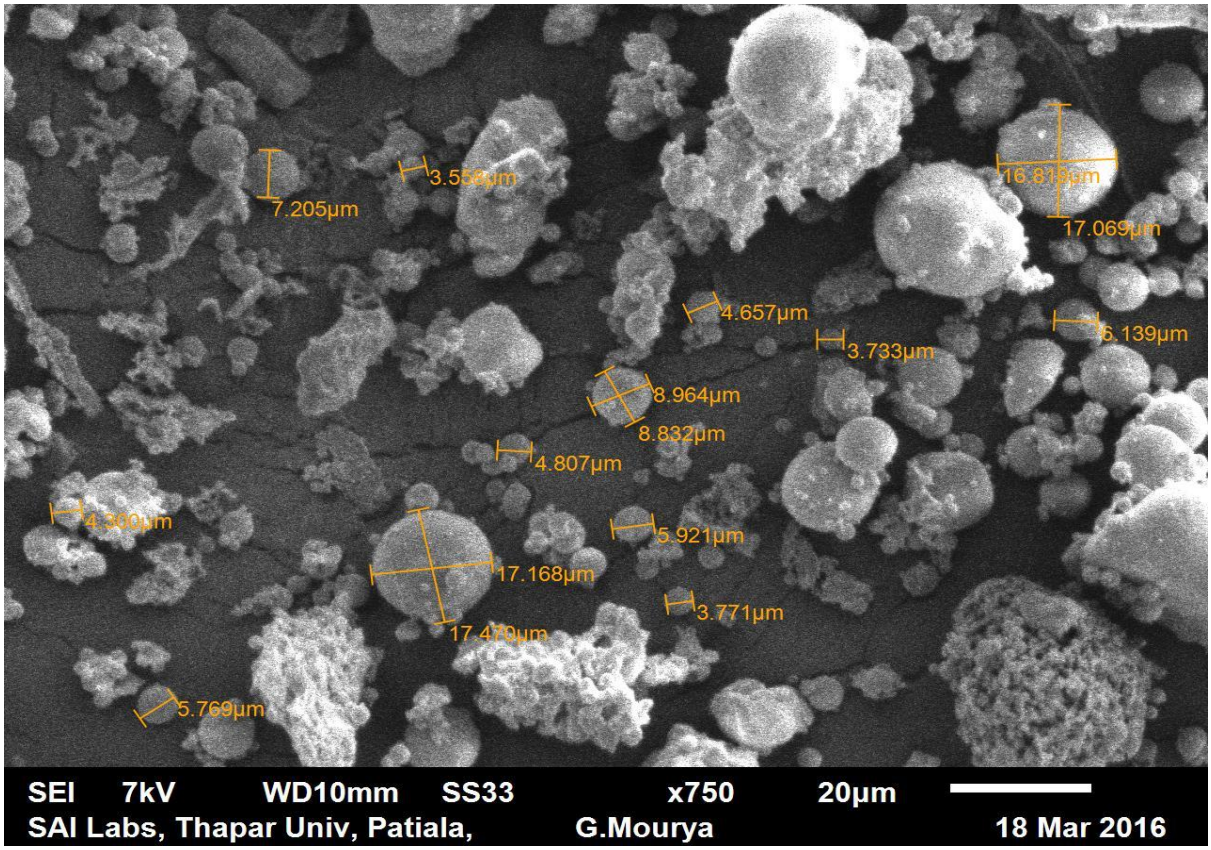


**Figure 3.13:** SEM picture of fly ash 2 from power plant 2

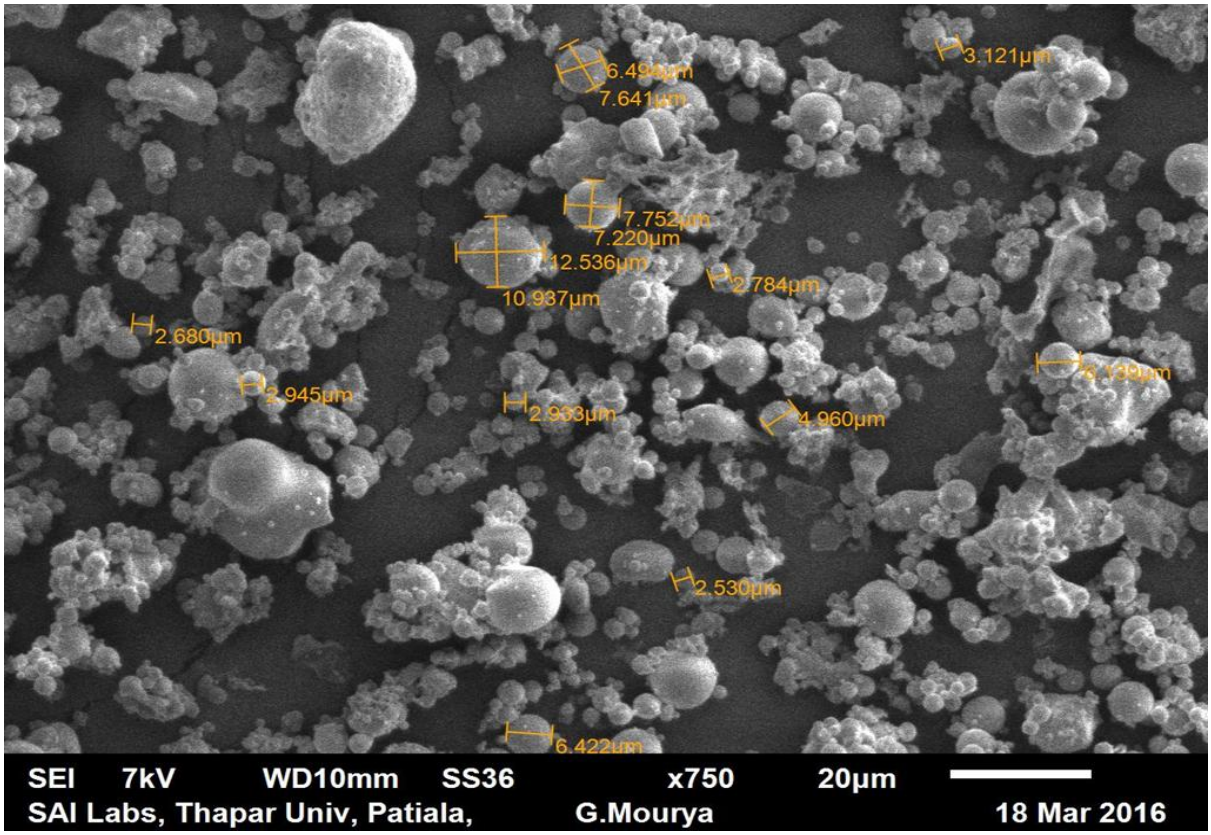


**Figure 3.14:** SEM picture of fly ash 3 from power plant 2

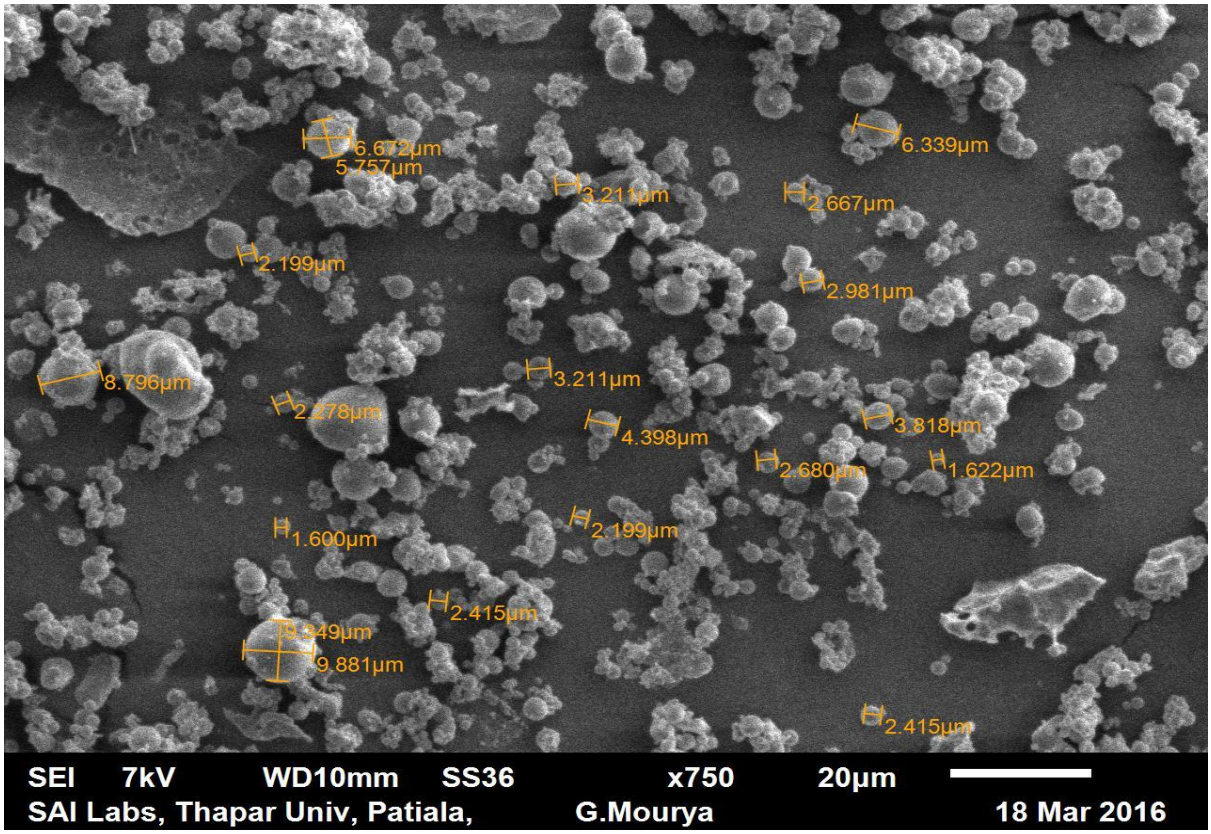


**Figure 3.15:** SEM picture of fly ash 4 from power plant 2

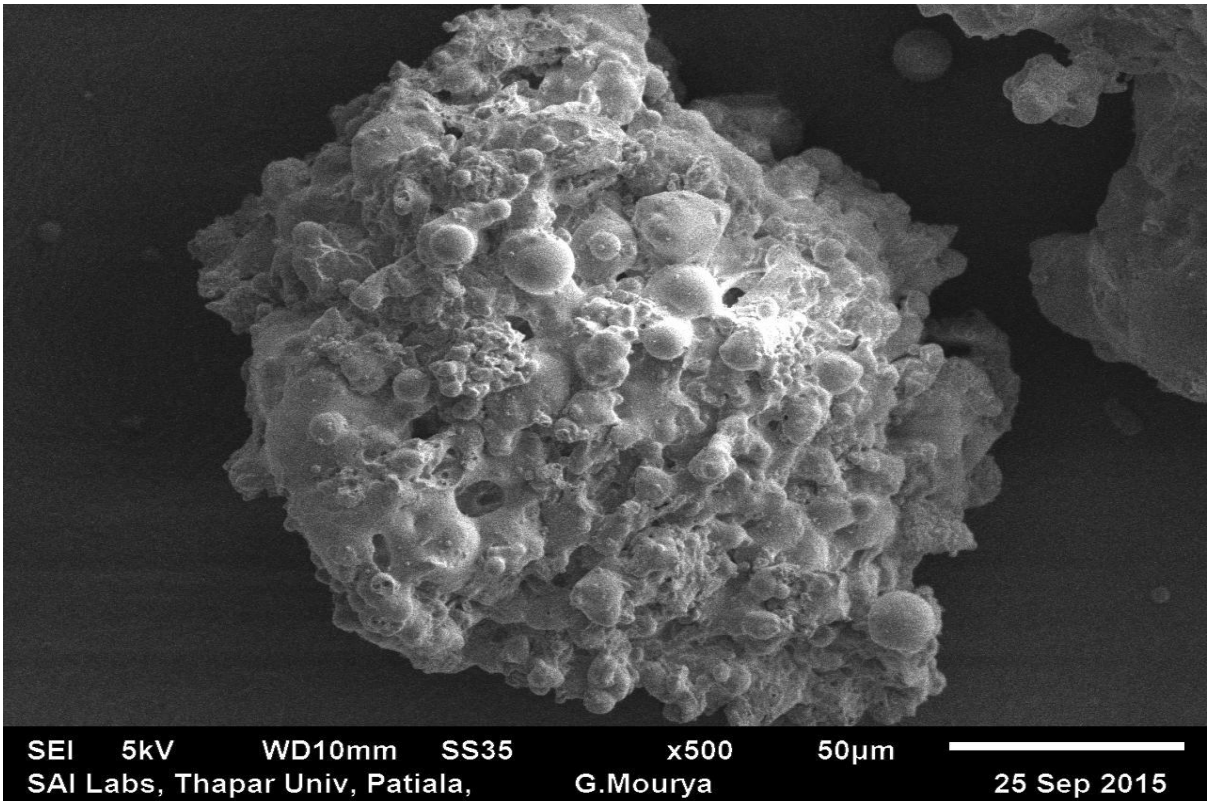


**Figure 3.16:** SEM picture of fly ash 1 from power plant 5

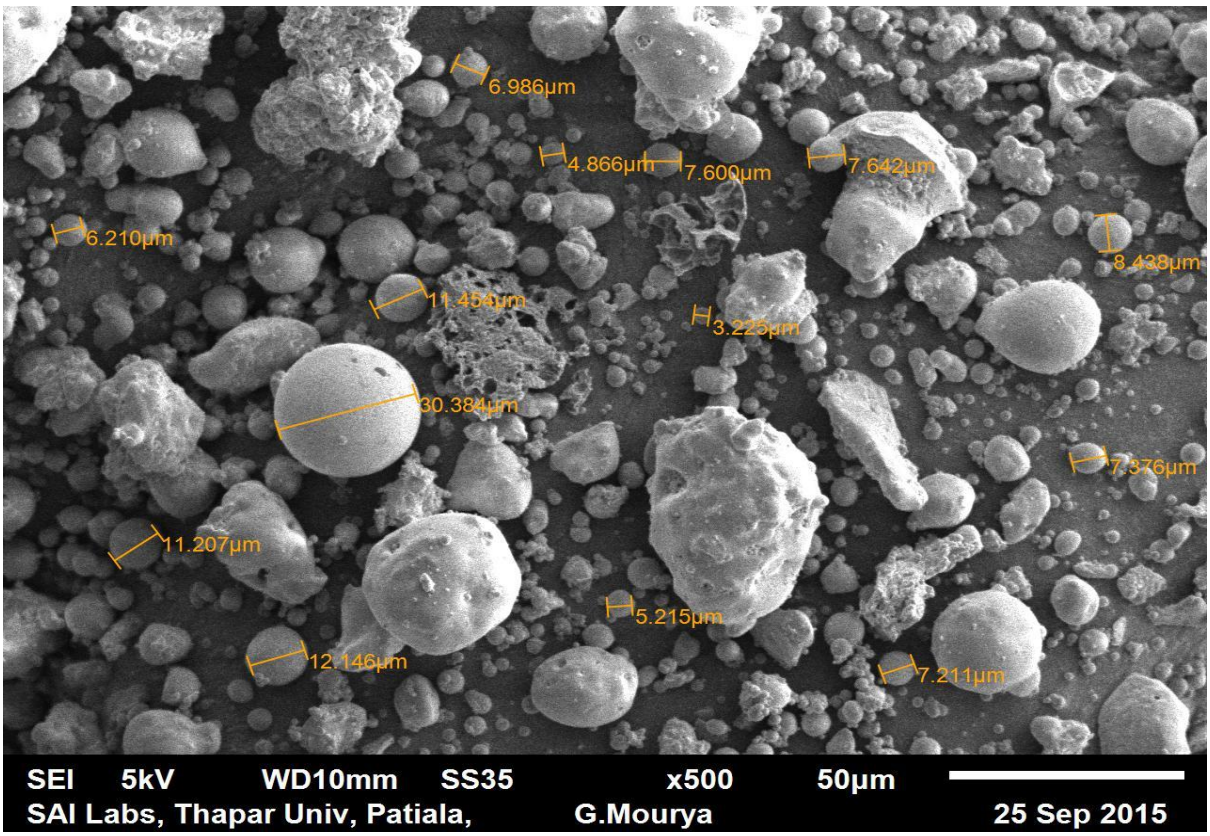


**Figure 3.17:** SEM picture of fly ash 2 from power plant 5

A figure 3.8 to 3.11 shows the SEM pictures of field 1, 2, 4 and 7 fly ash samples of power plant 1 at a magnification of $500^x$ and Fig. 3.12 to 3.15 shows that of fly ash from the first four fields of ESP hoppers belonging to power plant 2 at a magnification of $750^x$.SEM pictures of power plant 2 presents that the size of the particles reduces from the field-1 fly ash to field-4, comparing this four samples which are magnified at the same level, it can be stated that the fly ash 4 has a larger number of particles with very small particle size than others. Figure 3.16 shows the magnified picture of an agglomerate.

### 3.2.2 Particle size distribution

Mean particle size and the particle size distribution of the materials were determined by using laser diffraction method in the laboratory in Delhi, India. The Fig. 3.18 to 3.21 shows the distribution curve of volume density and cumulative volume with variation in particle size for first four fields of fly ash belonging to power plant 2.

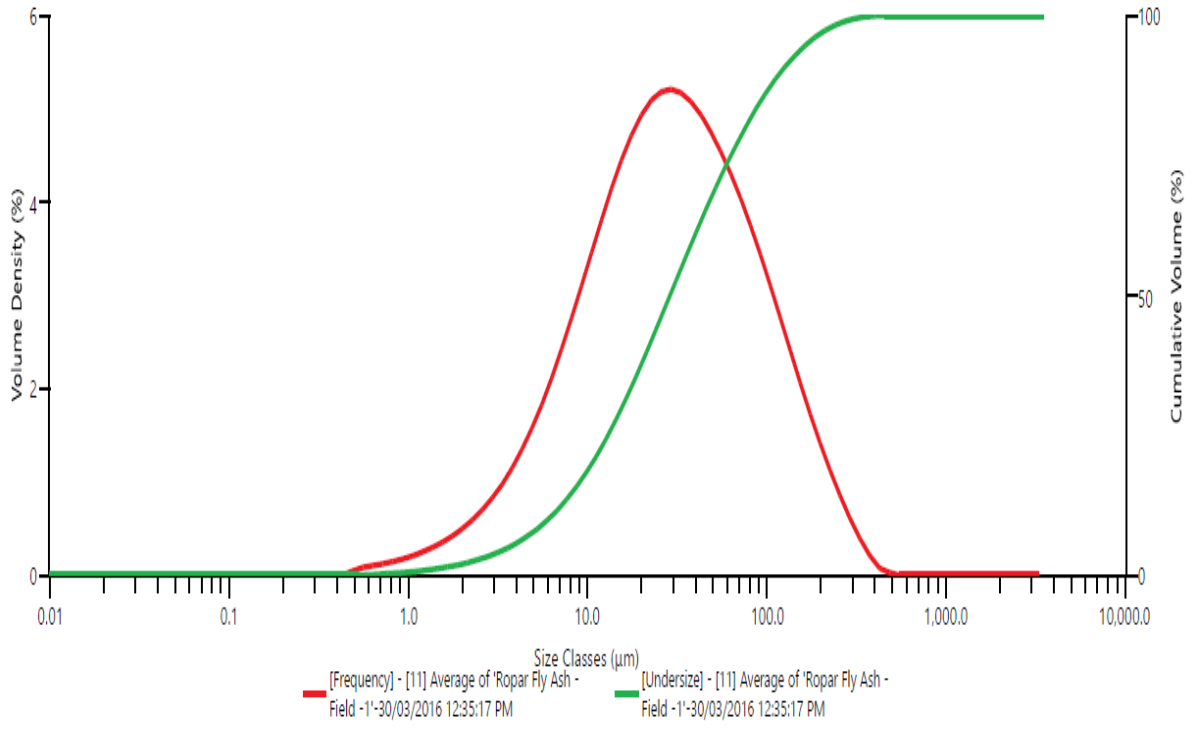


**Figure 3.18:** Size distribution analysis of fly ash 1

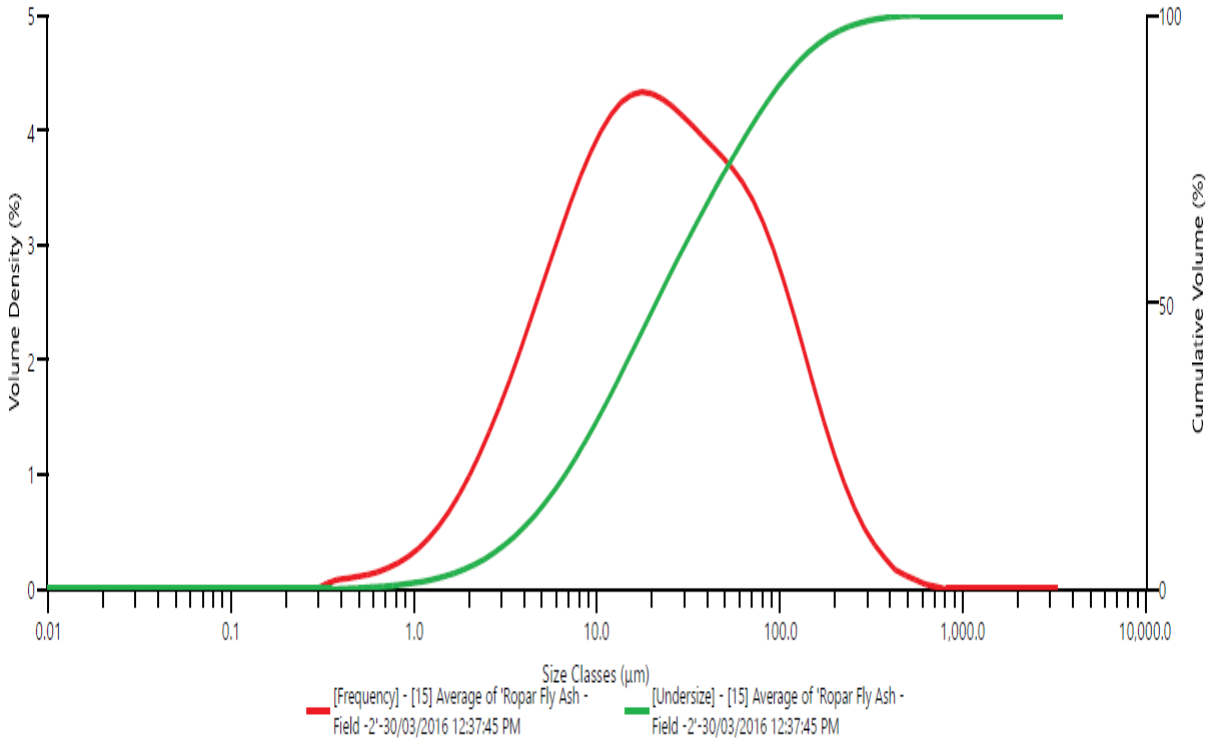


**Figure 3.19:** Size distribution analysis of fly ash 2

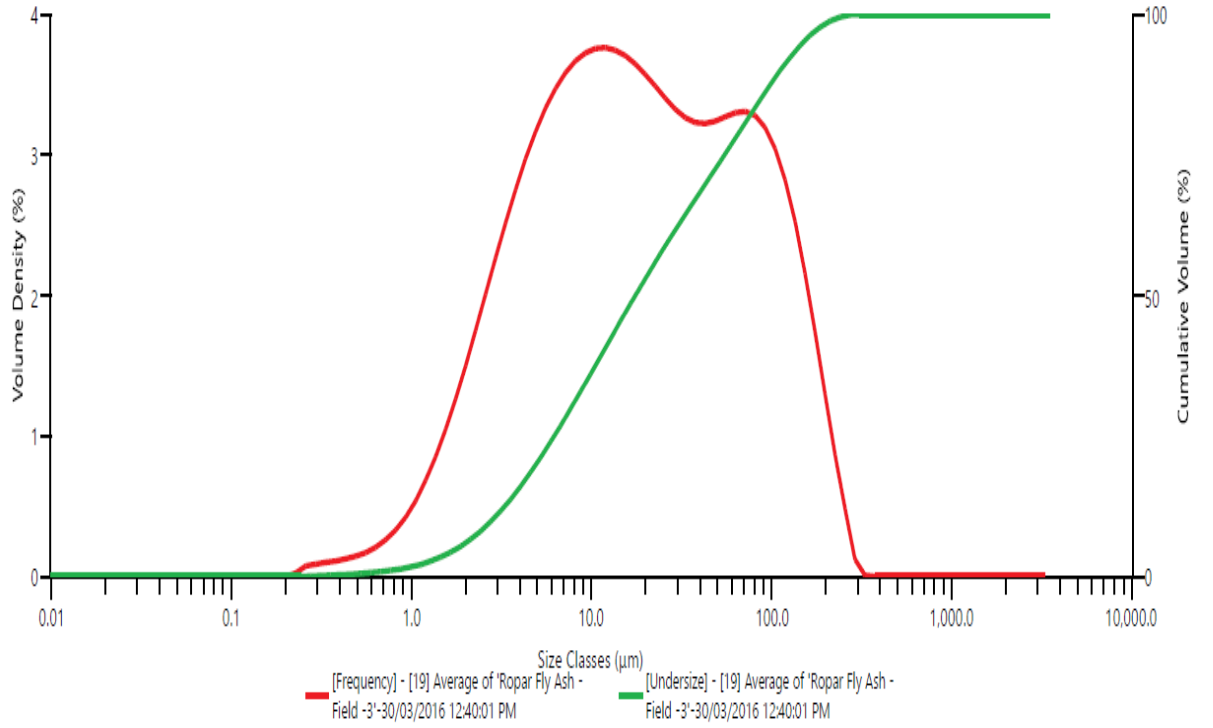


**Figure 3.20:** Size distribution analysis of fly ash 3

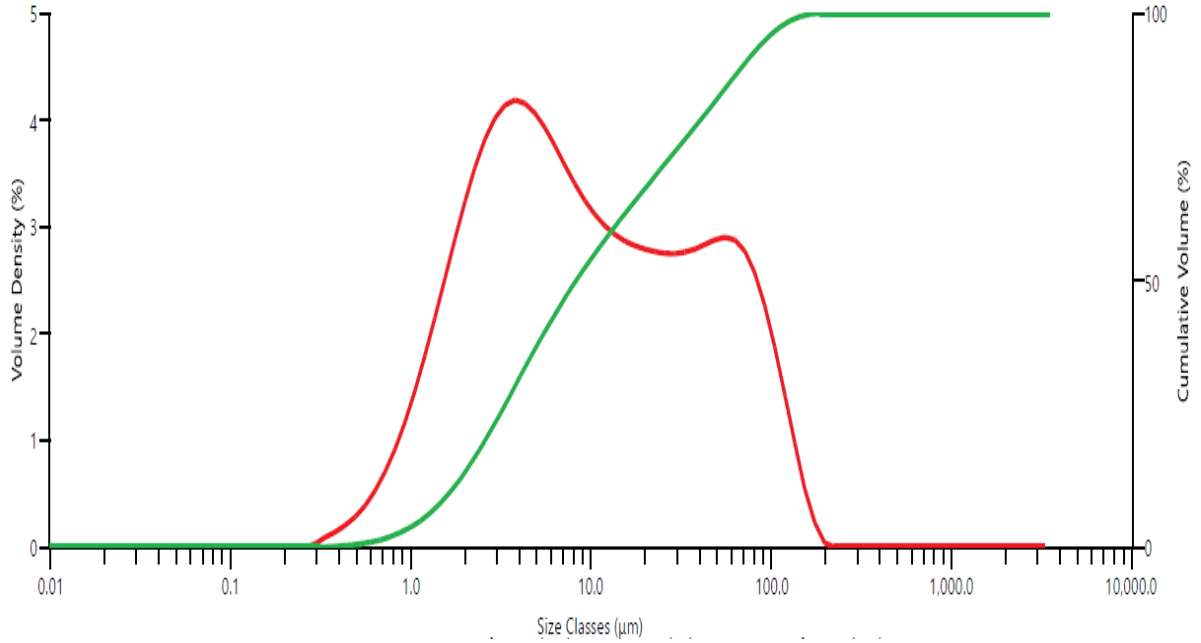


**Figure 3.21:** Size distribution analysis of fly ash 4

The fly ash collected from the power plant 2 is found to be highly cohesive and estimated to have high tendency for compactness. Hence to prove the same the fly ash (as received from the power plant) of known mass was rammed in sand rammer until a further reduction in the volume was not observed. A cylindrical specimen is formed (shown in figure 3.22) which indicates the high bonding strength of the particles. The bonding strength of the fly ash from the field-7 is observed to be very high comparatively from the other field fly ash because of very small particle size and high cohesiveness. The cylindrical specimen of field-1 couldn't be shaped because of its less compactness.

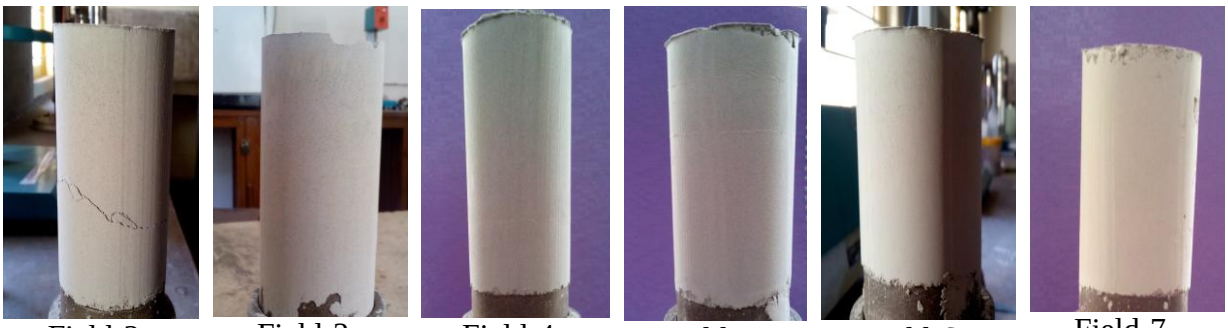


**Figure: 3.22:** Cylindrical specimen of fly ash from power plant 2

**Table 3.2:** Physical properties of powders

| Powder No | Material | $d_{10}$ (µm) | $d_{50}$ (µm) | $d_{90}$ (µm) | $\rho_p$ (kg/m$^3$) | $\rho_{tb}$ (kg/m$^3$) | $\rho_{lb}$ (kg/m$^3$) |
|---|---|---|---|---|---|---|---|
| 1 | Fly ash 1 from P1 | 42 | 139 | 316 | 2015 | _ | 848 |
| 2 | Fly ash 2 from P1 | 23 | 102 | 235 | 2014 | _ | 839 |
| 3 | Fly ash 3 from P1 | 18 | 69 | 170 | 2025 | _ | 818 |
| 4 | Fly ash 4 from P1 | 6 | 21 | 63 | 2025 | _ | 759 |
| 5 | Fly ash 1 from P2 | 6 | 28 | 120 | 2140 | | 686.8 |
| 6 | Fly ash 2 from P2 | 3 | 21 | 63 | 2120 | 1019 | 677.4 |
| 7 | Fly ash 3 from P2 | 2 | 17 | 111 | 2290 | 977 | 674.0 |
| 8 | Fly ash 4 from P2 | 1 | 8 | 69 | 2101 | 983 | 596.3 |
| 9 | Fly ash 5 from P2 | 1 | 4 | 29 | 2500 | 723 | 590.2 |
| 10 | Fly ash 6 from P2 | 1 | 4 | 25 | 2430 | 909 | 611.2 |
| 11 | Fly ash 7 from P2 | 1 | 4 | 33 | 2560 | 1102 | 494.3 |
| 12 | Fly ash 1 from P3 | 20 | 103 | 235 | 2030 | _ | 794.4 |
| 13 | Fly ash 2 from P3 | 4 | 25 | 235 | 2299 | _ | 769.5 |
| 14 | Fly ash 1 from P4 | 16 | 87 | 238 | 2080 | _ | 798.7 |
| 15 | Fly ash 2 from P4 | 7 | 35 | 105 | 2078 | _ | 777.1 |
| 16 | Fly ash 1 from P5 | 38 | 126 | 202 | 2060 | _ | 677 |
| 17 | Fly ash 2 from P5 | 5 | 48 | 170 | 2200 | _ | 857.8 |
| 18 | Mustard powder | 56 | 266 | 656 | _ | _ | _ |

### 3.2.3: Mode of flow

Researchers developed diagrams for predicting mode of flow by determining the relationship between different particle and bulk parameters. Geldart [1973] classified bulk material into four groups, A, B, C and D by utilizing basic bulk material parameters of the average particle diameter and particle density.

If the material falls within the A or C groups, it is highly likely to be conveyed in fluidized dense phase. If the material appears in B category it is more likely to be in dilute phase flow. In case of D type material whose density is relatively low has the ability to be conveyed in plug flow. The comparison of Geldart chart with the mode of flow data is shown in Fig. 3.17. From this diagram it is indicative that the materials undergoing tests fall under A/C boundary and are capable to easily fluidized and conveyed in fluidized dense phase.

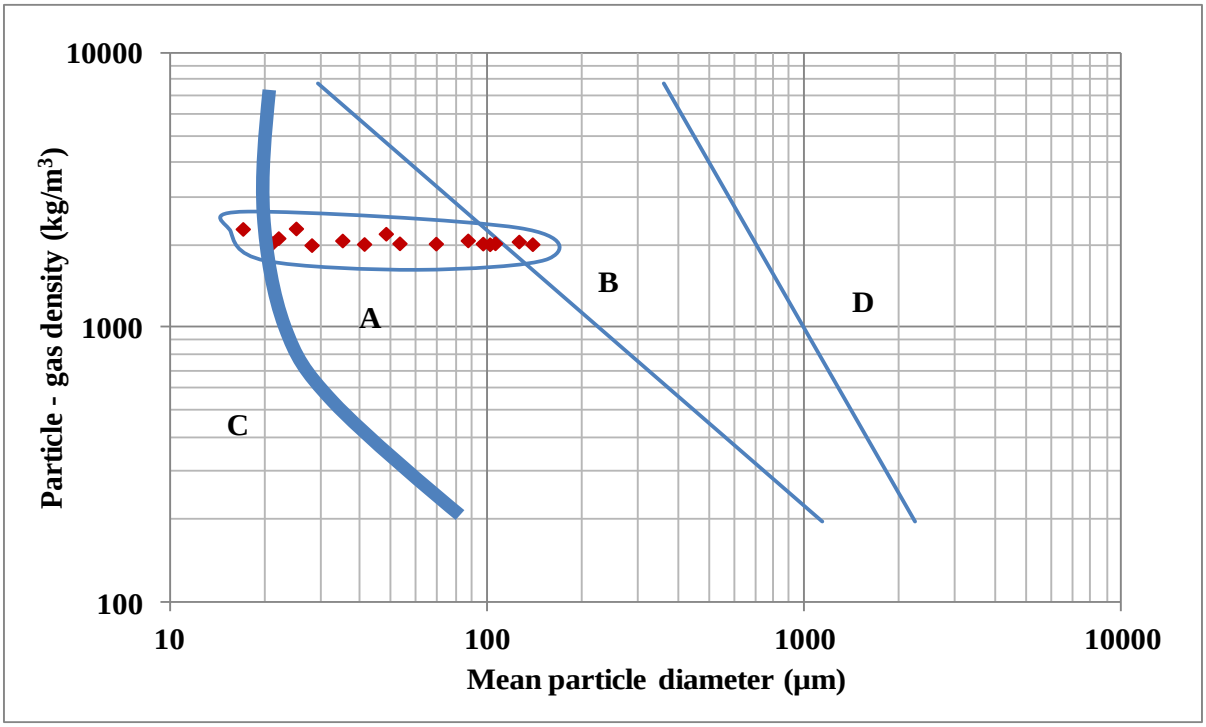


**Figure 3.23:** Geldart classification diagram with mode of flow data

Pan [1999] developed a bulk material classification diagram with three modes of pneumatic flow PC1, PC2 and PC3 by considering the particle diameter and loose poured bulk density. PC1 is for fluidized dense phase, PC2 for plug flow and PC3 for dilute phase. Fig. 3.18 clearly shows that the materials fall into the category of fluidized dense phase flow.

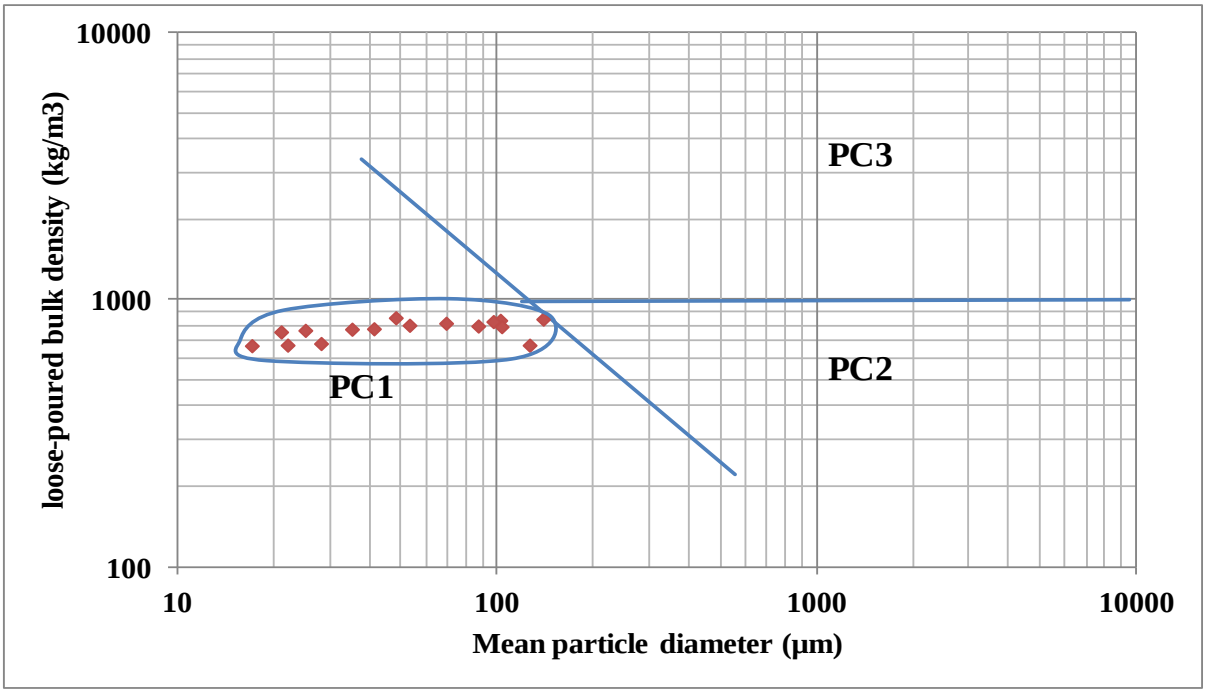


**Figure 3.24:** Pan pneumatic conveying prediction diagram with mode of flow data

# Chapter 4

# Yield stress measurement

## 4.1 Results and Discussion of yield stress

Experiments were conducted on fly ash samples from two different power plants, mustard powder and the mustard paste prepared from it. Tests carried out under fluidized and un-fluidized condition of materials belonging to power plant 1 to discover the effect of aeration on the yield stress values whereas only under un-fluidized condition of materials belonging to power plant 2 and mustard. Shear stress values are observed at varying strain rates corresponding to spindle speeds varying from 0.1 to 3.0 RPM. The extreme left value of shear stress is considered as the yield stress of the respective powders.

### 4.1.1 Yield stress test on mustard

The initial experimental procedure is processed on mustard powder by choosing vane spindle V-75 at two different spindle immersion depths of 1.6 cm and 3.4 cm. The mean particle size of mustard powder is 266 µm with the particle size distribution of 56 µm – 656 µm.

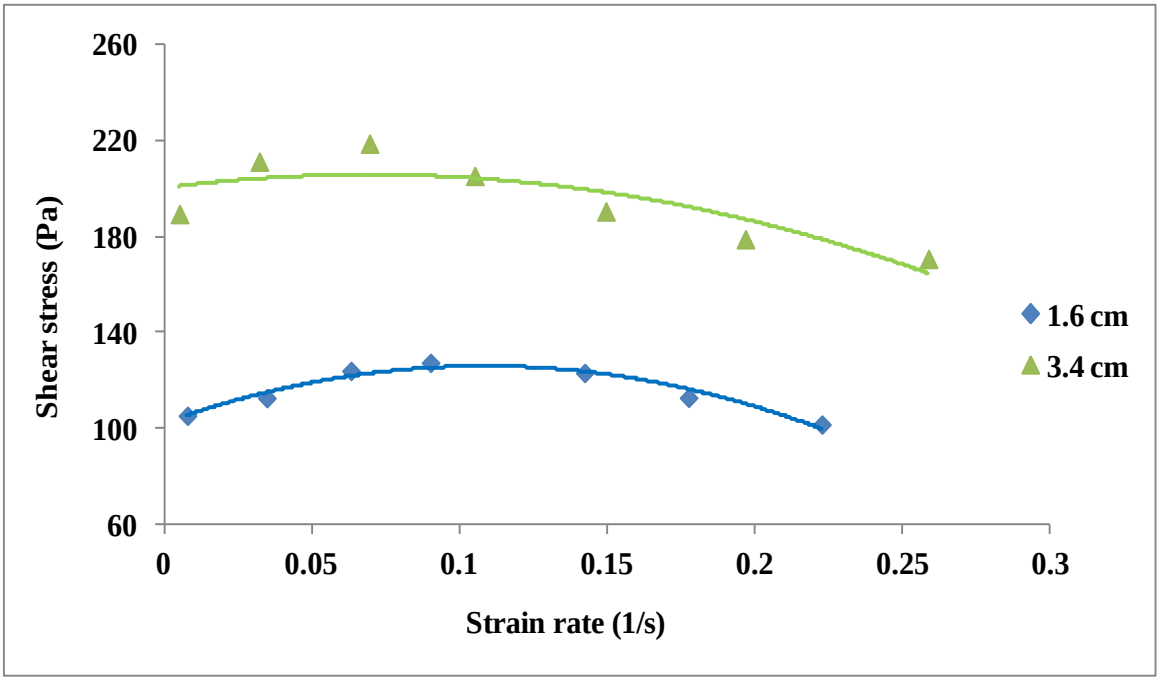


**Figure 4.1:** Shear stress versus rate of strain for mustard powder under un-fluidized condition

From the Fig. 4.1 it can be elucidated that the shear stress value initially increases with increase in strain rate at lower strain rates, then continues to drop down with increasing strain rate. The reason predicted for this behaviour from practical observations is that as the spindle starts rotating, the spindle vanes impel the material to rotate along with them, simultaneously the material endeavour to move away from the spindle vanes and creating air pockets between the vanes. At lower speeds the non cohesive powders easily move into to the air pockets and hence almost same amount of material stays in contact with the spindle vanes throughout the period of spindle rotation, so it requires larger force to rotate inside the material. At higher spindle speeds the material between the spindle vanes is thrown away from the spindle vanes due to centrifugal forces and cannot get back into their original position. Hence the material content in contact with the spindle vanes is reducing continuously in the time of spindle rotation resulting in lesser yield stress values. From the figure an other information that could be extracted is that with an increase in the depth of spindle immersion the stress of the material increases. This is for the reason that as the depth of immersion increases loaded material onto the spindle vane increases and hence requires larger force to rotate. From Fig. 4.1 it was found that the yield stress value at 1.6 cm of spindle depth is 100 Pa and at 3.4 cm is 200 Pa.

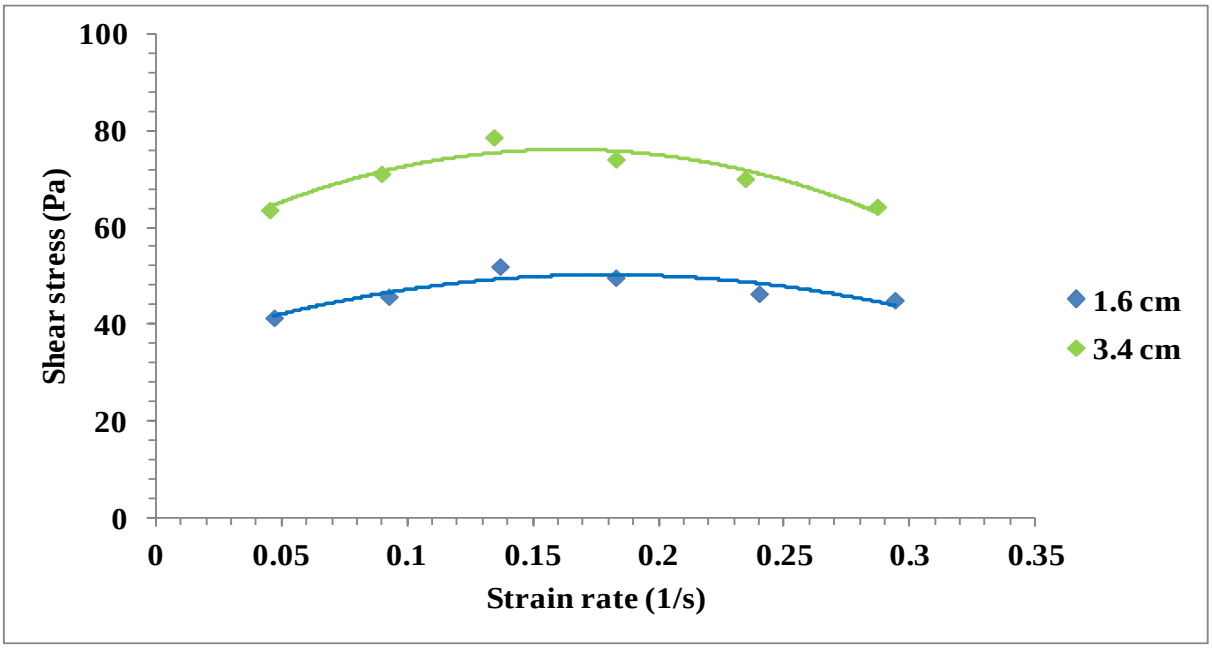


**Figure 4.2:** Shear stress versus rate of strain for mustard paste

By micro-analysis, it can be stated that the difficulty of powder flow over the fluids is due to the molecular shape and the molecular surface texture. Liquids have the smoother

surfaces, hence the stress required to move or slide over the layers is very less. Where in case of powders, the irregular shapes of the molecules cause interlocking of molecules; therefore the spindle undergoes more amount of stress to slide one layer of powder over another. In order to reduce the interlocking of the particles mustard paste is prepared from the mustard powder by adding some amount of water content into it. Mustard paste is considered as bingham plastic fluid. This test is conducted to compare the behaviour of powder materials with bingham plastic fluids. Yield stress test is conducted on this paste at two depths of 1.6 cm and 3.4 cm. The shear stress versus strain rate diagram for mustard paste is shown in Fig. 4.2. It has been observed that the yield stress value is reduced considerably (36 Pa at 1.6 cm and 52 pa at 3.4 cm of spindle depth) with the addition of water into the mustard powder. It can be anticipated that the particle-particle bondage is broken by the added water content and therefore smoothens the surface. Hence there is a reduction in inter-particle forces acting between the particles and the spindle vanes rotate smoothly inside the paste resulting in lesser value of the yield stress.

### 4.1.2 Yield stress tests on fly ash from power plant 1

The three fly ash samples powder 1, 2 and 3 are collected from the field 1, 4 and 7 of ESP hopper and are having a particle size of 132, 69 and 21 μm respectively. Due to larger mean particle size, powder 1 has shown bubbling nature when tests are performed under aerated condition (shown in Fig. 4.3).

**Figure 4.3:** Bubbling of powder 1 at fluidized condition

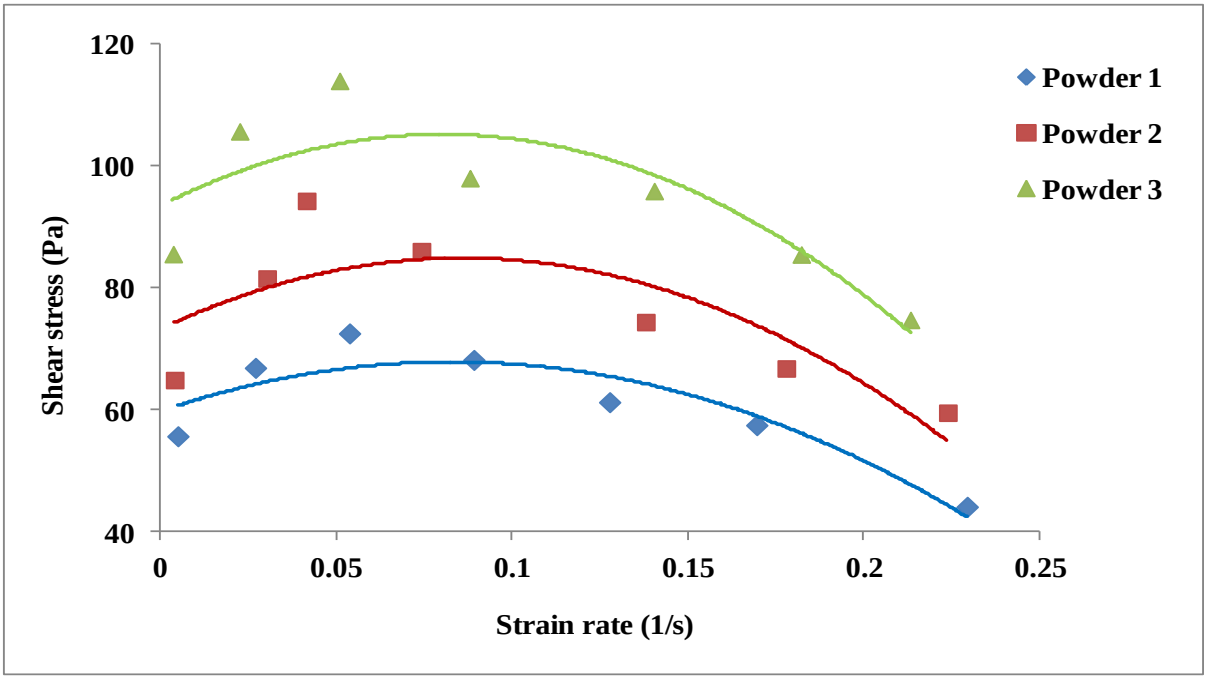


**Figure 4.4:** Shear stress versus rate of strain for different particle sizes (powder no.1, 2 and 3) under fluidized condition

Figure 4.4 shows the comparative diagram of shear stress versus strain rate for powder 1, 2 and 3 at a spindle depth of 1.6 cm under fluidized condition. It can be observed from the figure that as particle size decreases the shear stress values increases with strain rate. Powder 3 being more cohesive compared to powder 1 and 2, shows higher stress value under fluidized condition.

**Figure 4.5:** Channelling in powder 3

Powder 3 has a mean particle size of 21 μm which is cohesive in nature. It was observed during experiments that the channelling occurs as shown in Fig.4.5 during fluidization of fine and cohesive powders. The air escapes through the passages formed and uniform fluidization has not occurred, which created uncertainty in recording the values of yield stress, especially at high depths.

Figure 4.6 to 4.8 shows comparison of stress values at three different depths for powder 1, 2 and 3 under un-fluidized condition. The stress values increases with increasing spindle depth of immersion. The more the depth of immersion, more the amount of powder acts on the spindle, hence force required by the spindle to rotate is high. Comparing powder 1 from Fig. 4.4 (fluidized condition) and depth 1 of powder 1 from Fig. 4.6 for un-fluidized powders, it can be observed that when the powder is aerated (fluidized) stress required by the spindle is reduced from 115 Pa to 60 Pa. Similarly for powder 2 and 3 at depth 1 the stress value recorded at aerated condition is less when compared to the un-fluidized condition. Strain rate decreases with increasing depth of immersion, which represents a higher time requirement for spindle rotation.

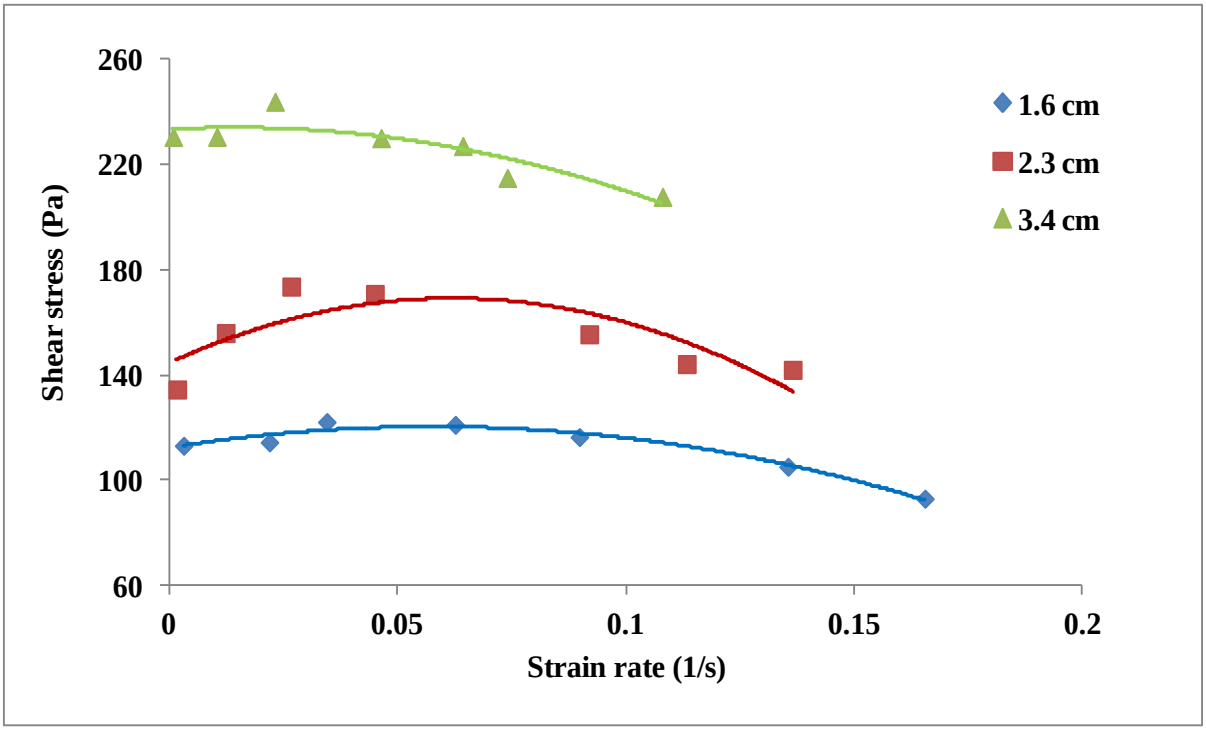


**Figure 4.6:** Shear stress versus rate of strain for powder 1 under un-fluidized condition

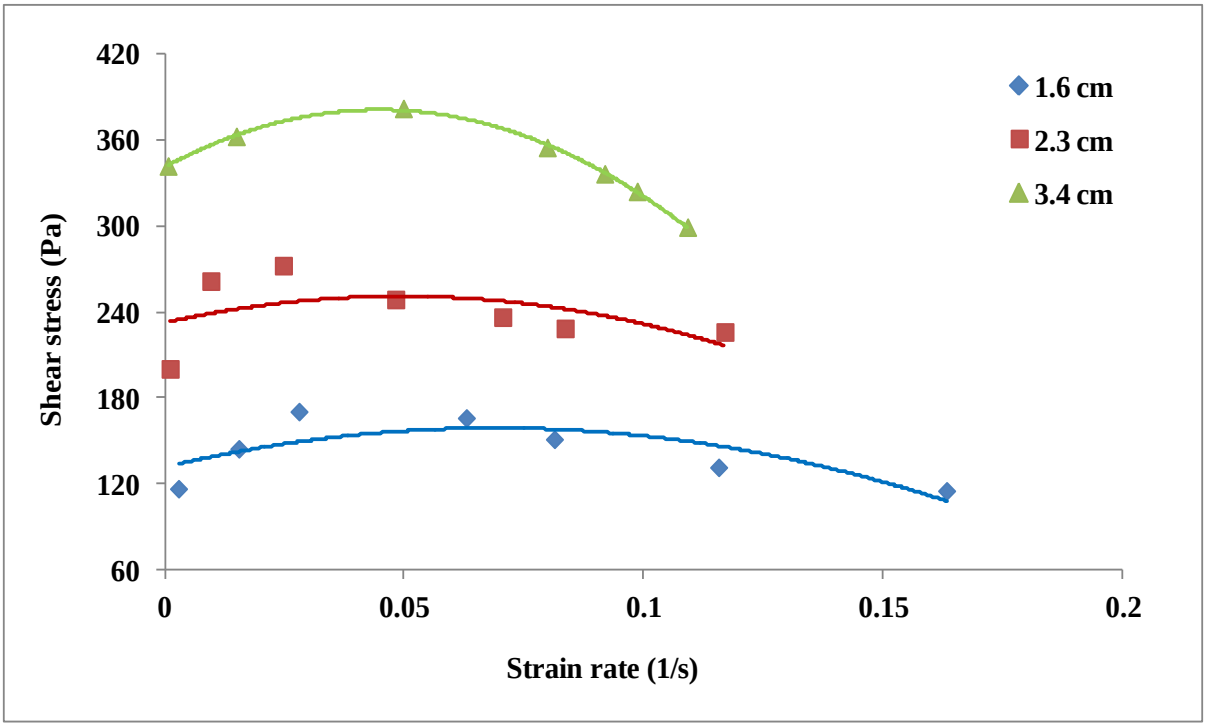


**Figure 4.7:** Shear stress versus rate of strain for powder 2 under un-fluidized condition

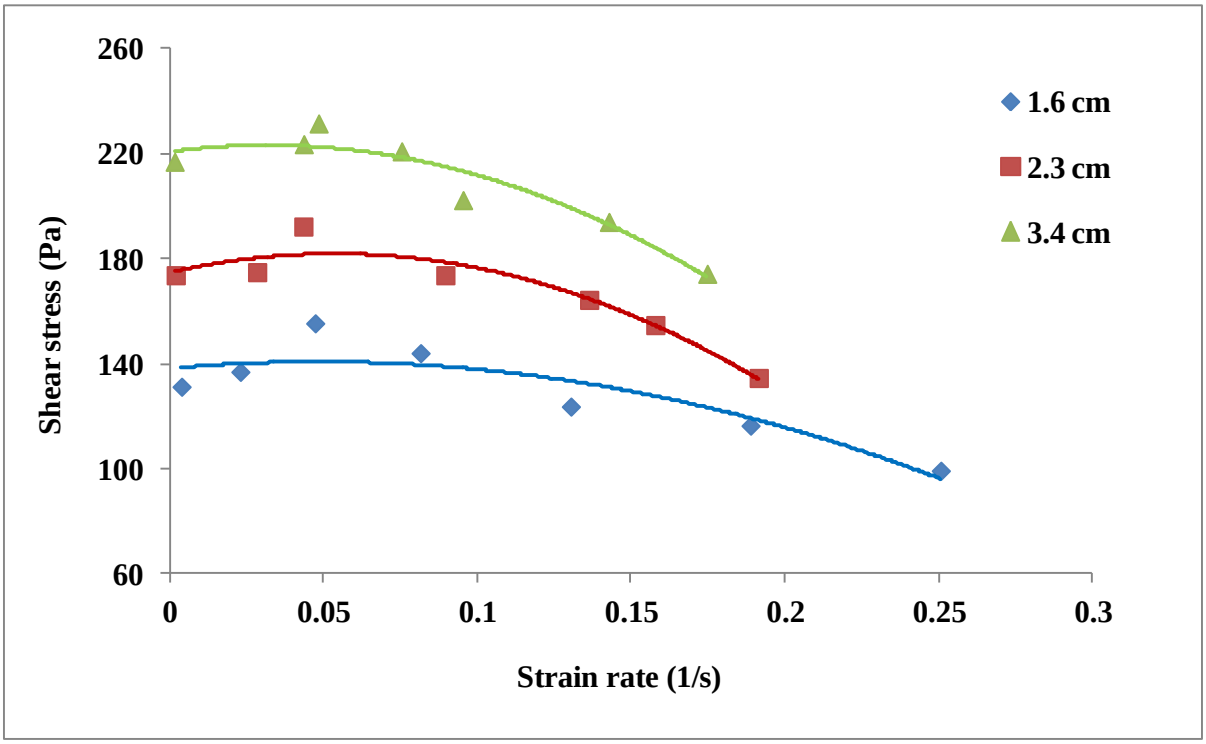


**Figure 4.8:** Shear stress versus rate of strain for powder 3 under un-fluidized condition

### 4.1.3 Yield stress tests on fly ash from power plant 2

In this section the shear stress variation with strain rate at two different depths for all seven fields of ESP hoppers from power plant 2 have been discussed. The average particle size range of this fly ash is 4μm to 28μm which comes under the Geldart group C materials well known for their cohesiveness.

It has been observed practically that higher the cohesiveness the particles have higher intensity to form agglomerates due to increased inter-particle forces (Vander waal's forces), hence on applying little external force they tend to compact and behave as a solid. Tests conducted on such materials on the state of as received from the power plant (un-conditioned) may result in an uncertain value of stress, due to its non-uniform nature throughout the container. Unlike free flowing materials the cohesive materials once deformed cannot be able to flow back to its original position, the impression of spindle immersion remains on the material. The test performed on cohesive material (on a un-conditioned state) that which shows its non flowability nature is shown in Fig. 4.9.

**Figure 4.9:** Immersion of spindle left over after test on cohesive powders

To get rid of the agglomerates and to ensure the uniform distribution of powders in the container, sieving is performed. Due to the high bonding nature of the cohesive powders the particles blocked the fine holes of the sieve (which stands as a proof of the sticky nature of the cohesive powders) and the same is shown in the Fig. 4.9

**Figure 4.10:** Powder blocking the fine holes of sieve mesh

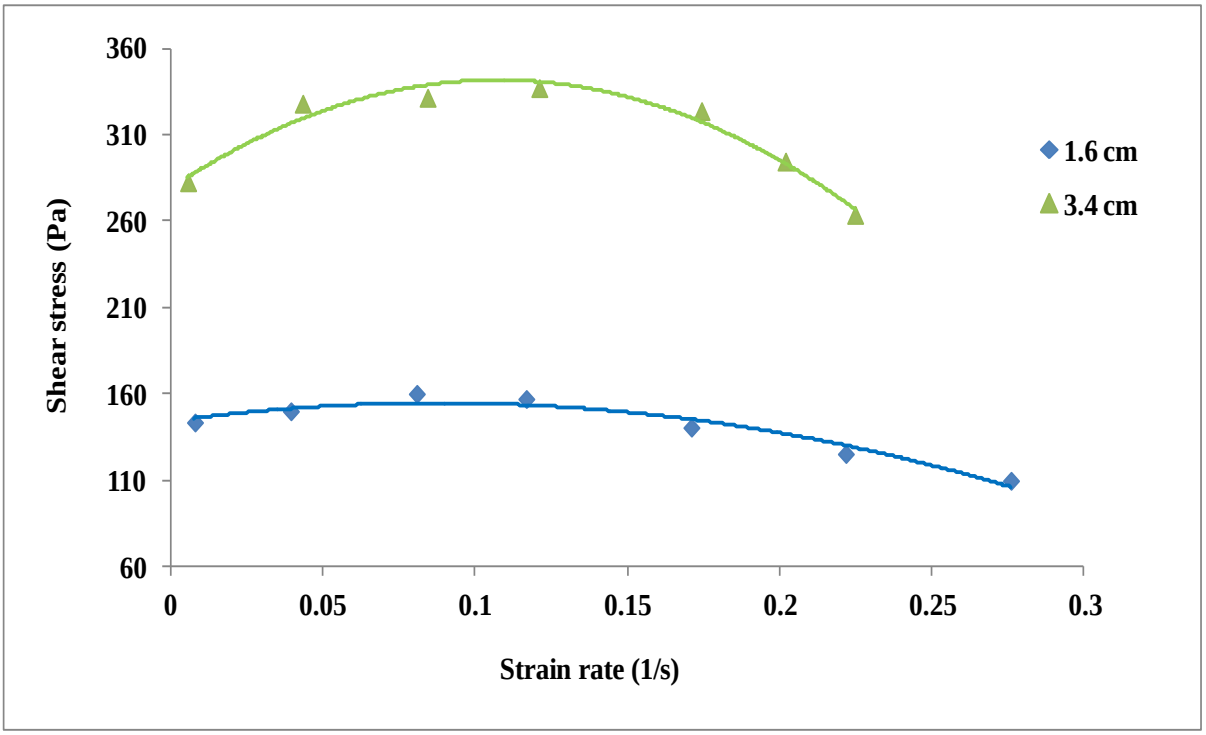


**Figure 4.11:** Shear stress versus rate of strain for field-1 powder under un-fluidized condition

Field 1 of power plant 2 has smaller particle size compared to field 1 of power plant 1 exhibiting larger yield stress value because of its cohesive nature. Figure 4.11 shows the variation of stress with strain rate of fly ash 1 of power plant 2 whose mean particle size is 28µm. The particle size distribution is of range 13µm to 279µm. The extreme left value of stress at the Y-coordinate is considered as the yield stress value. For fly ash 1 the yield stress value determined at a depth of 1.6 cm is 140Pa and at a depth of 3.4 cm is 280Pa which represents an increase in stress required to enhance the powder to flow with increasing the depth of spindle immersion.

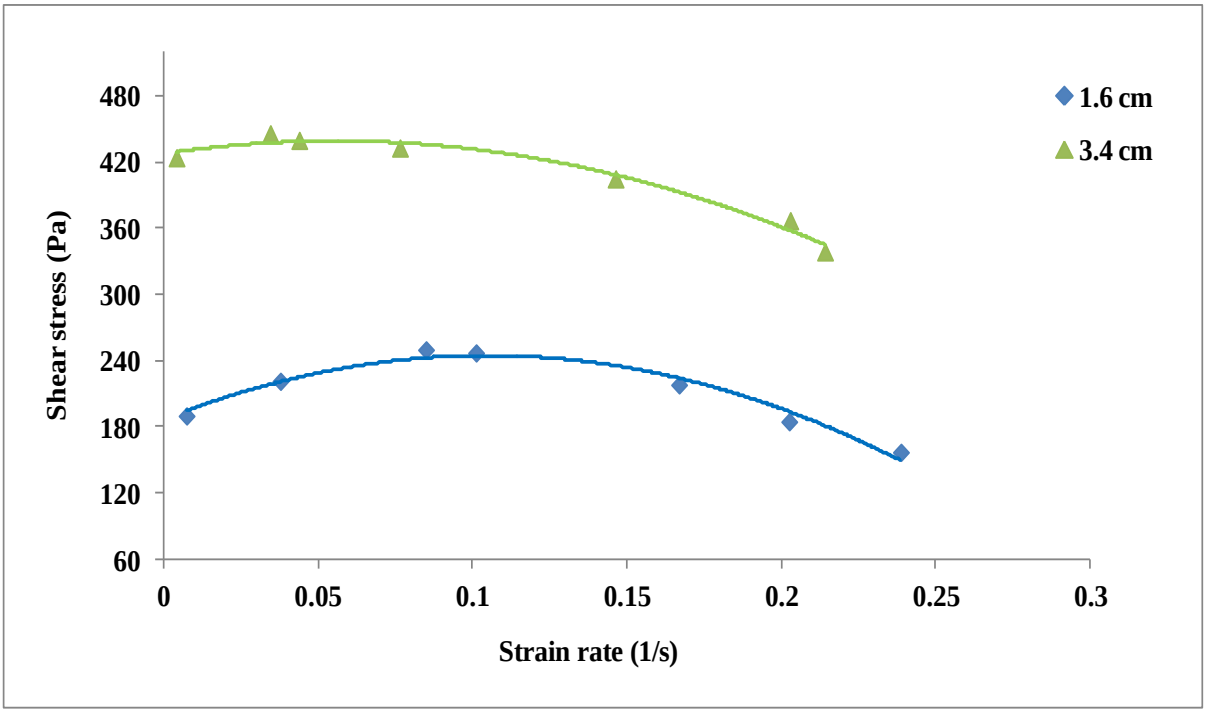


**Figure 4.12:** Shear stress versus rate of strain for field-2 powder under un-fluidized condition

The corresponding yield stress values determined for fly ash 2 of power plant 2 at depths 1.6cm and 3.4 cm are 180 Pa and 425 Pa respectively are shown in Fig. 4.12. The mean particle size of fly ash is 21µm. Comparatively the yield stress values determined for fly ash 2 are higher than that for fly ash 1. The reason for the increase in yield stress can be predicted as the smaller mean particle size and the wide particle size distribution of 9µm to 302µm. Powders with wide particle size distribution have a higher tendency of packing, hence spindle requires more force to deform the powder.

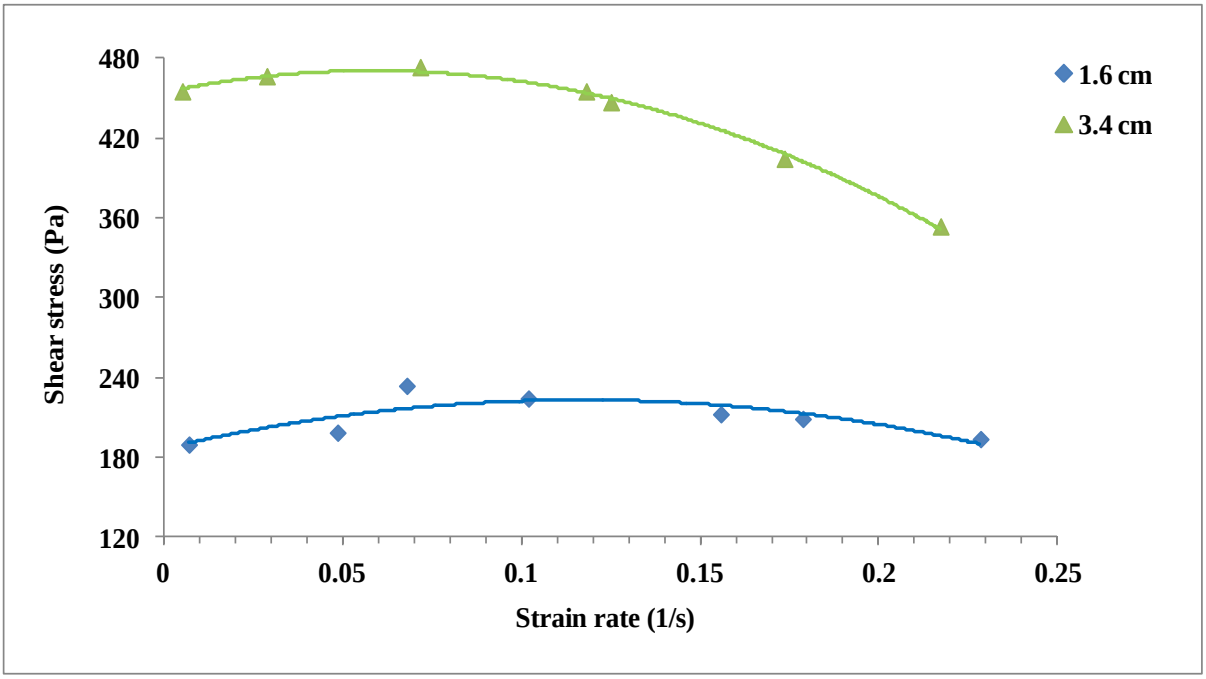


**Figure 4.13:** Shear stress versus rate of strain for field-3 powder under un-fluidized condition

Figure 4.13 shows the variation of stress with strain rate for fly ash 3 which has a mean particle size of 18μm. The yield stress values determined at depths 1.6 cm and 3.4 cm are 180 Pa and 455 Pa respectively. Noticeable increase in stress value is obtained at a larger depth of spindle immersion.

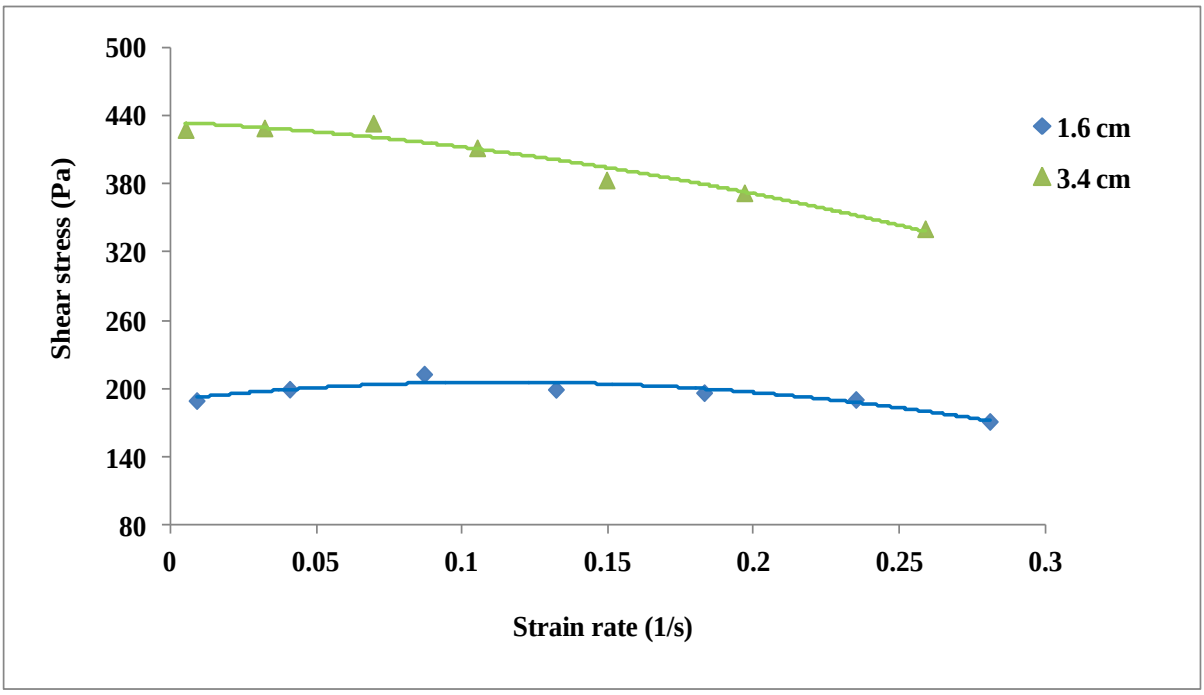


**Figure 4.14:** Shear stress versus rate of strain for field-4 powder under un-fluidized condition

Figure 4.14 shows the results of the fly ash 4 having a mean particle size of 8 µm. The yield stress values are 190 Pa and 440 Pa at depths 1.6 cm and 3.4 cm respectively. It was noticed that the decrease in particle size increased the yield stress value. This is due to the increase in inter-particle/electrostatic forces between the particles.

Figures 4.15 to 4.17 present the yield stress values of fly ash 5, 6 and 7. All the three powders have a mean particle size of 4 µm and particle size distribution of 3 µm to 105 µm, 3 µm to 100 µm and 3 µm to 98 µm respectively. Since there is not much variation in the particle size or particle size distribution, all the three fields show almost the same yield stress value at larger spindle depth.

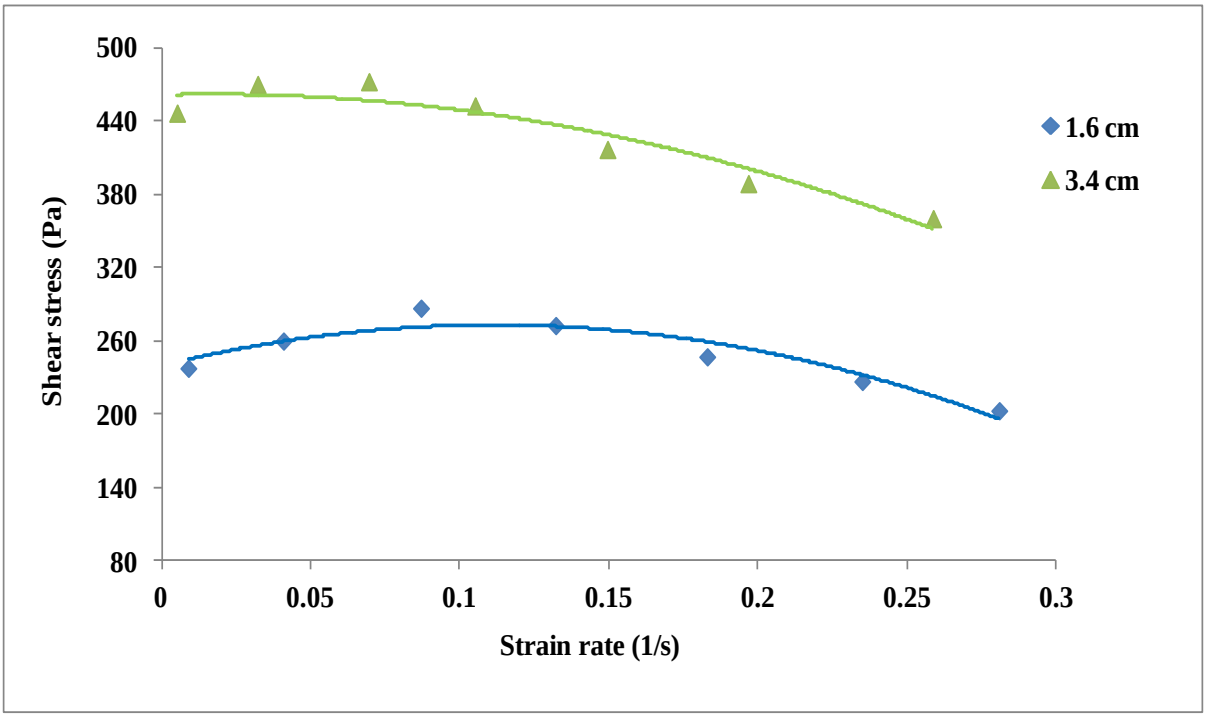


**Figure 4.15:** Shear stress versus rate of strain for field-5 powder under un-fluidized condition

The shear stress versus strain rate graph of fly ash from the field-5 is shown in Fig. 4.15. From the figure the determined yield stress value of fly ash 5 at depth 1.6 cm and 3.4 cm are 230 Pa and 460 Pa respectively.

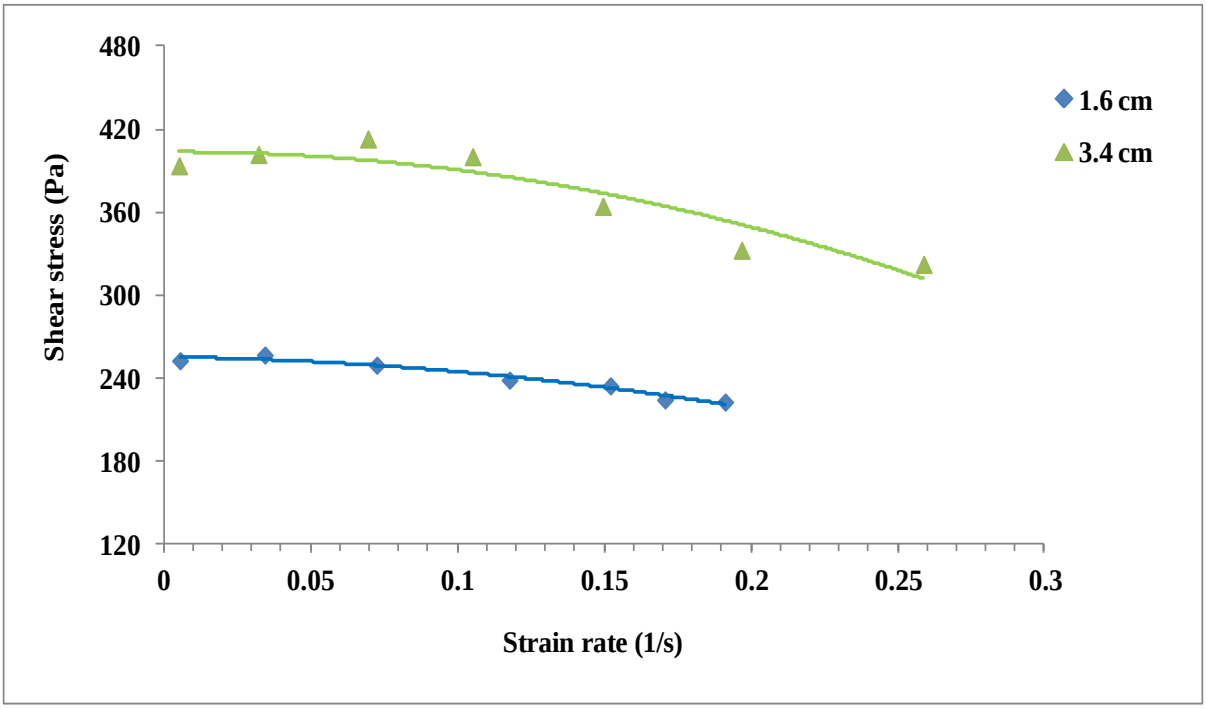


**Figure 4.16:** Shear stress versus rate of strain for field-6 powder under un-fluidized condition

The yield stress value of fly ash 6 at 1.6 cm depth is 260 Pa and at 3.4 cm is 400 Pa has shown in Fig.4.16

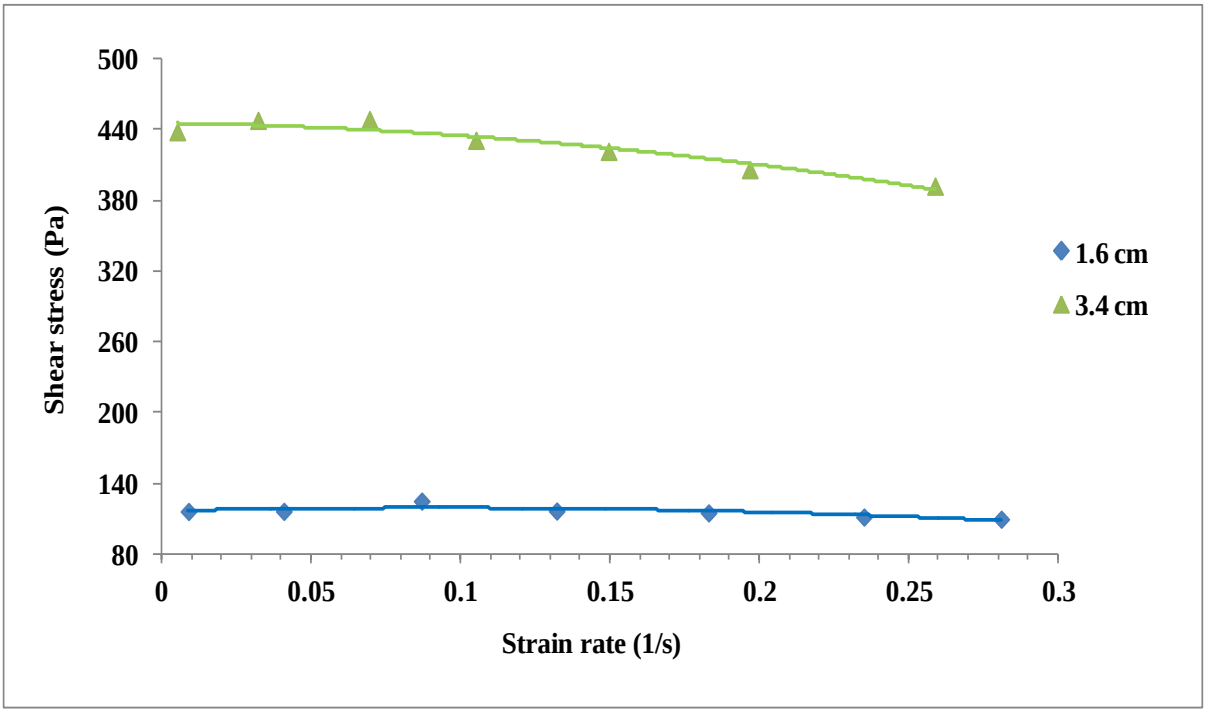


**Figure 4.17:** Shear stress versus rate of strain for field-7 powder under un-fluidized condition

Figure 4.18 and 4.19 shows the comparison of shear stress values of all seven fields of fly ash at depths 1.6 cm and 3.4 cm respectively.

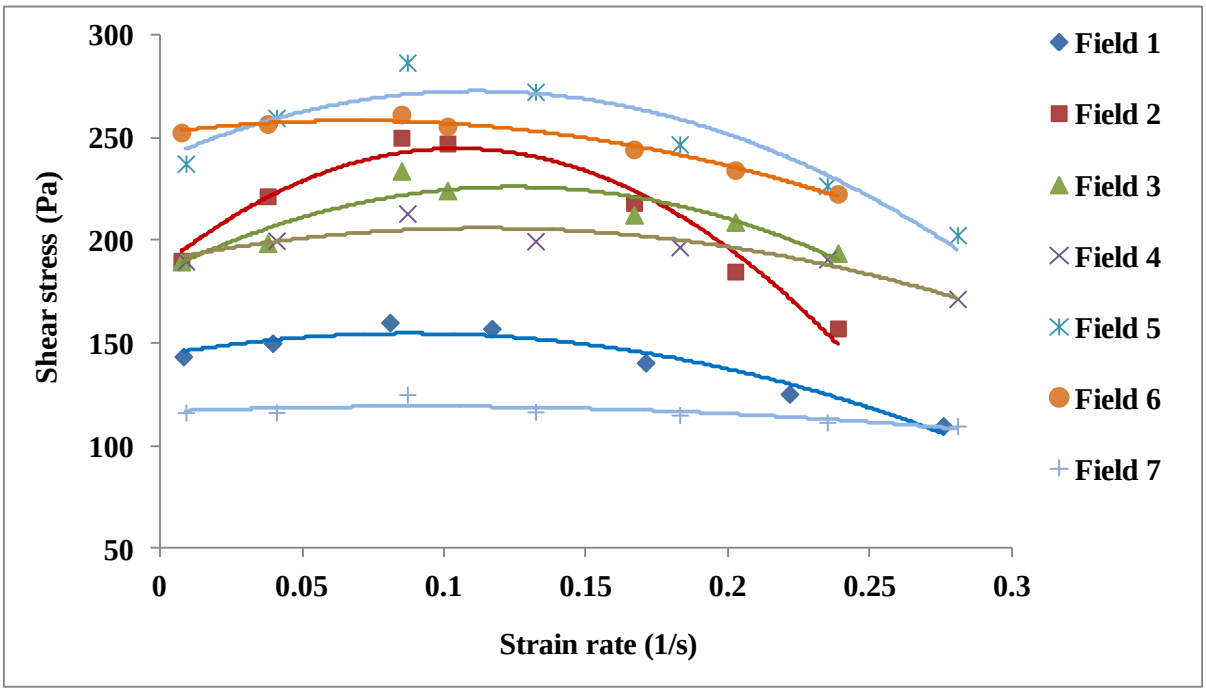


**Figure 4.18:** Shear stress versus rate of strain for powders of all 7 fields under un-fluidized condition at a spindle depth of 1.6 cm

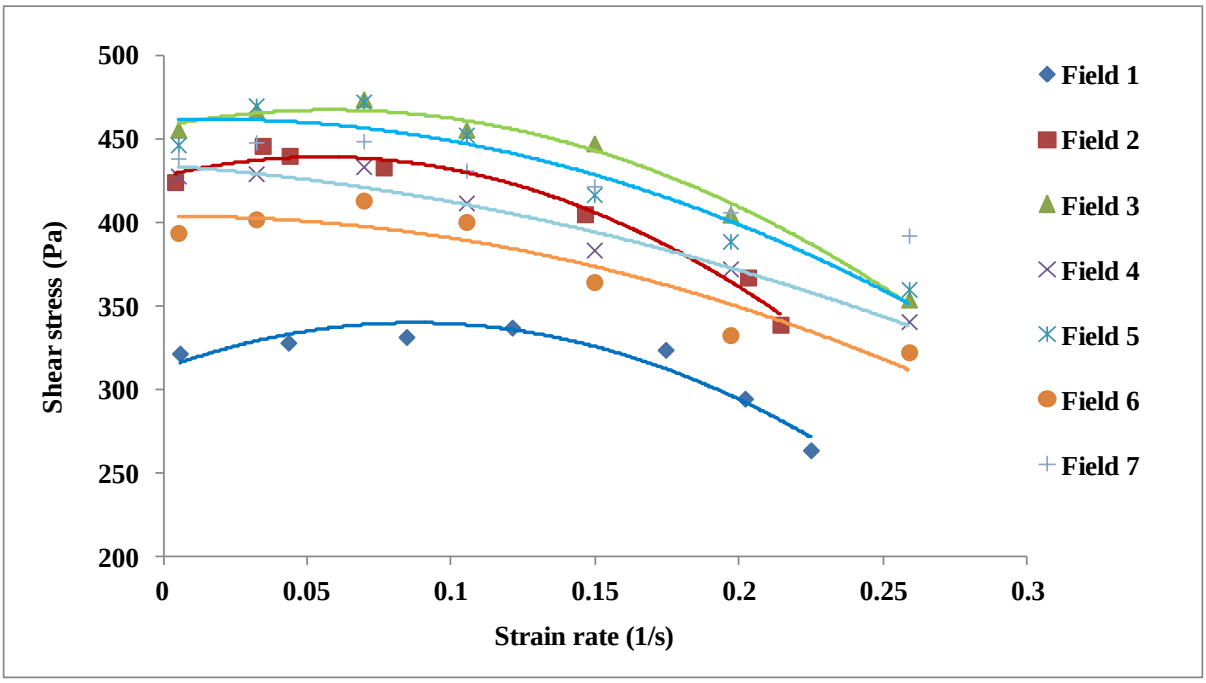


**Figure 4.19:** Shear stress versus rate of strain for powders of all 7 fields under un-fluidized condition at a spindle depth of 3.4 cm

From Fig. 4.19 it can be observed that the shear stress value at different spindle speeds for field 1 fly ash is lower whose particle size is 28 μm and are higher for field 2 and field 3 comparatively (i.e; stress values increased with reduced particle size). From the graph it can be elucidated that the fly ash of field 4, 5, 6 and 7 have lesser yield stress values compared to field 3. The fly ash of field 5, 6 and 7 have almost nearby values, perhaps for the reason all the three fly ash samples have same mean particle size with almost same particle size distribution of 1 μm – 29 μm, 1 μm – 25 μm and 1 μm - 33 μm respectively.

The determined yield stress values of each material under un-fluidized condition of powders at different depths are presented in following table 4.1.

**Table 4.1:** Yield stress values under un-fluidized condition

| **S.No** | **Material** | **$d_{50}$ (μm)** | **Yield stress at Depth 1 (Pa)** | **Yield stress at Depth 2 (Pa)** | **Yield stress at Depth 3 (Pa)** |
|---|---|---|---|---|---|
| 1 | Fly ash 1 of P1 | 139 | 112 | 144 | 234 |
| 2 | Fly ash 2 of P1 | 69 | 130 | 230 | 340 |
| 3 | Fly ash 3 of P1 | 21 | 138 | 172 | 223 |
| 4 | Fly ash 1 of P2 | 28 | 142 | _ | 280 |
| 5 | Fly ash 2 of P2 | 22 | 180 | _ | 428 |
| 6 | Fly ash 3 of P2 | 18 | 186 | _ | 458 |
| 7 | Fly ash 4 of P2 | 9 | 188 | _ | 430 |
| 8 | Fly ash 5 of P2 | 5 | 236 | _ | 464 |
| 9 | Fly ash 6 of P2 | 4 | 255 | _ | 396 |
| 10 | Fly ash 7 of P2 | 4 | 120 | _ | 446 |
| 11 | Mustard powder | 266 | 100 | _ | 206 |
| 12 | Mustard paste | _ | 34 | _ | 54 |

## 4.2 Conclusions

Based on the experimental investigation and practical observation the following conclusions can be made:

- Yield stress value depends upon the particle properties such as particle size and particle shape. A powder material of irregular shape has a high tendency of interlocking, hence requires larger force to enhance the flow.
- Mustard paste prepared from the same mustard powder showed similar behaviour with reduced yield stress value because of bond breakage between the particles and surface smoothening by the presence of water molecules in-between. Powder materials behave as non-newtonian bingham plastic fluids.
- Shear stress values increases with increase in strain rate at lower speeds and then continues to drop down with increasing strain rate. As the depth of spindle immersion increases the loaded material on the spindle increases resulting in higher yield stress value.
- Aerated powders behave as fluids hence show reduced yield stress values compared to un-fluidized powders.
- In high depth of spindle immersion it has been noticed that cohesive powers require higher stress values to enhance the flow.

# Chapter 5

# Fluidization and de-aeration

## 5.1 Introduction

The minimum fluidization velocity ($U_{mf}$) is the main parameter to design the fluidization operation. The point of $U_{mf}$ represents the point of transition from fixed bed to fluidized bed. It depends upon particle and bulk properties of the powders such as particle density ($\rho_p$), bulk density ($\rho_b$), mean particle size ($d_{50}$), particle size distribution and shape, besides it also depends on surface characteristics (adhesion, moisture, cohesion and electrostatics). To find $U_{mf}$, experimental or theoretical procedures can be approached. Experimentally $U_{mf}$ is found by measuring the pressure drop per unit length with increasing and decreasing air flow rate.

As experimental approach is usually time consuming, several researchers have proposed empirical models by multi regression analysis, providing relation between Archimedes number and Reynolds number which showed good fit in researchers own experimental data. The model should consider all the properties of conveying material for better prediction. Researchers follow their own method for model prediction, hence specifying a generalized model for $U_{mf}$ prediction has become almost difficult. In this study an experimental data of fly ash from power plant 1 has been adopted from literature and validated the empirical models predicted by certain researchers (Xie and Geldart [1995], Abrahamsen and Geldart [1980], Vasconcelos and Mesquita [2011], Wen and Yu [1966], Xu and Zhu [2008], Hariprasasd et al [2007]). All the models have under predicted the $U_{mf}$ value for fine powders. A new model is proposed by regression analysis on available experimental data and material properties, it has been noticed that the model is best suitable for fine powders. In order to establish the truth of correctness of the model, experiments are conducted on fine and cohesive materials of fly ash samples collected from different ESP hoppers of power plant 2, 3, 4 and 5.

### 5.1.1: Validation of existing models on adopted experimental data of fluidization

Several correlations can be found in the literature to determine the minimum fluidization velocity by using the physical properties of the materials. These correlations were based on

both the experimental data on different products and by considering that the pressure drop per unit length is equal to the net gravity force per unit area during incipient fluidization.

**Abrahamsen and Geldart [1980]** examined the effect of gases on powder behaviour by using fluidization column of internal diameter 0.15 m made of Perspex material. They used 23 different powders with mean particle size varying from 20 to 72 μm and particle density varying between 1100 to 4600 kg/m$^3$. The results show that powder belongs to Geldart category A will behave like category B powder when the gas changes from air with hydrogen. Eq. (5.1) was reported to provide good predictions for finding minimum fluidization velocity on their fine powders.

$$U_{mf} = \frac{0.009\left(\rho_s - \rho_g\right)^{0.934} g^{0.934}\, d_{50}^{1.8}}{\mu_g^{0.87}\, \rho_g^{0.066}} \tag{5.1}$$

**Wen and Yu [1966]** proposed a generalized relationship between Reynolds and Archimedes numbers to determine the minimum fluidization velocity. They have developed the correlation based on the well known Ergun equation for the fixed bed pressure drop. They have plotted a large number of published data points on the graph between $Re_{mf}$ and Ar, found that their correlation shows greater accuracy. The model also covers the widest range of Reynolds number ($0.001 < Re_{mf} < 4000$). The expression was given as:

$$U_{mf} = \frac{\mu_g}{\rho_g\, d_{50}} \{ 1135.7 + 0.0408\, Ar)^{0.5} - 33.7 \tag{5.2}$$

**Xie and Geldart [1995]** studied the effect of temperature and gases on $U_{mf}$ and $U_{mb}$ for twelve different FCC powders having a particle size varying from 26 μm to 137 μm. They found that gas absorption in FCC powders has considerable effect on fluidizing behavior. The minimum fluidization velocity decreases with the rise in temperature. They experimentally determined the minimum fluidization velocity and provided the following correlation:

$$U_{mf} = \frac{\varepsilon_{mf}^3}{1-\varepsilon_{mf}} \frac{(\rho_s - \rho_g)\, g\, d_{50}^2}{180\, \mu_g} \tag{5.3}$$

**Vasconcelos and Mesquita [2011]** studied the fluidization characteristics of alumina fluoride having different particle size in two rectangular and one circular permeameter. They compared the $U_{mf}$ values obtained from equation (5.4) with several correlations reported in literature and experimental data. It was found that values of $U_{mf}$ as predicted by Vasconcelos were found in good agreement with experimental values with error less than 5 %. The expression for minimum fluidization velocity was given as:

$$U_{mf} = 0.21(Ar)^{0.25} \frac{(\varphi_s)^{0.7}}{(1.05\ \varepsilon_{mf})^{0.7}} (d_{50}\ g)^{0.5} \quad (5.4)$$

**Xu and Zhu [2008]** developed a new correlation for finding minimum fluidization velocity for fine particles by modifying the well known Ergun equation by taking into account the inter-particle forces. They found satisfactorily good results for particles belonging to different Geldart groups from the prediction made by new correlation. Their model is provided by equation 5.5

$$Re_{mf}^2 + \frac{85.71(1-\varepsilon_{mf})}{\varphi_s} Re_{mf} = E_G + E_C \quad (5.5)$$

$$E_G = 0.57\ \varphi_s\ \varepsilon_{mf}^3 Ar$$

$$E_C = 4.79 \text{ x } 10^{-9} \frac{\varphi_s\ \varepsilon_{mf}^{0.52} \rho_g d_{50}}{L_o\ \mu_g^2}$$

$$\varepsilon_{mf} = 0.77(d_{50} \text{ x } 10^{-6})^{-0.124}$$

**Hariprasad et al. [2007]** investigated into the effect of temperature on the minimum fluidization velocity ($U_{mf}$). 9 different Group B (Geldart classification) materials were used in the temperature range of 298 to 973K and provided the following correlation for the minimum fluidization condition:

$$Re_{mf} = \frac{Ar}{1502} \quad (5.6)$$

The above models (Eqs. 5.1 to 5.6) were used to predict the minimum fluidization velocity for fly ash.

**Table: 5.1:** Adopted experimental data of fly ash from 7 ESP hoppers of power plant 2

| ESP field no. | $d_{50}$ (µm) | $\rho_s$ (kg/m$^3$) | $\rho_b$ (kg/m$^3$) | $W_{fo}$ (m/s) | Experimental $U_{mf}$ (m/s) |
|---|---|---|---|---|---|
| 1 | 139 | 2015 | 848 | 0.68 | 0.0285 |
| 2 | 102 | 2014 | 839 | 0.45 | 0.016 |
| 3 | 97 | 2025 | 818 | 0.43 | 0.018 |
| 4 | 69 | 2025 | 759 | 0.25 | 0.03 |
| 5 | 53 | 2030 | 780 | 0.16 | 0.036 |
| 6 | 41 | 2018 | 830 | 0.094 | 0.04 |
| 7 | 21 | 2032 | 804 | 0.026 | 0.122 |

The results of comparisons of predicted minimum fluidization velocity from models versus experimental data are shown in Figure 5.1.

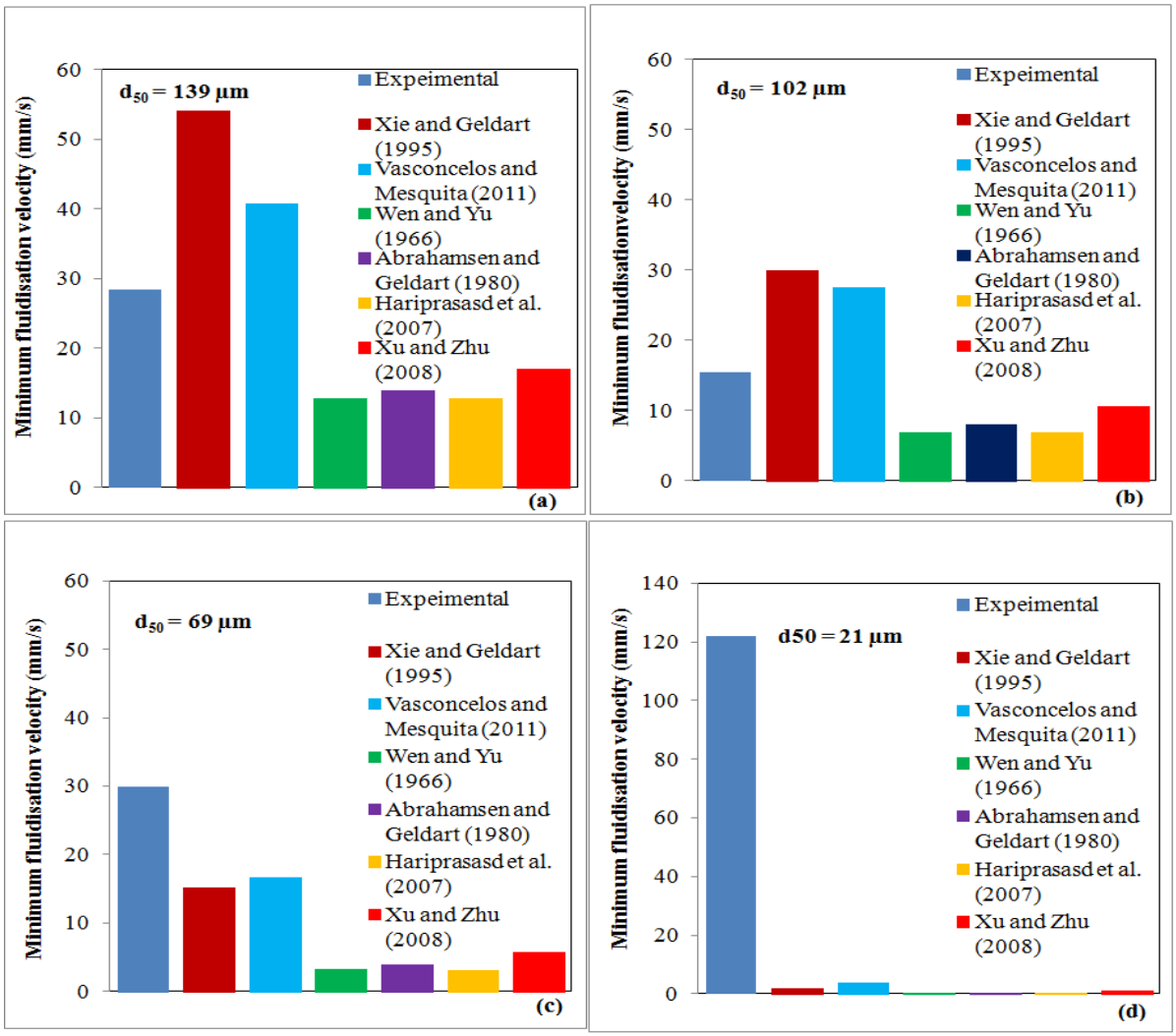


**Figure 5.1:** Validation of existing models for provided experimental data.

From Fig. 5.1 it can be observed that for all four fly ash samples of average particle size ($d_{50}$) 139 µm, 102 µm, 69 µm and 21 µm the $U_{mf}$ predicted from the existing models is different from the experimental values of $U_{mf.}$ For fly ash of $d_{50}$ 139 µm and 102 µm (which fall under Geldarts A/B boundary), models of Xie and Geldart (1995), Vasconcelos and Mesquita (2011) over predicted the $U_{mf}$ values. The model of same authors has under predicted the value of $U_{mf}$ for d50 = 69 µm (falls under Geldarts group A classification), but are near to the experimental values. The models proposed by the remaining researchers under predicted the $U_{mf}$ for all fly ash samples. It is clearly observed that none of the models are valid for estimating the $U_{mf}$ values of d50 = 21 µm (Falls under Geldart's A/C boundary). As it is evident that the existing models are unable to predict the minimum fluidization velocity reliably for very fine powders (finer fly ash), a new model format to represent the minimum fluidization condition has been developed.

### 5.1.2: Proposed model for prediction of minimum fluidization velocity

At $U_{mf}$ the hydrodynamic forces on the particles $F_d$ balances with or exceeds the gravitational forces $F_g$, when the air passes through the packed bed of particles.

$$F_g + F_d = 0 \tag{5.7}$$

The net gravitational force on the bed of particles must consider the weight W of the particles and the buoyancy forces $F_b$.

$$F_g = W - F_b$$
$$= (\rho_p - \rho_f) g V_p \tag{5.8}$$

The drag force on the bed of particles can be calculated by calculating the pressure drop across the bed and multiplying it by the cross-sectional area of the column. The pressure drop through a porous medium is a function of bed voidage (ξ), flow velocity or superficial air velocity (U) and particle properties ($D_e$, $\Phi_s$).

$$\nabla P = f\ (\xi, U, D_e, \Phi_s)$$

The drag force on the bed of particles is given as,

$$F_d = \nabla P A H \tag{5.9}$$

Balancing the forces as indicated in Eq. 5.7, using equation 5.8 for $F_g$ and Eq. 5.9 for $F_d$, results in an expression that can be solved for $U_{mf}$.

Considering all the forces, particle and fluid properties, Ergun proposed a correlation.

$$\left(\frac{\Delta P}{L_o}\right)_{drag} = \frac{150(1-\xi_b)^2 \mu_g U}{{\xi_b}^3 (\Phi_s d_p)^2} + \frac{1.75(1-\xi_b)\rho_g U^2}{{\xi_b}^3 \Phi_s d_p} \tag{5.10}$$

The first part in the above equation manages the pressure drop due to viscous forces and the second part manages the pressure drop due to inertial forces. This is a generalized equation of pressure drop. Viscous forces dominate at low Re and inertial forces dominate at higher Re [Xu and Zhu, 2006].

Instead of balancing the forces, some other methods of predicting $U_{mf}$ were developed by several researches based on correlation between Re and Ar. In this study besides the non-dimensional numbers like Re number and particle properties alone and another parameter considered in developing the correlation is the settling velocity in the calm air of round particles ($W_{fo}$), and is given as:

$$\log_{10}(Re_p) = K\,(W_{fo}/U_{mf})^{\,n} \tag{5.11}$$

Where, the $Re_p$ is given as:

$$Re_p = \frac{\rho_s W_{fo} d_{50}}{\mu_g} \tag{5.12}$$

'K' and 'n' in the equation 7 are the power function constant and exponent, respectively.

To determine the values of 'K' and 'n' in the equation (5.11), the experimental values of $U_{mf}$ of the all the 7 fly ash samples have been used, as given in table 5.1

Using the experimental data of minimum fluidization velocity for fly ash, the following model has been developed:

$$\log_{10}(Re_p) = 2.308\,(W_{fo}/U_{mf})^{\,0.157} \tag{5.13}$$

Figure 5.2 shows the plot of the model through the experimental data points. The high value of $R^2$ indicates a good fit. Figure 5.3 shows the experimental versus predicted (using the newly developed model) values of $U_{mf}$.

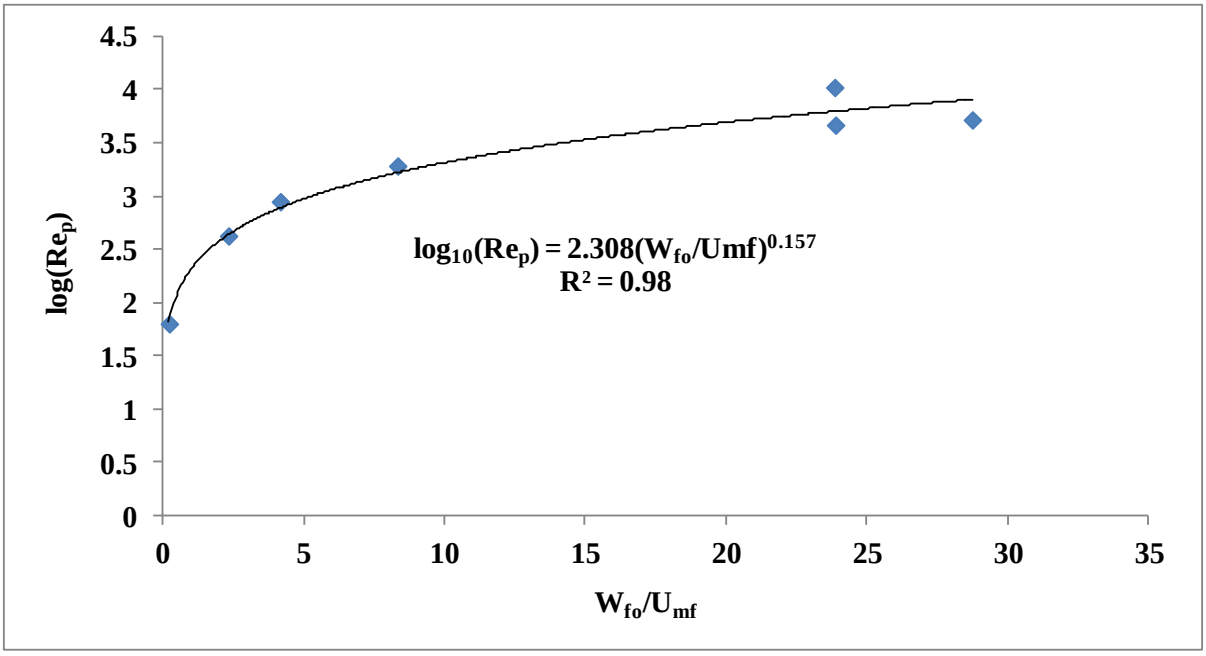


**Figure 5.2:** Plot of the new developed model representing minimum fluidization condition

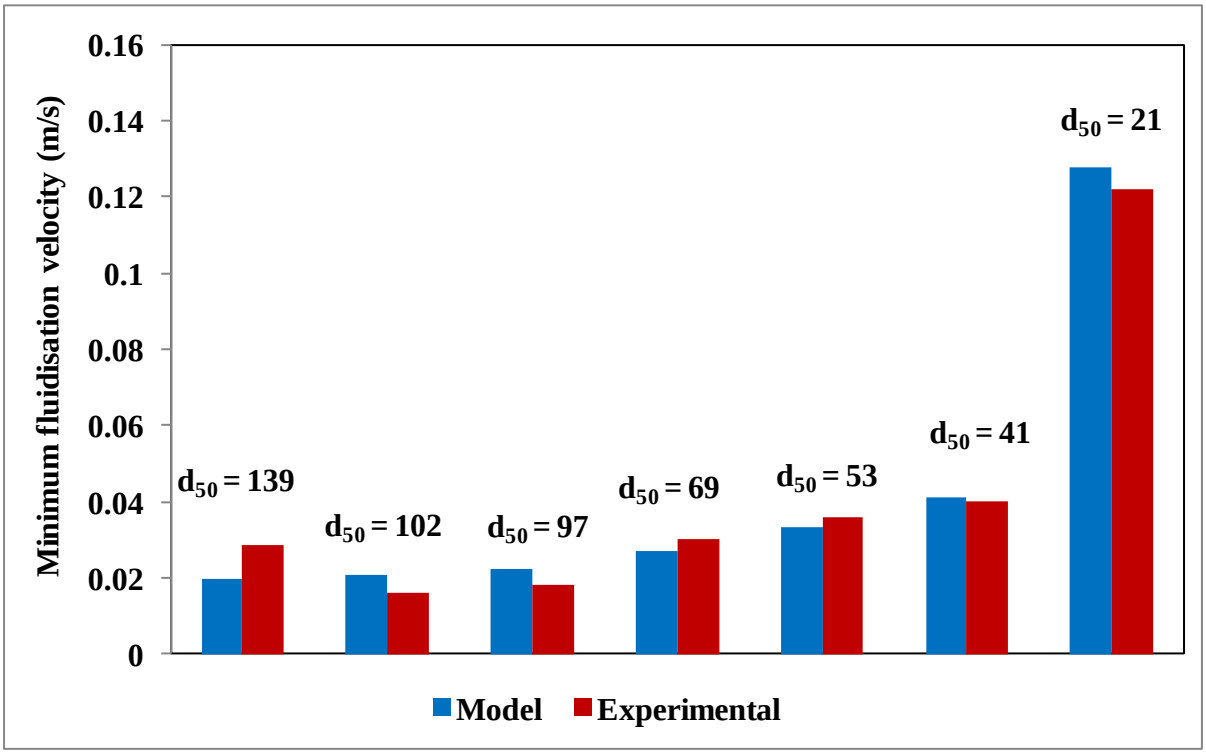


**Figure 5.3:** Experimental versus model predicted values of $U_{mf}$ ($d_{50}$ in μm)

## 5.2: Experimental results of fluidization test on fly ash samples from power plants

The experimental results obtained will be uncertain if standardization is not followed. For example the pressure drop value across the bed at varying flow rates represents the transfer of bed from fixed to fluidized, but they depend upon how the experiment is performed and the experience of the person. This means that the different conditions and equipments that were used by different researchers in former made it difficult to find consistency of results across the researchers. Hence, following a standard method of measurement is necessary. This study follows the detailed guidelines on procedure and process provided by Klinzing et.al [2003], Williams [2008] and Chawla, Masters of Engineering thesis [2015].

In previous studies, experimental work is conducted on little standardized fluidization set up. Certain modifications to the experimental setup are made as an effort to standardize the equipment. The materials subjected to fluidization tests in the present work are very fine, which fall under group A/C classification. Unlike powders belonging to group A and B, it is difficult to fluidize Group C powders which generally results in gas bypassing via the formation of channels, they lift as a plug of bulk material or vertical and inclined cracks are formed (shown in figure 5.4) by fluidizing.


**Figure 5.4:** Difficulties in fluidization of cohesive powders

The difficulty in fluidization is not only due to the reason that the cohesive forces such as Van der Waals, electrostatic, capillary forces are larger than the gravitational forces, but also due to the fact that the drag forces are exerted by the gas on the particles is not

sufficient enough for fluidization. From the experimental observations, it was found that the cohesive particles tend to form agglomerates (which appear as large particles belonging to group B and D as shown in Fig. 5.5) due to high inter-particle forces and they no more behave as an individual particle, therefore the fine and cohesive particles can be fluidized as agglomerates of the original fine particles at excess gas velocity above the actual $U_{mf}$ required for fluidizing primary particles, which is already noticed by Shabanian et al. [2012]. To overcome all these problems and improve the quality of fluidization of group C particle agglomerates various assisting methods have been proposed and implemented in literature. These methods include the application of external generated forces by acoustic, electric or mechanical fields or mechanical vibrations; using a centrifugal fluidized bed or tapered fluidized bed, addition of foreign particles or the use of micro-jets as the secondary air supply. Hence, in this experimental process the fluidization setup is updated with an external secondary air supply hose at the bottom of the bed which acts as a micro-jet to breakdown channelling and achieves the proper fluidization of these powders.

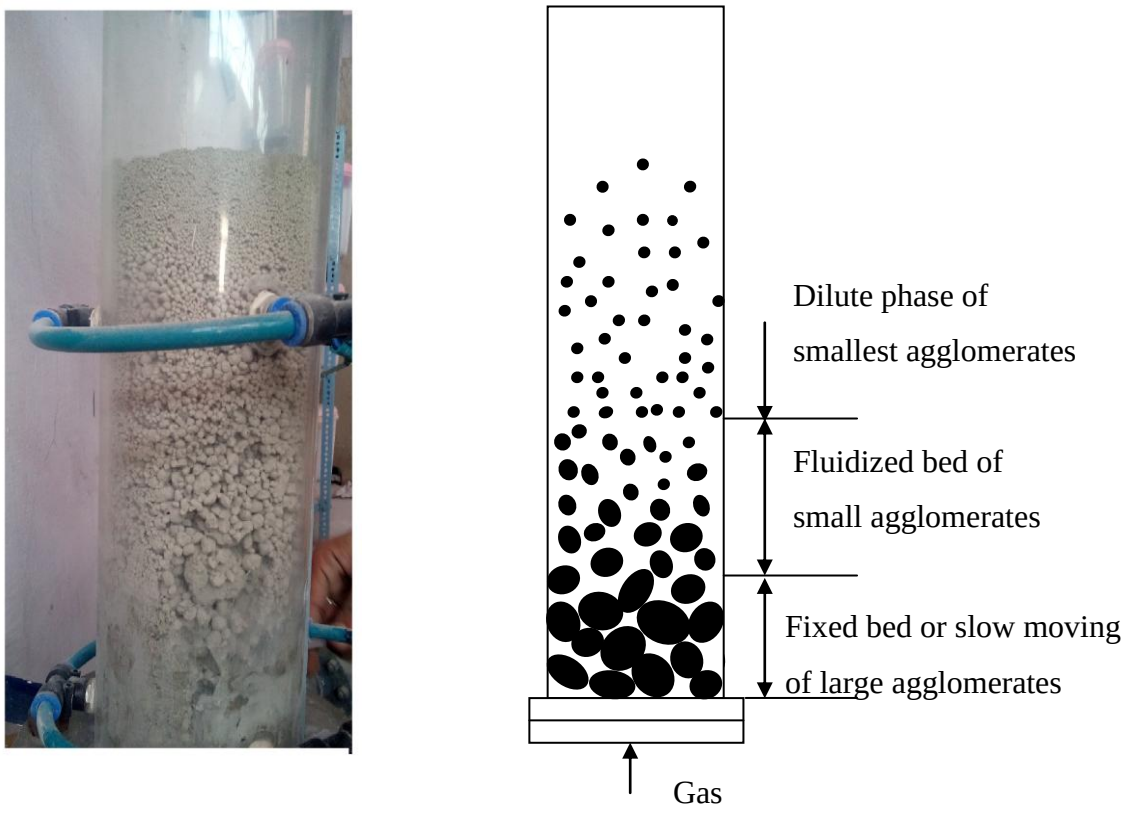


**Figure 5.5:** Actual and schematic diagram of agglomerate formation in fluidized bed

Behaviour of powders depends upon many factors, one of them is particle size. Material properties such as bulk density, particle density and air carrying capacity of powders change with particle size. The main focus of this particular chapter is to find the minimum fluidization velocity of the fine powders and analyze the effect of particle size on it; and compare the experimental values with theoretically calculated values of the proposed model. Experimentally $U_{mf}$ is determined by superimposing two graphs formed between superficial air velocity and pressure drop per unit length with increment and decrement in air mass flow rates and marking an intersection point of both the graphs. This method is adopted from the Bachelor of Engineering thesis of Williams, [2008]. The results for the fly ash powders from the power plant 2 are provided below.

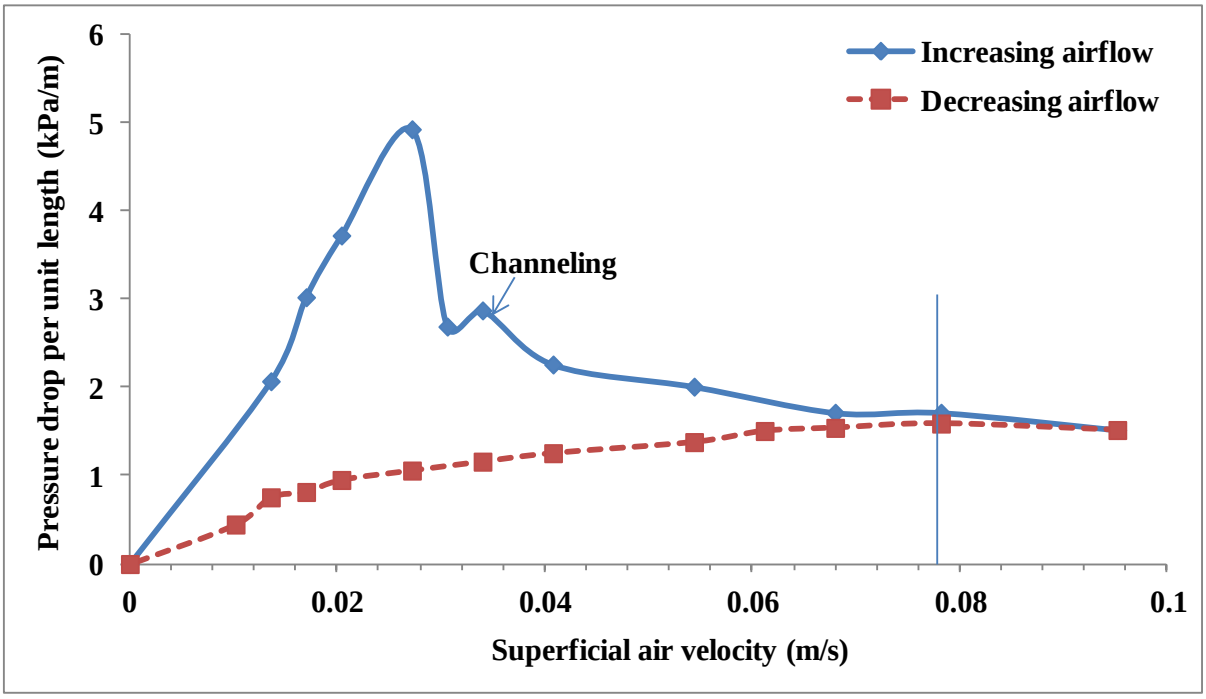


**Figure 5.6:** Fluidization test of fly ash 1 of power plant 2

Fly ash 1 has a mean particle size ($d_{50}$) of 28 µm and particle size distribution range of 6 µm - 120 µm. The fluidization behaviour of this is portrayed in Fig. 5.6. Initially with increasing air flow rate, pressure drop increased to an extreme point after which it is decreased as the fluidized bed lift has been started. The maximum pressure drop is obtained at a superficial air velocity of 0.027 m/s. With little more increase in air mass flow rate channelling is observed, followed by air bubbling and then complete fluidization. During increasing mass flow rate larger fluctuations in pressure drop readings were observed after channelling until complete fluidization is attained. The air flow rate is increased up to the

maximum superficial air velocity of 0.095 m/s, at which the bed height is observed to be increased by 5 cm from the initial bed height. The air mass flow rate is gradually decreased from the fully fluidized state. A smooth, gradually decreasing pressure drop curve is obtained with decreasing air mass flow rate. From the intersection point of increasing and decreasing air flow rate curves, the minimum fluidization velocity obtained is 0.074 m/s.

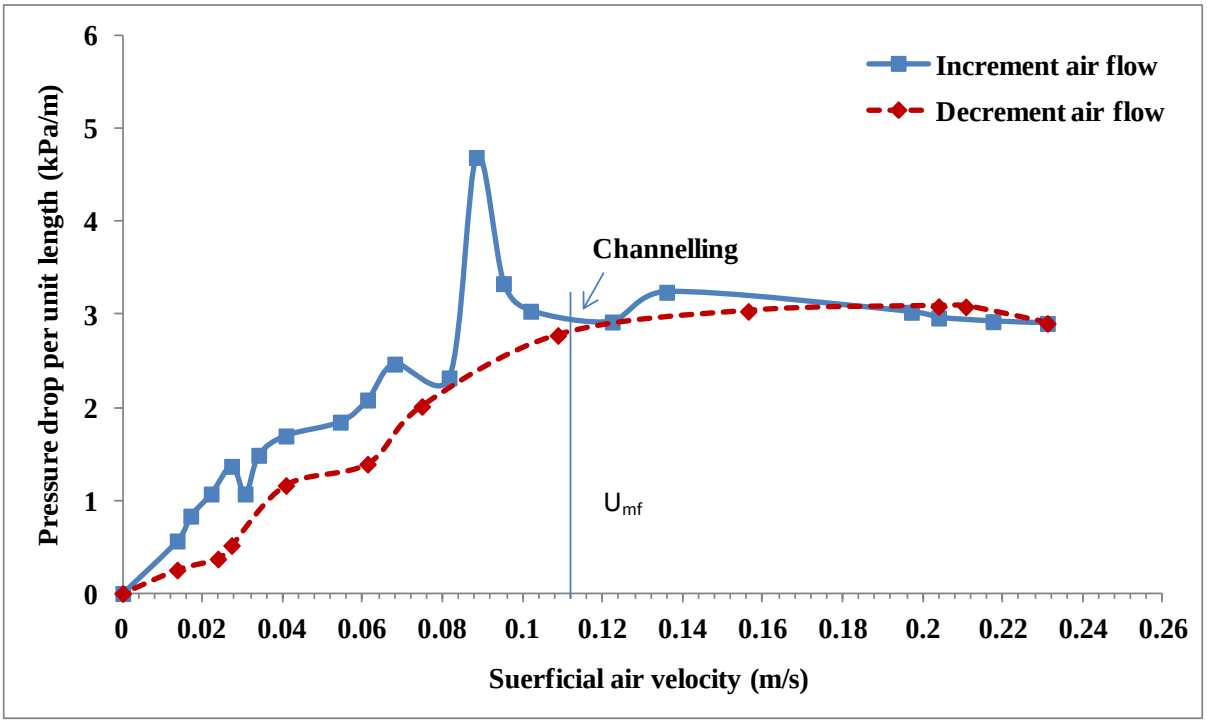


**Figure 5.7:** Fluidization test of fly ash 2 of power plant 2

Fly ash 2 is from the second field ESP hopper whose mean particle size ($d_{50}$) is 21 µm and having a particle size distribution range of 3 µm – 112 µm. From Fig. 5.7 it can be observed that with increasing air flow the pressure drop increased till a point and dropped suddenly, after which the pressure drop remained almost constant with further increase in air flow. The maximum pressure drop is obtained at a superficial air velocity of 0.088 m/s. After complete fluidization by decreasing air flow the pressure drop is not significant in the superficial air velocity range of 0.23 m/s to 0.12 m/s. After 0.12 m/s the further reduction in air flow rate resulted in a gradual reduction in pressure drop. The curves of increasing and decreasing air flow rate are separated after a point of superficial air velocity and hence from the superimposition of both the curves the minimum fluidization velocity is determined as 0.112 m/s.

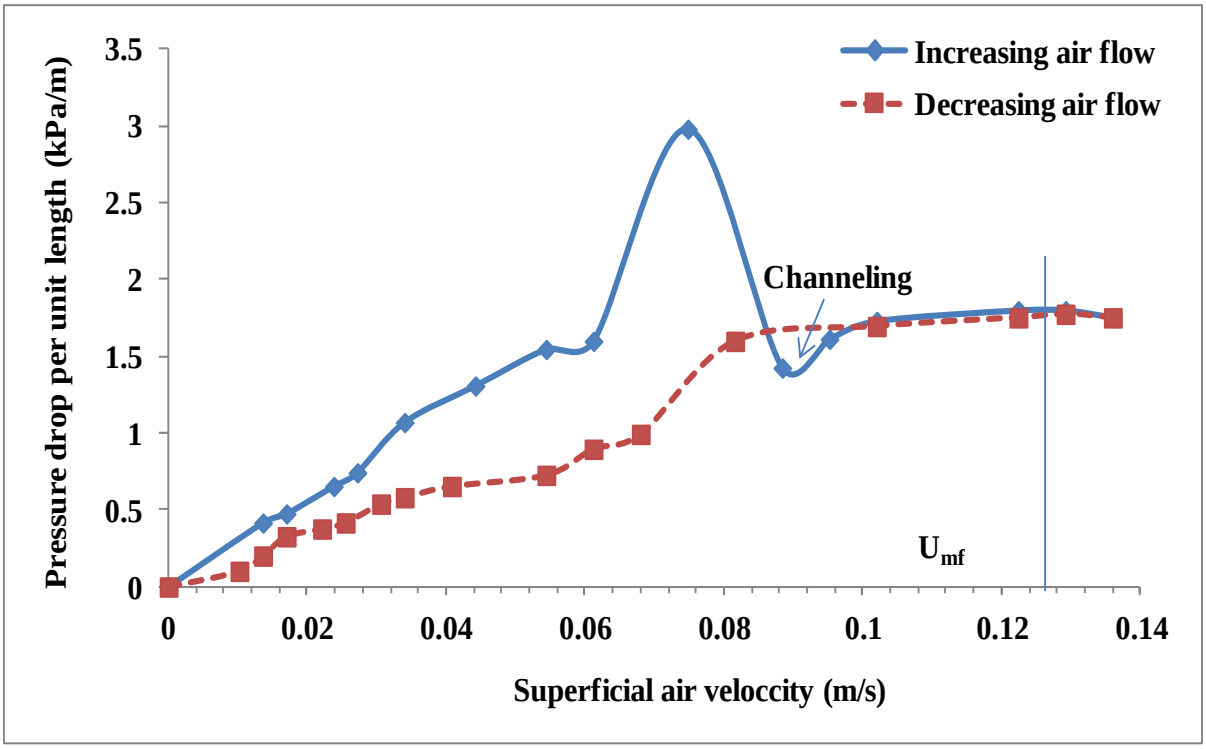


**Figure 5.8:** Fluidization test of fly ash 3 of power plant 2

Figure 5.8 shows the fluidization behaviour of fly ash 3. The mean particle size ($d_{50}$) of the powder is 17 µm. The extreme pressure drop of 3 kPa/m is attained at the superficial air velocity of 0.074 m/s. From both the increasing and decreasing airflow rate curves it can be noticed that there is a sudden raise and drop in pressure drop respectively. Fly ash 3 has wider particle size distribution compared to fly ash 1. Due to this wide particle size distribution the particles have a high tendency to get packed under very small external forces, hence the bed got compacted with gradual increase in air flow rate by which there is sharp change in pressure drop. The further increase in air flow rate lead to bed breakage and channelling by which air passages have been formed and the air got escaped. Therefore, there is a sudden drop in pressure. The fully fluidized state is attained with a further more increase in air flow rate. The minimum fluidization velocity is found to be 0.126 m/s. After this point of velocity there is little considerable change in pressure drop.

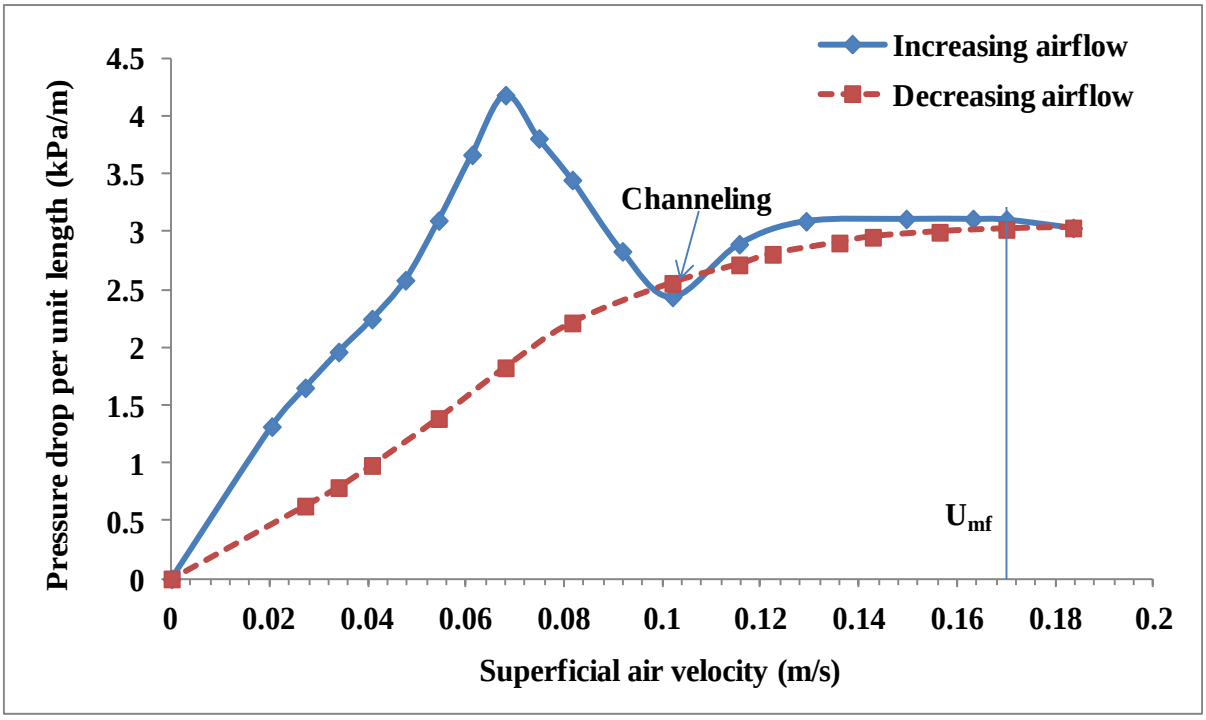


**Figure 5.9:** Fluidization test of fly ash 4 of power plant 2

Figure 5.9 shows the fluidization behaviour of fly ash 4 whose mean particle size is 8 µm. The maximum pressure drop of 4.18 kPa/m is attained at 0.067 m/s of superficial air velocity. Complete fluidization is reached by increasing the air flow rate after channelling. After the fully fluidization state, further increase in air flow rate tended to agglomeration and segregation as shown in Fig. 5.5. Since the fly ash is cohesive, agglomerates are formed. Larger agglomerates got settled down at the bottom of the bed and the smaller agglomerates undergo dilute kind of fluidization on the top surface. With the decreasing air flow rate the curve obtained is smooth and gradually decreasing pressure drop curve. The cause for this behaviour may be predicted as a result of agglomeration. Inter-particle forces are high in case of cohesive materials; therefore the minimum fluidization velocity required for fluidization of this fly ash sample was high. The $U_{mf}$ determined from the superposition of increasing and decreasing air flow rate curves is 0.17 m/s.

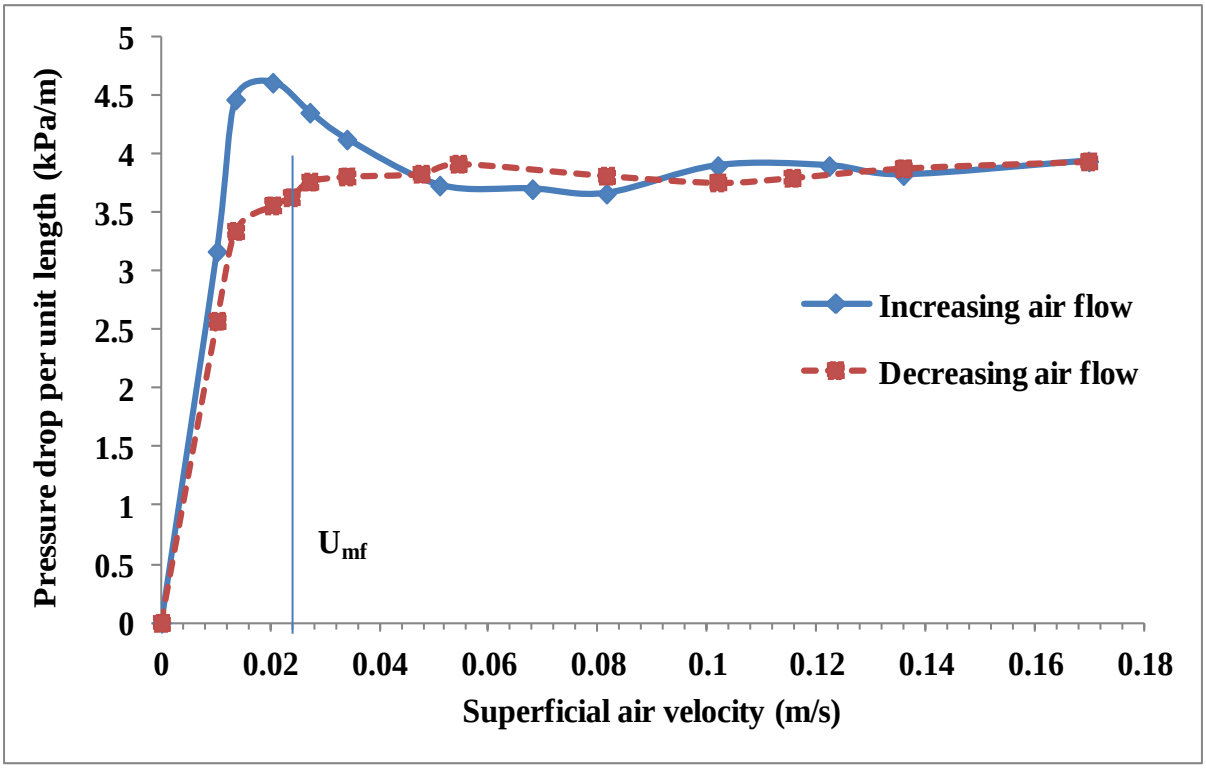


**Figure 5.10:** Fluidization test of fly ash 1 from power plant 3

Figure 5.10 shows the fluidization behaviour of fly ash 1 collected from the first field ESP hopper of power plant 3, the determined mean particle size is 106 µm with particle size distribution range is 20 µm to 235 µm which indicates that the powder is not cohesive in nature. While increasing the air flow rate steep increase in pressure drop across the bed has obtained until a maximum pressure drop of 4.61 kPa/m at a superficial velocity 0.02 m/s. The reduction in pressure drop after this point indicates the initiation of fluidization. Comparing with the fly ash samples of power plant 2 there is no steep drop in pressure while increasing the air flow after maximum pressure drop, which represents no channelling during the process of fluidization. After complete fluidization has occurred the pressure drop almost remained constant. By decreasing the air flow from the maximum supplied velocity to zero the pressure drop remained same until the superficial velocity reached 0.027 m/s. After this velocity the further reduction in air flow showed a curvature with small radius beyond that the minute change in air flow resulted in a sudden drop of pressure. This kind of behaviour of the powder is due to the quick de-aeration process, which represents that the powder has less/little air carrying capability. The same has been observed during the experimental process that there is a sudden drop in bed height in fraction of seconds. From the superimposition of the graphs the determined minimum fluidization velocity is 0.024 m/s.

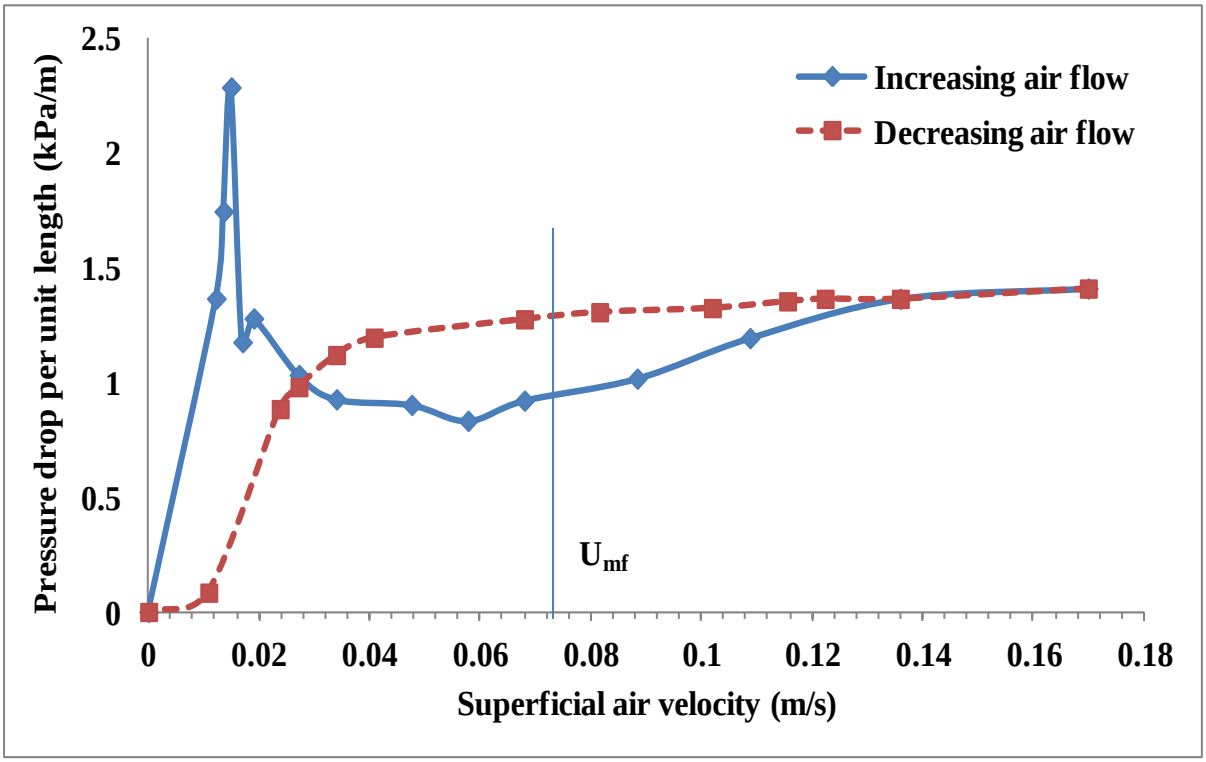


**Figure 5.11:** Fluidization test of fly ash 2 from power plant 3

The mean particle size of this fly ash is 25 µm and the particle size distribution is 4 µm to 103 µm. This fly ash comes under the group of cohesive powders; the un-stability in pressure drop of increasing air flow curve indicates the occurrence of channelling. As discussed above figures for fly ash 1, 2, 3 and 4 from the power plant 2 the pressure drop is sudden while increasing the air flow during fluidization. From the graph it can be extracted that while decreasing the air flow rate the pressure drop remained almost same until 0.08 m/s of superficial air velocity beyond which a noticeable change is pressure drop has been displayed. Comparing Fig. 5.10 with 5.11 it can be stated that with decreasing superficial air velocity there is a gradual change in pressure drop with a large radius of curvature in case of fly ash 2, which indicates that the fly ash 2 has high capability to retain air and takes more time for de-aeration. The determined minimum fluidization velocity for fly ash 2 is 0.073 m/s.

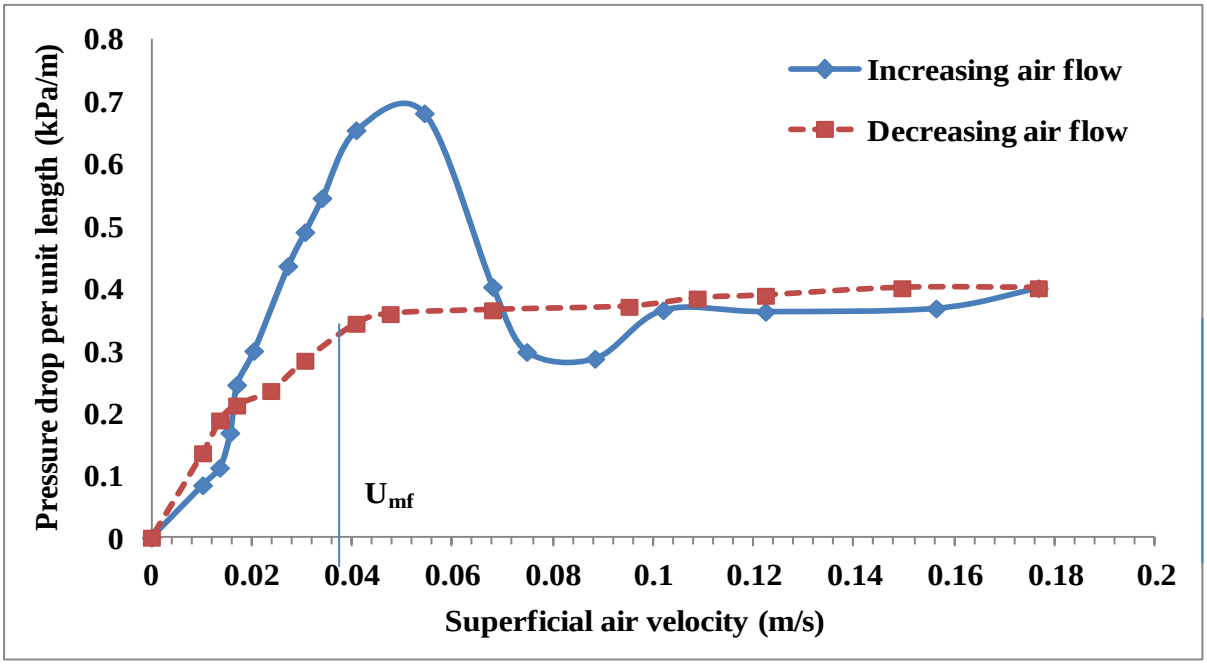


**Figure 5.12:** Fluidization test of fly ash 1 from power plant 4

Figure 5.12 shows the fluidization behaviour of fly ash 1 belonging to power plant 4. The mean particle size is 87 µm and the particle size distribution is 16 µm to 238 µm. It can also be seen from the figure that the pressure drop is not varying considerably by reducing air flow until 0.047 m/s of superficial air velocity. Further reduction in air flow resulted in a gradual change of pressure drop. The minimum fluidization velocity determined is 0.038 m/s.

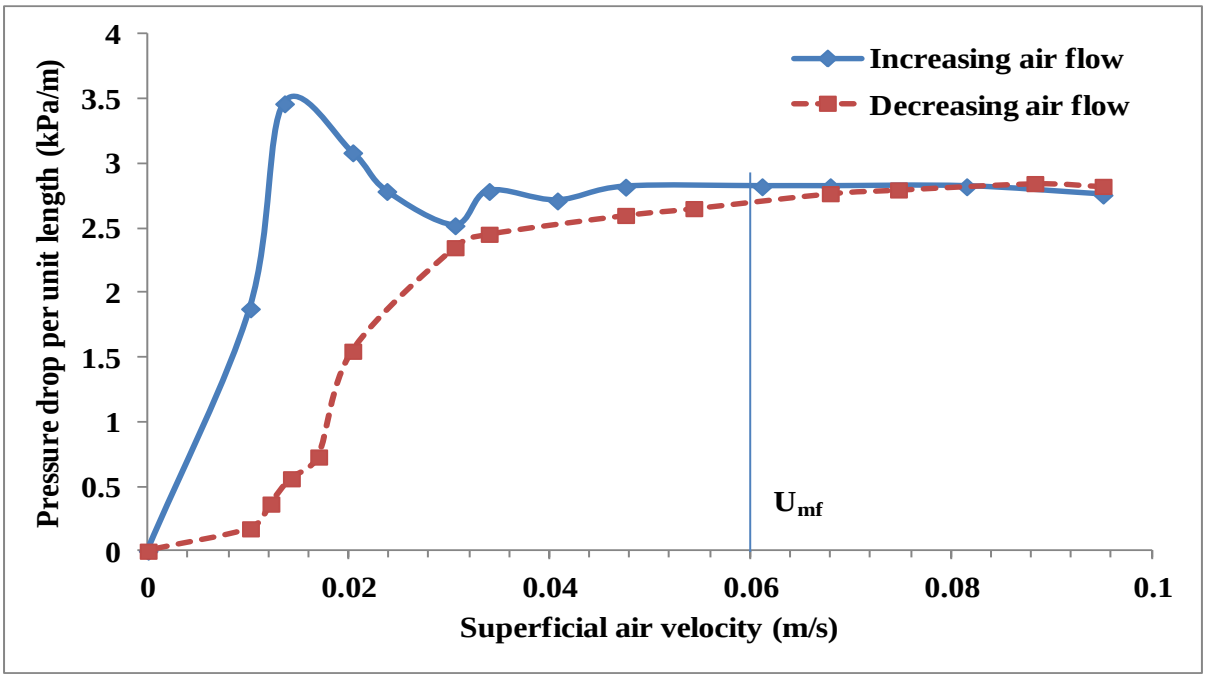


**Figure 5.13:** Fluidization test of fly ash 2 from power plant 4

The fly ash 2 has the mean particle size of 35 µm and the particle size distribution range of 7 µm - 105 µm. The considerable variation in pressure drop with the decreasing air flow is observed after 0.067 m/s of superficial air velocity. The minimum fluidization velocity of the fly ash is 0.06 m/s (shown in Fig. 5.13).

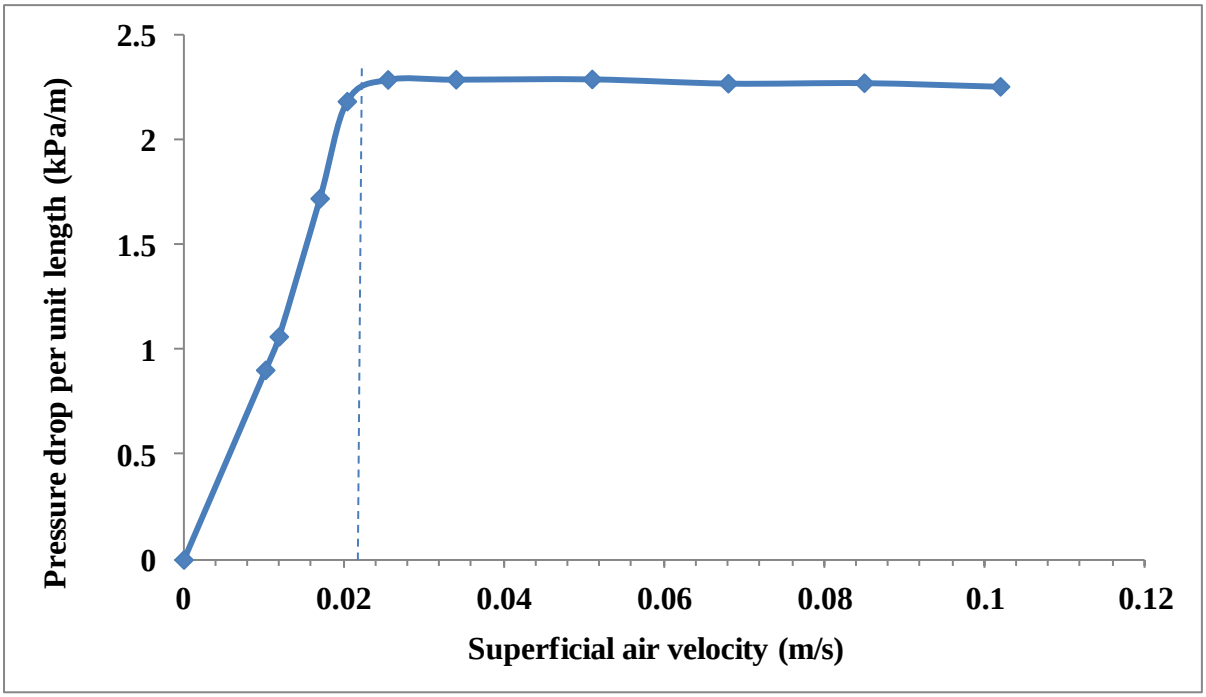


**Figure 5.14:** Fluidization test of fly ash 1 from power plant 5

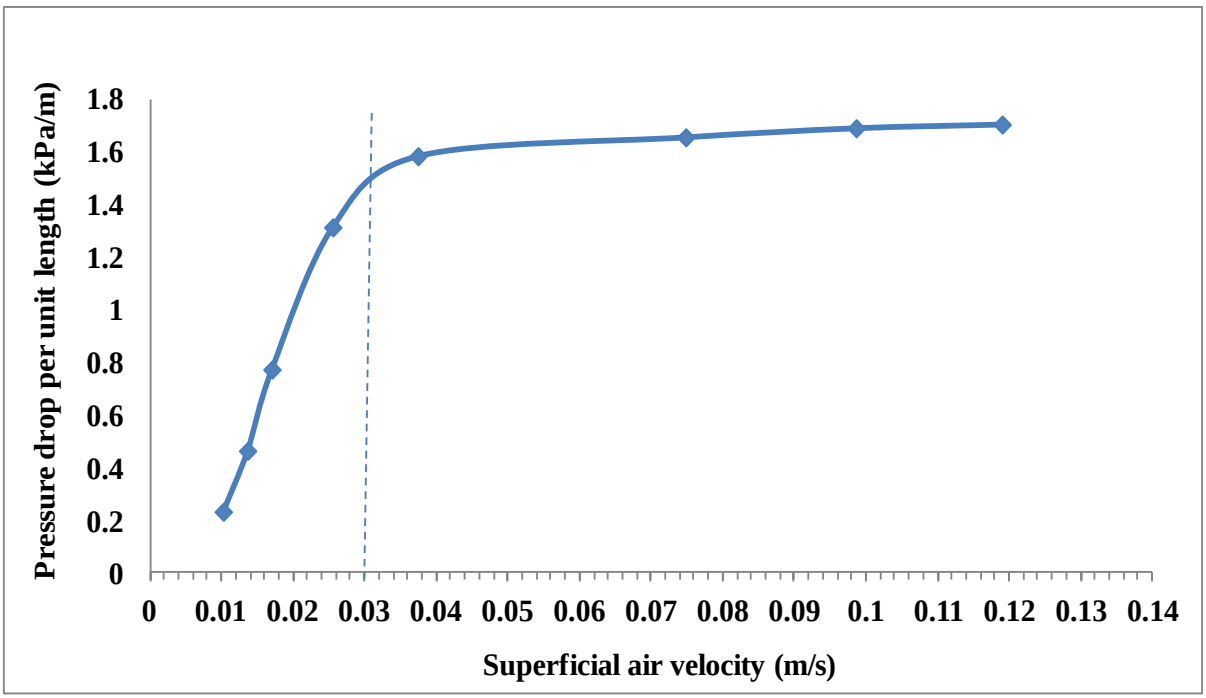


**Figure 5.15:** Fluidization test of fly ash 2 from power plant 5

Figure 5.14 and 5.15 shows the fluidization behaviour of fly ash material (belonging to power plant 4) with the decreasing air flow. Fly ash 1 has a mean particle size of 126 µm and fly ash 2 has a mean particle size of 48 µm. From the comparison of Fig. 5.14 and 5.15 it has been figured out that the powder with large particle has a sudden drop in pressure with the sharp edge of change in pressure curve, whereas the powder with small particle size shows the gradual change in pressure with smooth radius of curvature in a pressure drop curve.

## 5.3: Validation of new proposed model

In order to ensure the suitability of the predicted models for fine powders, experimental $U_{mf}$ values for certain powders have been determined and compared with the predicted $U_{mf}$ values based on the proposed model. The physical properties of the powders and the experimental and predicted $U_{mf}$ are given in the Table 5.2.

**Table 5.2:** Experimental and predicted $U_{mf}$ values

| S.No | Powder | $d_{50}$ (µm) | $\rho_s$ (kg/m$^3$) | $W_{fo}$ | Model | Expeimental $U_{mf}$ | %Error |
|---|---|---|---|---|---|---|---|
| 1 | Fly ash 1 of P2 | 28 | 2000 | 0.048 | 0.06819 | 0.080 | -13.242 |
| 2 | Fly ash 1 of P2 | 21 | 2120 | 0.029 | 0.11639 | 0.108 | 7.7693 |
| 3 | Fly ash 1 of P2 | 17 | 2290 | 0.023 | 0.15684 | 0.126 | 24.4786 |
| 4 | Fly ash 1 of P2 | 8 | 2101 | 0.005 | 11.7060 | 0.170 | Unstable |
| 5 | Fly ash 1 of P3 | 106 | 2030 | 0.475 | 0.02149 | 0.024 | 19.3902 |
| 6 | Fly ash 1 of P3 | 25 | 2299 | 0.043 | 0.07049 | 0.064 | 17.4963 |
| 7 | Fly ash 1 of P4 | 87 | 2080 | 0.37 | 0.02304 | 0.038 | -23.174 |
| 8 | Fly ash 1 of P4 | 35 | 2078 | 0.076 | 0.04743 | 0.060 | -20.939 |
| 9 | Fly ash 1 of P5 | 126 | 2060 | 0.61 | 0.02014 | 0.022 | -12.412 |
| 10 | Fly ash 1 of P5 | 48 | 2200 | 0.14 | 0.03180 | 0.030 | 6.0232 |
| 11 | Fly ash 1 of P1 | 139 | 2015 | 0.67 | 0.01966 | 0.028 | -30.694 |
| 12 | Fly ash 1 of P1 | 102 | 2014 | 0.45 | 0.02193 | 0.016 | 37.085 |
| 13 | Fly ash 1 of P1 | 97 | 2025 | 0.43 | 0.02242 | 0.018 | 24.594 |
| 14 | Fly ash 1 of P1 | 69 | 2025 | 0.25 | 0.02633 | 0.030 | -12.204 |
| 15 | Fly ash 1 of P1 | 53 | 2030 | 0.16 | 0.03150 | 0.036 | -12.746 |
| 16 | Fly ash 1 of P1 | 41 | 2018 | 0.094 | 0.04055 | 0.040 | 1.4489 |
| 17 | Fly ash 1 of P1 | 21 | 2032 | 0.026 | 0.13229 | 0.122 | 8.4366 |

The $U_{mf}$ of fly ash 4 of P2 has been over predicted, the error in estimation is very high, which showed that the model is not valid for the highly cohesive powder. Figure 5.16 shows the plot of the model through the experimental data points. The high value of $R^2$ indicates a good fit. Figure 5.17 shows the experimental versus predicted values of $U_{mf}$.

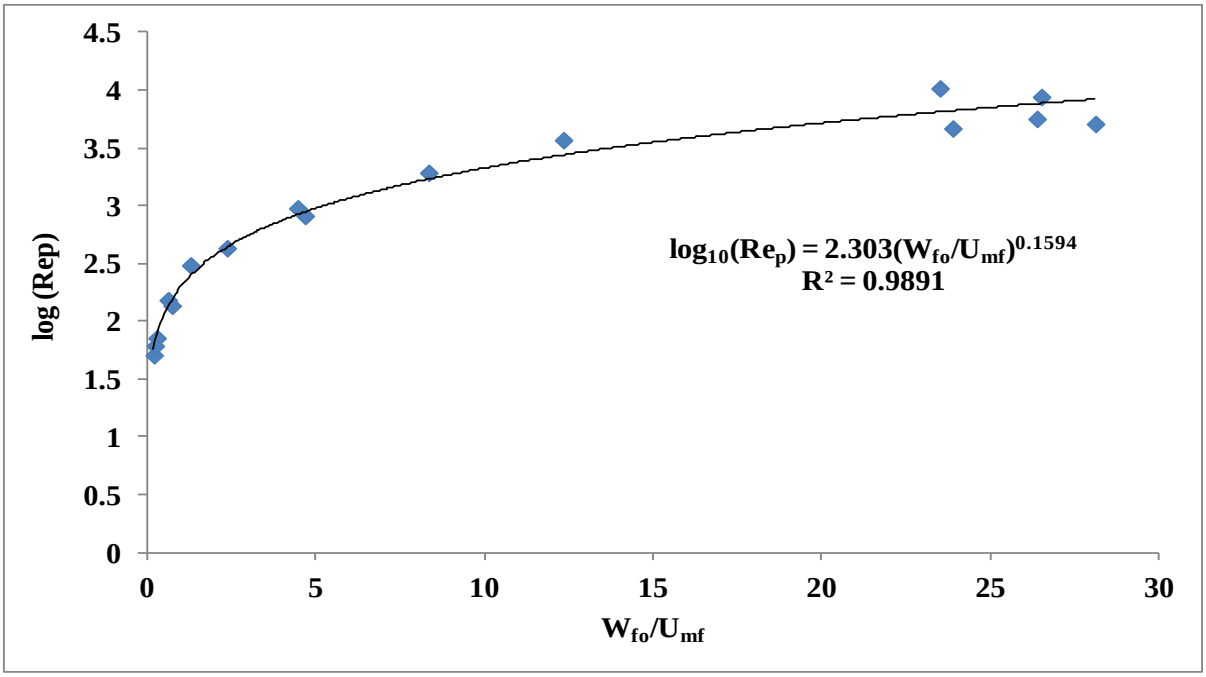


**Figure 5.16:** Plot of the new developed model representing minimum fluidization condition

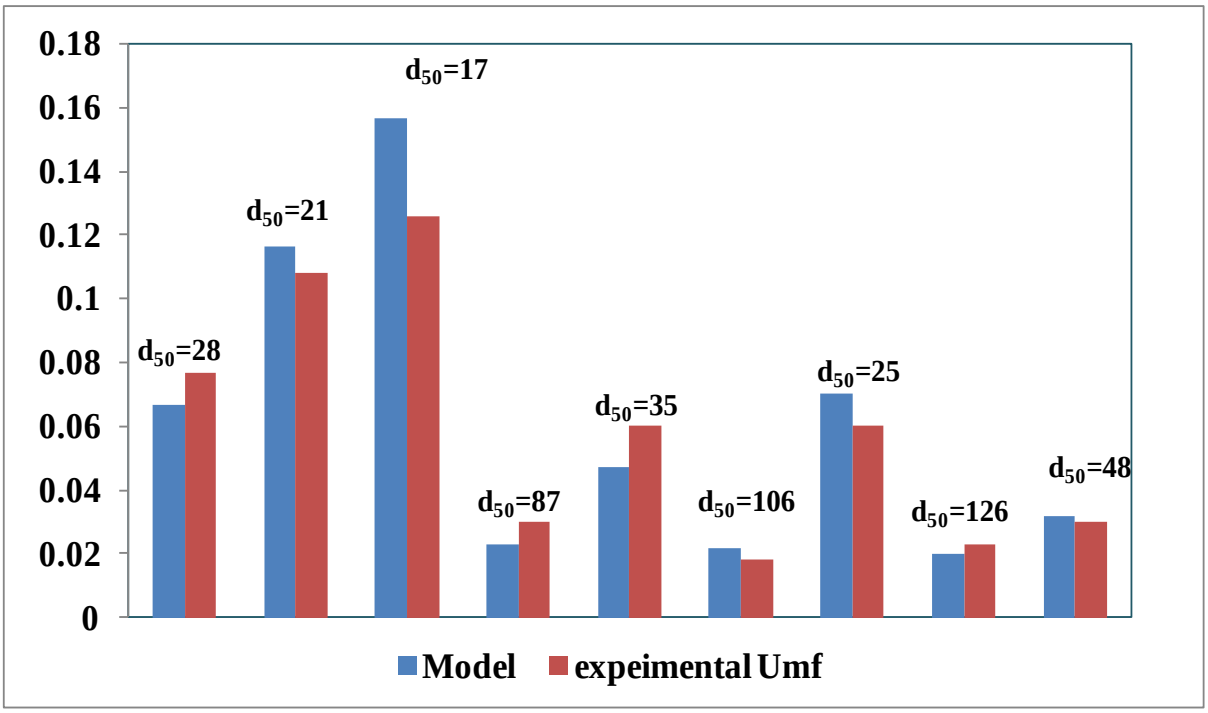


**Figure 5.17:** Experimental versus model predicted values of $U_{mf}$ ($d_{50}$ in μm)

Figure 5.16 shows that the developed correlation as mentioned in Eq. 5.11 well predicted the $U_{mf}$ value for the fly ash with R square value of 0.98. The comparative bar diagrams of predicted and experimentally calculated $U_{mf}$ values show the suitability of the model.

## 5.4 Conclusions

Based on the experimental investigation into the minimum fluidization velocity of fine powders the following conclusions could be made:

- Most of the correlations developed by researchers for predicting $U_{mf}$ found to be not reliable for very fine powders. A new model proposed based on experimental data using a dimensionless parameter ratio of settling velocity ($W_{fo}$) to minimum fluidization velocity and Reynolds number; which showed good fit with experimental values.
- Several experiments conducted on fly ash samples from different power plants having different particle size and size distribution evince that the new model predicts the $U_{mf}$ values approximately for fine powders and the error in prediction is less for powders which falls in the boundary of A/C group.
- The model failed to predict the $U_{mf}$ value of fly ash with mean particle size of 8 µm (highly cohesive powder). This specifies that the $W_{fo}$ plays no considerable role in case of highly cohesive powders, hence the model is lacking in with a parameter which reveals the fluidization behaviour.
- Powders with larger particle size have less air retention capacity and hence the pressure drop versus superficial air velocity plot with decreasing air flow rate is a curve with a sharp change and small radius of curvature, whereas the plot for smaller particle size powders it is a curve with gradual change having a larger radius of curvature.
- Highly cohesive powders when aerated form agglomerates and hence tend to behave as particles with larger particle size exhibiting lesser air retention capacity.

# Chapter 6

# Conclusion and Future scope of work

## 6.1 Conclusion

Based on the investigation into behaviour of fine powders the following conclusions can be made:

- The mustard paste which is considered as the bingham plastic fluid resulted in lesser value of yield stress when compared to mustard powder. The cause of reduction in stress value is due to reduced bondage among the particles by introducing water content into the powder to prepare a paste.
- The behaviour of shear stress varying with strain rate curve for fly ash resembled same as for mustard paste. It has also been found that the yield stress value of powders highly depends upon their physical properties such as particle size, size distribution and cohesive forces among the particles.
- As the depth of spindle immersion increases the obtained yield stress value increases, which implies that the yield stress value is directly related to the change in depth of spindle immersion.
- The model proposed for predicting the minimum fluidization velocity by experimental data fit using dimensionless parameters; ratio of settling velocity in the calm air of round particles to the experimental minimum fluidization velocity and the Reynolds number was found to predict the $U_{mf}$ values very close to experimental values especially for the powders belonging to A/C boundary.
- It was found that the model over predicts $U_{mf}$ value for highly cohesive powders. The cause for this is due to the settling velocity ($W_{fo}$) value which is very low for particles with particle size less than equal to 10 μm. This states that the model is lacking with a parameter which highly influences the fluidization behaviour of highly cohesive powders.
- The sudden change in pressure gradient versus superficial air velocity curve with a very small radius of curvature indicates the very little potential of the powder to retain air in it. The larger the radius of curvature of the curve higher is the air carrying capability of the powder.

## 6.2 Future scope of work

Future scope of work includes:

- Further investigation into the yield stress behaviour of other powders other than fly ash has to be conducted to ensure that the powders have similar behaviour as bingham plastic fluids.
- More tests have to be conducted on fluidized powders to analyze the fluid like behaviour of powders and relate the rheology properties with the fluidization and minimum transport boundary.
- The proposed model for minimum fluidization velocity has to be validated for powders other than fly ash to check its reliability.
- The present developed model doesn't include the rheology properties. Hence a model has to be developed for fluidized dense phase flow by including the air particle parameters; minimum fluidization velocity, permeability and rheology property yield stress for designing the pneumatic conveying system efficiently.

# REFERENCES


Abrahamsen, A.R and Geldart, D. 1980. Behaviour of Gas Fluidized Beds of Fine Powders Part I. Homogenous expansion, *Powder Technology*, 26 : 35-46.

Barletta, D., Donsì, G., Ferrari, G & Poletto, M. (2007). A rotational tester for the characterization of aerated shear flow of powders. *Particle and Particle Systems Characterization*, *24*(4-5), 259–270.

Bheeni, C.. (2015). ME Dissertation: An experimental investigation into the rheology of fine powders for modelling fluidized dense-phase pneumatic conveying, Thapar University.

Bruni, G., Tomasetta, I., Barletta, D., Poletto, M & Lettieri, P. (2009). Sensitivity analysis on a rheological model for the flowability of aerated fine powders. *Chemical Engineering Transactions*, *17*, 735–740.

Chawla, A. (2015). ME Dissertation; An investigation into the effects of variation of particle size on the fluidization and de-aeration characteristics of powders to assess dense-phase pneumatic conveyability, Thapar university .

Chen, W. (2013). PhD Dissertation: The rheology of aerated fine powders : theory and application in pneumatic conveying systems, University of New Castle.

Escudero, D & Heindel, T. J. (2013). Minimum fluidization velocity in a 3D fluidized bed modified with an acoustic field. *Chemical Engineering Journal*, *231*(July), 68–75.

Freeman, R. E., Cooke, J. R & Schneider, L. C. R. (2009). Measuring shear properties and normal stresses generated within a rotational shear cell for consolidated and non-consolidated powders. *Powder Technology*, *190*(1-2), 65–69.

Geldart, D., Abdullah, E. C & Verlinden, A. (2009). Characterisation of dry powders. *Powder Technology*, *190*(1-2), 70–74.

Gupta, S. K., Agarwal, V. K., Singh, S. N., Seshadri, V., Mills, D., Singh, J & Prakash, C. (2009). Prediction of minimum fluidization velocity for fine tailings materials. *Powder Technology*, *196*(3), 263–271.

Hirota, M., Sogo, Y., Marutani, T & Suzuki, M. (2002). Effect of mechanical properties of

powder on pneumatic conveying in inclined pipe. *Powder Technology*, *122*(2-3), 150–155.

Jiliang, M., Xiaoping, C & Daoyin, L. (2013). Minimum fluidization velocity of particles with wide size distribution at high temperatures. *Powder Technology*, *235*, 271–278.

Johanson, K. (2009). Effect of particle shape on unconfined yield strength. *Powder Technology*, *194*(3), 246–251.

Kalman, H., Satran, A., Meir, D & Rabinovich, E. (2005). Pickup (critical) velocity of particles. *Powder Technology*, *160*(2), 103–113.

Krantz, M., Zhang, H & Zhu, J. (2009). Characterization of powder flow: Static and dynamic testing. *Powder Technology*, *194*(3), 239–245.

Mallick, S. S. (2009). PhD Dissertation: Modelling of fluidized dense-phase pneumatic conveying of powders, University of Wollongong

Mallick, S. S & Wypych, P. W. (2009). Minimum transport boundaries for pneumatic conveying of powders. *Powder Technology*, *194*(3), 181–186.

Pan, R. (1999). Material properties and flow modes in pneumatic conveying. *Powder Technology*, *104*(2), 157–163.

Pusapati, R & Rao, T. (2014). Fluidized bed processing: A review. *Indian Journal of Research in Pharmacy and Biotechnology*, *5674*(August), 1360–1365.

Sanchez, L., Vasquez, N., Klinzing, G. E & Dhodapkar, S. (2003). Characterization of bulk solids to assess dense phase pneumatic conveying. *Powder Technology*, *138*(2-3), 93–117.

Setia, G. (2012). ME Dissertation: Modelling Minimum transport boundary for Dense-phase pneumatic conveying of fine powders, Thapar University.

Seville, J. P. K., Willett, C. D & Knight, P. C. (2000). Interparticle forces in fluidization: A review. *Powder Technology*, *113*(3), 261–268.

Shabanian, J., Jafari, R & Chaouki, J. (2012). Fluidization of Ultrafine Powders. *International Review of Chemical Engineering*, *4*(1), 16–50.

Sharma, A. M., Kumar, A., Patil, K. N & Huhnke, R. L. (2013). Fluidization characteristics of a mixture of gasifier solid residues, switchgrass and inert material. *Powder Technology*, *235*, 661–668.

Shaul, S., Rabinovich, E & Kalman, H. (2012). Generalized flow regime diagram of fluidized beds based on the height to bed diameter ratio. *Powder Technology*, *228*, 264–271.

Turki, D & Fatah, N. (2008). Behavior and fluidization of the cohesive powders: Agglomerates sizes approach. *Brazilian Journal of Chemical Engineering*, *25*(4), 697–711.

Xie, H. Y & Geldart, D. (1995). Fluidization of FCC powders in the bubble-free regime: effect of types of gases and temperature. *Powder Technology*, *82*(3), 269–277.

Xu, C & Zhu, J. (2006). Parametric study of fine particle fluidization under mechanical vibration. *Powder Technology*, *161*(2), 135–144.

Zhang, L., Hou, J., Bi, X. T., Grace, J. R., Janke, T & Arato, C. (2012). Fluidization characteristics and charging behavior of fly ash in a vibro-fluidized bed. *Powder Technology*, *215-216*, 235–241.

# Appendix A

The following equations are used to calculate the shear stress and strain rate values after each packet of data is obtained from the YR-1

Shear stress is given as:

$$\boldsymbol{\tau} = \frac{\mathbf{T} \times \mathbf{YMC} \times \mathbf{TK}}{10}$$

*Where:*

$\tau$ = Yield stress (Pa)

TK = Model torque constant for RVYR-1 (TK =1)

YMC = Yield multiplier constant of used spindle (YMC = 40 for V-75)

T = % Torque reading

Strain rate ($\dot{\gamma}$) is the rate of deformation caused by strain in a material within a corresponding time.

$$\dot{\boldsymbol{\gamma}} = \frac{\boldsymbol{\gamma}}{\mathbf{t}}$$

Strain is given as:

$$\boldsymbol{\gamma} = \boldsymbol{\theta}_{\mathbf{M}} - (\mathbf{S} \times \mathbf{T})$$

*Where:*

$\gamma$ = Strain (rad)

$\theta_M$ = Angular rotation of motor shaft (rad)

$$\theta_M = \omega \times t \times \frac{2\pi}{60}$$

S = Radial spring factor (rad / %torque)

$$S = \theta_{cal} \times (2\pi) \times 0.01$$

$\omega$ = Rotational speed (RPM)

t = time of test (seconds)

$\theta_{cal}$ = Spring windup angle (revolutions)

$$\theta_{cal} = \frac{V_{cal} \times t_{cal}}{60000}$$

$V_{cal}$ = Calibration speed (fixed at 0.1 RPM)

$t_{cal}$ = Calibration time (milliseconds)

(Time for 0% to 100% spring wind up during calibration)

$$t_{cal} = \frac{bi}{b_{cal}} \times \frac{V}{V_{cal}} \times 100$$

bi = Base increment (milliseconds)

$b_{cal}$ = Base increment calibration torque (% torque/base increment)

V = Speed (RPM)

# LIST OF PUBLICATIONS

**Referred Journals (Under Review) – 2 Nos.**

**Chaudhry, B., Tejaswi, K., Setia, G and Mallick S.S**. An Experimental Investigation into the Rheology of Fine Powders for Modelling Fluidized Dense-Phase Pneumatic conveying. Powder technology.

**Chawla, A., Tejaswi, K., Mallick S.S and Setia,G.** An Investigation into Fluidization and De-aeration Characteristics of Powders to Assess Dense-Phase PneumaticConveyability. Powder Technology.